Federal University of Technology – Paraná

Postgraduate Program in Mechanical and Materials Engineering

Conrado Chiarello

Horizontal air-water two-phase slug flow: Eulerian and Lagrangian data analysis

Curitiba

2020

CONRADO CHIARELLO

HORIZONTAL AIR-WATER TWO-PHASE SLUG FLOW: EULERIAN AND LAGRANGIAN DATA ANALYSIS

Escoamento bifásico horizontal de ar e água em golfadas: análise Euleriana e Lagrangeana de dados

Dissertação apresentada como requisito parcial para obtenção do título de Mestre em Engenharia, do Programa de Pós-Graduação em Engenharia Mecânica da Universidade Tecnológica Federal do Paraná (UTFPR). Área de concentração: Engenharia Térmica.
Orientador: Moisés Alves Marcelino Neto.
Coorientador: Rigoberto Eleazar Melgarejo Morales.

CURITIBA

2020

Ministério da Educação
Universidade Tecnológica Federal do Paraná
Diretoria de Pesquisa e Pós-Graduação

TERMO DE APROVAÇÃO DE DISSERTAÇÃO Nº 394

A Dissertação de Mestrado intitulada**: Horizontal Air-Water Two-Phase Slug Flow: Eulerian and Lagrangian Data Analysis**, defendida em sessão pública pelo Candidato **Conrado Chiarello**, no dia 23 de outubro de 2020, foi julgada para a obtenção do título de Mestre em Engenharia Mecânica E De Materiais, área de concentração: Engenharia Térmica, linha de pesquisa: Mecânica dos Fluidos, e aprovada em sua forma final, pelo Programa de Pós-Graduação em Engenharia Mecânica E De Materiais.

BANCA EXAMINADORA:

Prof. Dr. Moisés A. Marcelino Neto – Presidente – UTFPR

Prof. Dr. Paulo H. D. dos Santos – UTFPR

Dr. Hendy T. Rodrigues – CENPES/PETROBRAS

A via original deste documento encontra-se arquivada na Secretaria do Programa, contendo a assinatura da Coordenação após a entrega da versão corrigida do trabalho.

Curitiba, **23 de outubro de 2020**.

To my friends, family and girlfriend. I would not have been here if it wasn't for you.

"In God we trust. All others must bring data."

W. Edwards Deming

Resumo

Escoamentos multifásicos são fenômenos recorrentes tanto em ambientes naturais – como nas erupções vulcânicas e no escoamento de sangue pelas veias – quanto nos ambientes industriais – como nas indústrias nuclear e petrolífera. O conhecimento sobre a hidrodinâmica do escoamento, assim como sua evolução ao longo da tubulação, é essencial para o correto dimensionamento de linhas de produção, equipamentos (como bombas e slug catchers) e para formular estratégias para otimizar a extração de óleo dos reservatórios. Um padrão de escoamento frequentemente reportado nas linhas de produção de petróleo é o padrão em golfadas, motivo pelo qual o presente estudo se concentra em sua investigação. Para a análise do escoamento, uma nova metodologia é proposta e aplicada aos dados extraídos nas dependências experimentais do Núcleo de Estudos Multifásicos (NUEM). O circuito experimental tem 35,6 m de comprimento e 26 mm de diâmetro interno e foi operado sob 18 diferentes condições experimentais de golfadas e monitorado ao longo de 5 diferentes estações de medição compostas por um par de sensores resistivos e distribuídas ao longo da tubulação. Os dados foram analisados usando um ponto de referência Euleriano, através do qual se encontram distribuições estatísticas para cada parâmetro em cada estação de medição para cada ponto experimental, e um ponto de referência Lagrangeano, que segue células unitárias ao longo da tubulação para avaliar as mudanças nos parâmetros hidrodinâmicos de estruturas individuais. Correlações são propostas baseadas nos resultados observados para a média e o desvio padrão dos parâmetros. Ainda, é feita a comparação com trabalhos na literatura de maneira a testar as correlações propostas, assim como propor correções às existentes. Ademais, detalhes do escoamento são investigados usando a metodologia proposta, que é capaz de fornecer informações adicionais pertinentes sobre o comportamento do escoamento – como a natureza intrinsicamente transiente do escoamento em golfadas, demonstrado pelas variações dos comprimentos dos pistões de líquido, cujo valor médio não varia significativamente, mas que é produto de variações abruptas positivas e negativas nos pistões individuais. Além disso, é demonstrado que a expansão do gás é um fenômeno diretivo em pontos de alta aeração, mas se torna menos pronunciado em escoamentos de baixa aeração – como o plug flow. Por fim, o comportamento das variáveis hidrodinâmicas ao longo da tubulação e os fenômenos associados a ele são profundamente investigados – fornecendo informações úteis para futura modelagem.

Palavras-chave: Escoamento multifásico, Escoamento horizontal em golfadas, Referencial euleriano, Referencial lagrangeano.

Abstract

Multiphase flows are recurrent phenomena both in natural environments – such as volcanic eruptions and blood flow through veins – and industrial environments – such as the nuclear and petroleum industries. Knowledge about the hydrodynamics of the flow as well as its evolution across the pipeline is essential to correctly design pipelines, equipments (such as pumps and slug catchers) and to formulate strategies to optimize the crude oil exploitation from reservoirs. A frequently reported flow pattern in oil pipelines is slug flow, reason why the present study focuses in its investigation. In order to analyze the flow, a novel methodology is proposed and applied to data retrieved in Multiphase Flow Center (NUEM) experimental facilities. The experimental loop has a length of 35.6 m and 26 mm internal diameter and was operated under 18 different slug flow conditions – varying gas superficial velocity from 0.3 to 2.5 m/s and liquid superficial velocity from 0.3 to 3.0 m/s – across 5 different measuring stations composed by a pair of two-wire resistive sensors distributed along the pipe. Data was analyzed using Eulerian reference frame (ERF), which provides distributions for each hydrodynamic parameter in each measuring station for every experimental point, and Lagrangian reference frame (LaRF), which follows unit cells across the pipeline in order to evaluate the change in hydrodynamic parameters of single structures. Correlations were proposed based on retrieved results for hydrodynamic parameters average values and standard deviation. Moreover, a comparison against previous works was made in order to test the presented correlations as well as to propose corrections to the existing ones. Furthermore, details of the flow were investigated using the developed methodology, which was able to provide additional and insightful information about the flow behavior – such as the intrinsically unsteady nature of slug flow, as slug lengths were found to oscillate at all times, even though average values did not report significant changes, which would indicate developed flow conditions. Moreover, it was shown that gas expansion is a driver phenomenon in heavily aerated points, but becomes lees pronounced in low aeration flows – such as plug flows.

Keywords: Multiphase flow, Horizontal slug flow, Eulerian reference frame, Lagrangian reference frame.

List of Figures

List of Tables

LIST OF SYMBOLS

Roman symbols

	Description	Unit
a	Wake effect constant	$[-]$
A	Area	$[m^2]$
b	Wake effect constant	$[-]$
B	Wake effect constant	$[-]$
C_0	Distribution parameter	$[-]$
C_∞	Drift velocity parameter	$[-]$
D	Tube diameter	$[m]$
D_x^y	Discrepancy between signals x and y	$[-]$
Eo	Eötvös number	$[-]$
f	Frequency	$[Hz]$
Fr	Froude number	$[-]$
f_S	Sensor acquisition frequency	$[Hz]$
g	Gravity acceleration	$\left[{}^{m}/_{s^2}\right]$
h_L	Liquid height	$[m]$
J	Mixture velocity	$[{}^{m}/_{s}]$
J_k	Phase k superficial velocity	$[{}^{m}/_{s}]$
K	Wake effect constant	$[-]$
L_k	Structure k length	$[m]$
Mo	Morton number	$[-]$
n	Number of bubbles	$[-]$
N_k	Structure k length in acquisitions	$[-]$
Q_k	Phase k volumetric flow rate	$\left[{}^{m^3}/_{s}\right]$
R	Cross-correlation maximum value	$[-]$
Re	Reynolds number	$[-]$
Sr	Strouhal number	$[-]$
T	Period	$[s]$
U	Sensor voltage reading	$[V]$
V_D	Drift velocity	$[{}^{m}/_{s}]$
V_k	Phase k actual velocity	$[{}^{m}/_{s}]$
V_{TB}	Elongated bubble translational velocity	$[{}^{m}/_{s}]$

Greek symbols

	Description	Unit
β	Intermittent factor	$[-]$
θ	Pipe inclination angle	$[rad]$
μ	Dynamic viscosity	$[Pa \cdot s]$
ρ	Density	$\left[{kg}/{m^3}\right]$
σ	Surface tension	$\left[{N}/{m}\right]$
σ_k	Parameter k standard deviation	$[Varies]$

Subscripts and superscripts

	Description
B	Bubble
c	Continuum
f	Film
G	Gas
h	Horizontal
i	i-th element
k	Phase k or Structure k
L	Liquid
p	Pipe
S	Slug
v	Vertical

Contents

1 Introduction

Multiphase flows are characterized by the flow of two or more phases in the same duct or channel simultaneously (Rosa, 2012). The presence of two or more phases increases substantially the complexity of the flow – the number of variables of a two-phase flow is considerably greater when compared to a single-phase flow, which often increases the difficulty of developing mathematical and numerical models to predict the characteristics of this kind of flow (Shoham, 2006).

Multiphase phenomena are present over a wide range of applications: besides the petroleum industry, which is the main concentration of this research, and the nuclear industry, pioneer in developing multiphase flow studies, this type of flows are also present in geophysical phenomena – such as volcanic eruptions and river flow with small particles, such as rock and sand –, and blood flow in human veins.

Petroleum is a mixture majorly constituted by organic compounds (Thomas, 2001). The multicomponent nature of this substance may imply in multiphase phenomena when extracting it. Often, substances such as crude oil, natural gas and water are present in the flow, which may contain small solid particles, such as sand, paraffins and hydrates. A common simplification adopted in order to model these flows is to consider that there are only two phases flowing through the tube: liquid and gas, which characterizes a two-phase flow.

Two phases, when flowing simultaneously in the same duct, tend to distribute themselves in some particular flow settings. These distributions are called flow patterns. Because flow pattern classification is subjective, the nomenclature and characterization may vary among authors. This work is going to follow the nomenclature proposed by Shoham (2006) for horizontal and near horizontal gas-liquid two-phase flow, as shown in Fig. 1.

Figure 1 – Flow patterns in horizontal and near-horizontal gas-liquid two-phase flow.

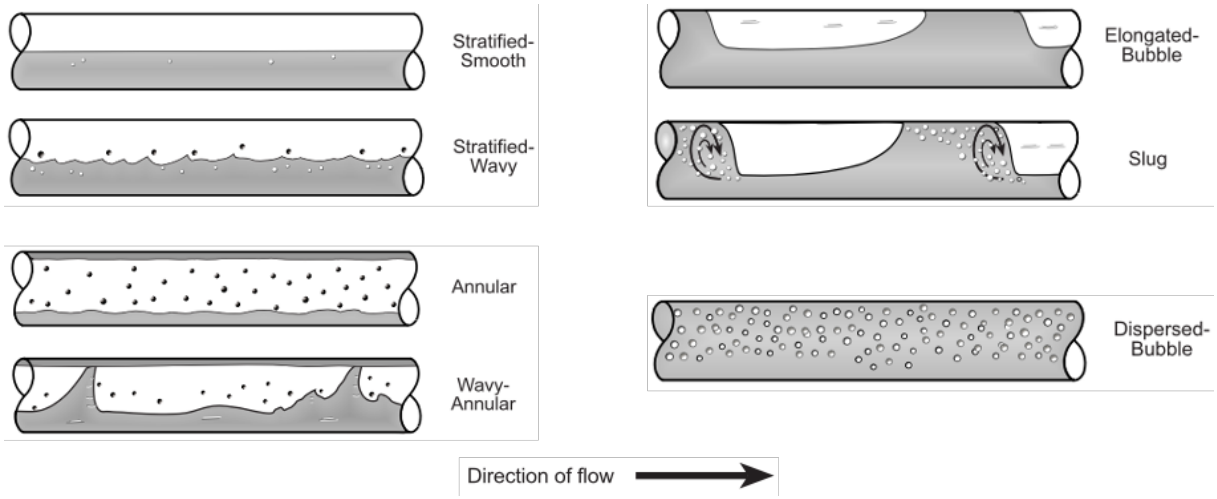

Source: adapted from Shoham (2006)

Depending on the flow conditions, transition between flow patterns may occur. Usually, these transitions are summarized and represented in a flow map. Figure 2 presents the Taitel and Dukler (1976) flow map for horizontal air-water two-phase flow at atmospheric pressure in a 1-inch diameter tube.

Figure 2 – Taitel and Dukler (1976) flow map for 1"air-water two-phase flow at atmospheric pressure

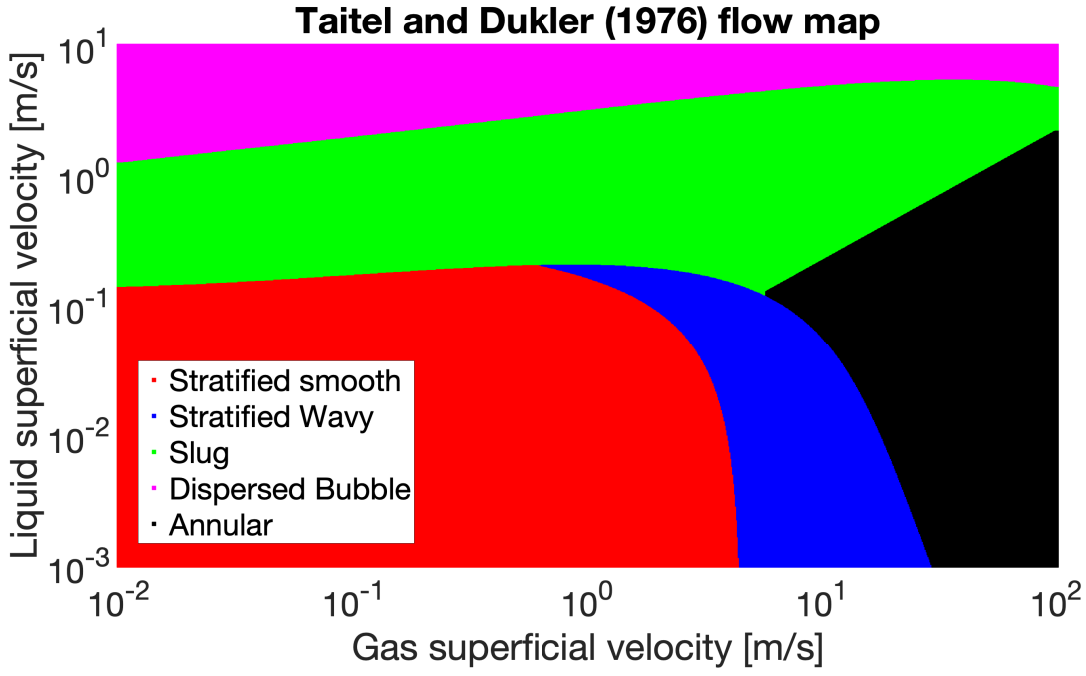

Source: Adapted from Taitel and Dukler (1976).

Among the presented flow patterns, Fanchi and Christiansen (2016) report that slug flow is frequently observed in oil and gas production. Slug flow is characterized by a basic unit structure, called unit cell, containing an elongated bubble and a liquid slug, which may contain dispersed bubbles. Figure 3 illustrates a slug flow unit cell.

Figure 3 – Slug flow unit cell.

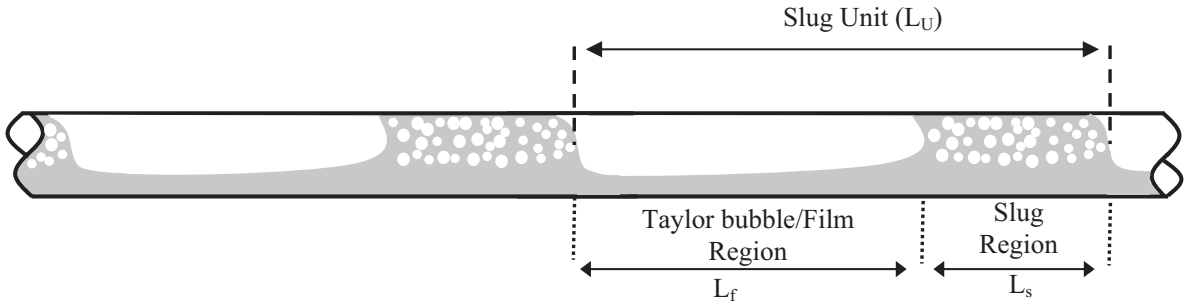

Source: Al-Safran (2016)

1.1 Relevance

Slug flow is characterized by the intermittent passage of two basic structures: the liquid slug and the elongated bubble. The non-stationary nature of this sort of flow substantially increases the difficulty to obtain essential flow parameters, such as pressure drop and unit cell frequency. Studying the effects of flow frequency in high-pressure three-phase flow, Kang et al. (1996) conclude that this hydrodynamic parameter speeds up the corrosive process in pipeline components.

In oil exploitation, the well head is connected to the platform using pipes, which usually follow the seabed terrain. In this sort of pipeline, horizontal two-phase flow is found and slug flow is frequently reported. Fig. 4 illustrates pipelines in oil exploitation.

Figure 4 – Oil extraction pipeline over the seabed.

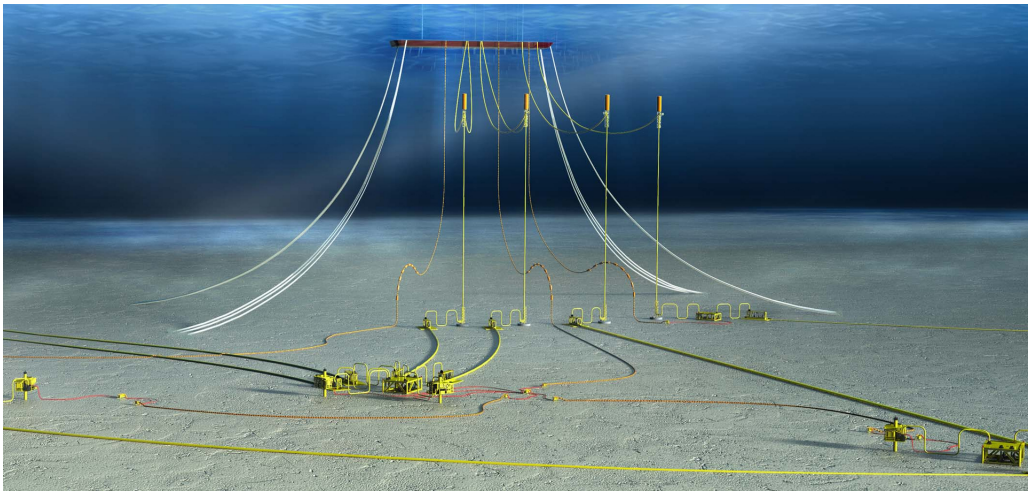

Source: OGE (2020)

Knowledge of the flow hydrodynamics and its evolution over time is essential to design pipeline equipment, as well as to formulate strategies to optimize crude oil extraction from natural reservoirs. In order to reproduce flow conditions found in oil exploitation, a physical model may be used, since the experimental approach is not feasible, given the extreme conditions of the flow. The physical model, though, should be validated using experimental data that reproduce a flow under bench scale conditions. As slug flow is an intrinsically transient flow, hydrodynamic parameters do not tend to follow deterministic correlations, but statistical distributions instead. Statistical analysis, hence, becomes an invaluable tool: finding the distribution which better fits the experimental data, its parameters – such as mean and standard deviation for normal distribution – may be used to predict the most probable values interval for each flow variable.

1.2 Objectives

The main goal of this work is to analyze data from an experimental study developed by Barros et al. (2019) to evaluate the detailed evolution of characteristic hydrodynamic parameters of a two-phase air-water slug flow in horizontal tubes, as well as to provide a novel methodology to retrieve data from a moving reference frame (Lagrangian referential).

In order to attain the proposed objective, this work will analyze data from the experimental horizontal circuit at Multiphase Flow Research Center (NUEM) facilities. After processing the experimental time series, characteristic slug flow parameters will be evaluated, namely, bubble translational velocity, unit-cell frequency, bubble and slug length and bubble and slug void fractions.

Among the specific objectives of this work, it is intended to apply two different

methodologies in order to extract information from the retrieved data: the Eulerian (or stationary) reference frame analysis – which consists in finding a statistical distribution which better fits the data obtained through the experimental circuit, as well as the statistical parameters of these distributions and fit correlations using known hydrodynamic variables – and the Lagrangian (or moving) reference frame analysis – which aims to identify and track unit cells across stations in order to monitor changes in hydrodynamic parameters. While the former is widely applied in literature, the latter is a novel methodology developed by the current work.

2 Literature Review

The present chapter synthetizes pertinent information present in academic literature which are used in this thesis. Section 2.1 starts the literature review with vertical and horizontal two-phase slug flow, progressing over a chronological order from relevant studies which provide the foundations of hydrodynamic models, detailing the main concepts and definitions involved in multiphase phenomena. Later on, characteristic parameters of slug flow are detailed in Section 2.2, gathering experimental studies and findings regarding these variables in literature, as it is the focus of the present work. Finally, Section 2.2 will be focusing on statistical evolution of hydrodynamic parameters of two-phase slug flow – bubble translational velocity and its peculiarities, frequency, void fraction and, at last, slug, bubble and unit cell lengths – for this is the main goal discussed by this work.

2.1 Two-phase slug flow

Slug flow is characterized by two structures which repeat themselves intermittently along the flow: the liquid slug and the elongated bubble, which, for vertical flow, is usually called Taylor bubble (Shoham, 2006; Yadigaroglu and Hewitt, 2018).

The liquid slug carries the liquid phase and may have some small dispersed bubble in it. The elongated bubble is a region mostly taken by the gas phase, containing a liquid film that flows around the bubble in vertical flows or underneath it in horizontal flows. This is the most remarkable difference between the flows. Behind the elongated bubble, there is a region of high instability caused by recirculation due to the chaotic dynamic of this sort of flow, namely, the wake region, represented in Fig. 5.

Figure 5 – Schematic representation of the wake region behind the elongated bubble.

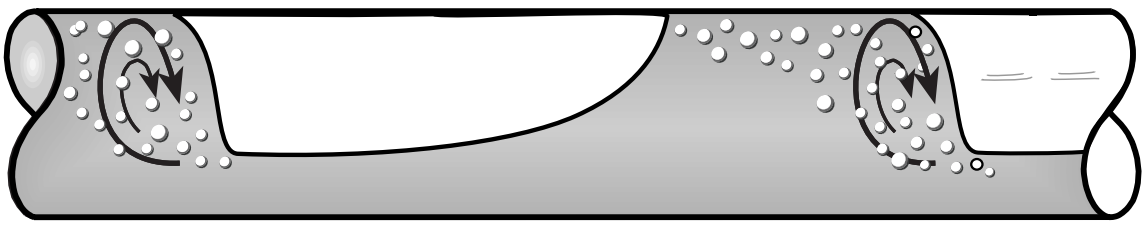

Source: adapted from Shoham (2006)

As multiple phases flow simultaneously through the same duct, new quantities to describe the flow arise. The first concept introduced is the phase fraction, often called

void fraction and liquid hold-up for gas-liquid two-phase flow. This parameter is defined by Shoham (2006) as the volume of the phase relative to the total volume, applied over an infinitesimal length. A practical way to calculate the phase fraction is to divide the area occupied by the given phase relative to the pipe cross-sectional area, as proposed by Yadigaroglu and Hewitt (2018), Eq. 2.1.

$$R_k = \frac{1}{A_p} \sum_{i=1}^{N} A_{k,i}, \tag{2.1}$$

where R is the phase fraction, k is the given phase, $A_{k,i}$ is the i-th piece of area of the phase k, N is the total number of disconnected pieces of area of the phase k and A_p is the cross-sectional area of the pipe. Because of the nature of its definition, phase fraction has an interesting property: the sum of all phase fractions within a given cross-sectional area must be equal to unity.

Ideally, phases velocities and volumetric flow rates would be known in any section of the pipe. Unfortunately, measuring these quantities is a difficult task. Another definition is made in order to contour this difficulty: the superficial velocity. Superficial velocities are defined by Shoham (2006) as the velocity the phase would have if it was flowing alone through the tube, Eq. 2.2.

$$J_k = \frac{Q_k}{A_p}, \tag{2.2}$$

where J_k is the superificial velocity of the phase k, Q_k is the volumetric flow rate and A_p is the pipe cross-sectional area.

As phase fraction is a ratio of areas, the fluid superficial and actual velocity may be related using this quantity, as per Eq. 2.3.

$$J_k = V_k R_k, \tag{2.3}$$

where Vk is the actual velocity of the phase k.

From the definition of superficial velocity, one more velocity may be calculated: the mixture velocity, defined by Shoham (2006) as the mixture volumetric flow rate, i.e. the sum of all phases flow rates, within the given cross-sectional area. Regarding two-phase gas-liquid flows specifically, the mixture velocity may be calculated as per Eq. 2.4.

$$J = J_L + J_G, \tag{2.4}$$

where J is the mixture velocity, J_L is the liquid superficial velocity and J_G is the gas superficial velocity.

In multiphase flow, dimensionless groups are often defined in order to describe the flow as an effort to extend the application of correlations to flows under different scales and conditions. They may arise as a ratio of forces or from the necessity of having dimensionless variables to study. Some common dimensionless numbers used to describe two-phase flows are found in Table 1.

Table 1 – Dimensionless numbers used in multiphase flow.

Number	Equation	Physical meaning
Reynolds	$Re = \frac{\rho V D}{\mu}$	Ratio of inertial to viscous forces
Froude	$Fr = \frac{V}{\sqrt{gD}}$	Ratio of inertial to gravitational forces
Eötvös	$Eo = \frac{\Delta\rho g D^2}{\sigma}$	Ratio of gravitational to surface tension forces
Morton	$Mo = \frac{g\mu_c^4\Delta\rho}{\rho_c^2\sigma^3}$	Dimensionless properties group
Strouhal	$Sr = \frac{fD}{V}$	Dimensionless frequency

Source: The author.

Besides the parameters cited above, each flow pattern has their own characteristic parameters. As this work is focused on slug flow, they are discussed in details up next.

2.2 Slug flow characteristic parameters

Slug flow has also characteristic parameters: bubble translational velocity, flow frequency, bubble and liquid slug void fraction and lengths. These parameters are used in order to design pipelines and equipment attached to it, such as pumps and slug catchers. Studies regarding these parameters are detailed up next.

2.2.1 Bubble translational velocity

Bubble translational velocity is a parameter of paramount importance, as it is often a key closure relationship in mechanistic models. Bubble translational velocity is defined by Taitel and Barnea (1990) as the velocity of the interface between the liquid slug and the elongated bubble, which is commonly associated to the entire slug unit cell, as experimental evidence supports that these velocities are almost identical and narrowly distributed around an average (Fabre, 2003).

In order to better understand bubble translational velocity, it is necessary to analyze each of its components individually. This velocity may be expressed as a function of three

major contributions: the relative velocity between gas and liquid, often called drift velocity, the mixture velocity and the wake effect modifier.

2.2.1.1 Drift velocity

The drift velocity is the relative velocity between phases, which can be directly retrieved when measuring the velocity of an elongated bubble flowing through stagnant liquid. Dumitrescu (1943) studied an infinite long bubble rising through quiescent liquid in a vertical tube and successfully obtained an analytical solution solving the potential flow differential equation for an inertial dominant flow, described in Eq. 2.5.

$$V_{TB} = 0.351\sqrt{gD}. \tag{2.5}$$

Although it might seem a simple solution at first glance, experimental evidence supports the agreement between the analytical solution and experimental measures (White and Beardmore, 1962).

Following similar approach, Benjamin (1968) retrieved the solution for an infinitely long bubble flowing through stagnant liquid in a horizontal pipeline. The potential flow differential equation was solved with slightly different boundary conditions: instead of a spherical top bubble, it was assumed that the bubble occupied the top portion of the pipe, forming a spherical cap. The solution is expressed in Eq. 2.6.

$$V_{TB} = 0.54\sqrt{gD}. \tag{2.6}$$

Even though the above equations have severe restrictions – as any analytical solution is expected to have –, they provide the foundations to the bubble translational velocity studies, often serving as a start point to experimental corrections regarding less restricted conditions – such as the Brown (1965) and Weber (1981) corrections for vertical and horizontal flow, respectively.

2.2.1.2 Mixture velocity

When flowing through moving liquid, the velocity of an elongated bubble is influenced by the moving stream. Nicklin et al. (1961) investigated these effects in vertical flows and, after conducting experimental tests, concluded that there is a linear relation between the translational velocity of the bubble and the mixture velocity, as shown in Eq. 2.7.

$$V_{TB} = C_0 J + V_D, \tag{2.7}$$

where C_0 is a constant, J is the mixture velocity and V_D is the drift velocity.

For vertical flows, it was found that C_0 is 2 for laminar and 1.2 for turbulent regimes. Theoretical background provided by Collins et al. (1978) sustains the claim that this constant is given by the ratio of the maximum velocity of the liquid in front of the bubble by the average velocity of the same flow.

Bendiksen (1984), emphasizing the assertiveness of the correlation proposed by Nicklin et al. (1961), gathered similar information for two-phase slug flow in declined, horizontal, inclined and vertical tubes, allowing a more general investigation of the influence of the moving stream in front of the bubble in its velocity. The author assumes as a first approximation that level and buoyancy effects may be treated individually, proposing the correlation found in Eq. 2.8.

$$V_D = V_D^h cos\theta + V_D^v sin\theta, \tag{2.8}$$

where V_D^h is the drift velocity for the horizontal case, V_D^v is the drift velocity for the vertical case and θ is the pipe inclination angle.

Carrying out experiments, Eq. 2.8 was verified to hold for all positive inclination angle range and for $Fr_L < 3.5$. For greater Fr_L values, it was observed that bubble centering takes place and the drift velocity is evaluated by Eq. 2.9.

$$V_D = V_D^v sin\theta. \tag{2.9}$$

The research also investigated the value of the constant C_0 for different inclinations. For vertical flow, the results showed agreement to those found by Nicklin et al. (1961), i.e., a constant value of 1.19-1.20. As bubble centering takes place – for Fr_L greater than 3.5 –, the same value was found. When Fr_L is less than 3.5, C_0 was found to be 1.05 for horizontal flows. For different inclinations, retrieved data suggested that C_0 is a combination of these values, according to Eq. 2.10.

$$C_0 = C_0^h + (C_0^v - C_0^h) sin^2\theta. \tag{2.10}$$

2.2.1.3 Wake effect

Behind the elongated bubble, there is a region characterized by its chaotic flow called bubble wake. This region substantially disturbs the liquid velocity profile behind the bubble. As reported by Collins et al. (1978), bubble velocity is influenced by the flow in front of its nose. Depending on the slug length separating two bubbles, liquid velocity profile ahead of the trailing bubble may not be fully developed, which implies in a higher peak velocity along the profile, culminating in the acceleration of the trailing bubble. This is called the wake effect.

Moissis and Griffith (1962) were the first to investigate such phenomenon. Using plastic, bullet shaped bubbles in vertical flow, velocities were measured for different separation distance – or slug lengths. Measured data suggested an exponential decay, as presented in Eq. 2.11.

$$\frac{V_{TB}^{trailing}}{V_{TB}^{leading}} = 1 + ae^{-b\frac{L_S}{D}}, \tag{2.11}$$

where a and b are experimental constants.

The exponential decay model holds for horizontal flow as well. Therefore, similar equations were developed for the horizontal case. Barnea and Taitel (1993) proposed a slightly different correlation, as shown in Eq. 2.12.

$$\frac{V_{TB}^{trailing}}{V_{TB}^{leading}} = 1 + Be^{-\beta\frac{L_S}{L_{stab}}}, \tag{2.12}$$

where B and β are experimental constants and L_stab is the slug stabilization length.

2.2.2 Frequency

Frequency is a parameter of major interest as well, as it brings most of the problems related to slug flow. Kang et al. (1996) reported that the corrosion rate is increased substantially as slug frequency increases. The flow intermittency is also responsible for stress cycling, arising the need to care about fatigue when designing structural components of the pipeline.

Two types of frequency are commonly used in modeling: the flow frequency and the unit cell frequency. Although these concepts seem similar, it must be stressed that they do not represent the same quantity; they are, though, related to each other.

2.2.2.1 Flow frequency

Flow frequency is defined as the number of unit cells per time, Eq. 2.13.

$$f = \frac{n}{T}, \tag{2.13}$$

where f is the flow frequency, n is the number of unit cells passed and T is the interval of time.

Flow frequency may oscillate for a small number of samples, but tends to converge to a steady value when bigger samples are analyzed. This is the physical frequency of the system, which should be used in order to design pipeline components.

2.2.2.2 Unit cell frequency

Frequency is defined as the rate of repetition of a given phenomenon; therefore, defining a frequency to a single unit cell seems to be physically inconsistent. The concept of unit cell frequency, though, should not be treated as a physical concept, but rather as a mathematical tool to assist in two-phase flow modelling instead. Unit cell frequency is defined as the inverse of the residence time of a unit cell, as shown in Eq. 2.14.

$$f_U = \frac{1}{T_B + T_S}, \tag{2.14}$$

where f_U is the unit cell frequency, T_B is the bubble passage time and T_S is the liquid slug passage time.

The unit cell frequency is related to the flow frequency, which is defined as the number of unit cells divided by time, as per Eq. 2.15. The time interval is, though, nothing but the sum of the unit cells individual times.

$$f = \frac{n}{T_1 + T_2 + \cdots + T_n}, \tag{2.15}$$

in which f is the flow frequency, n is the number of unit cells passed and Ti is the passing time of the i-th unit cell.

Combining Eq. 2.14 and 2.15,

$$f = \frac{n}{\frac{1}{f_{U1}} + \frac{1}{f_{U2}} + \cdots + \frac{1}{f_{Un}}}, \tag{2.16}$$

The concepts, although different, are related by a harmonic mean, as reported by Conte et al. (2017). While unit cell frequency may sound inconsistent at first glance, it is an important tool to evaluate flow frequency.

2.2.2.3 Frequency studies

A simple correlation to horizontal slug flow frequency was proposed by Gregory and Scott (1969). Measuring frequency for horizontal two-phase carbon dioxide-water slug flow in a 3/4"diameter tube, it was found that it depends on the slug velocity according to Eq. 2.17.

$$f = \frac{A}{V_S} + BV_S + C, \tag{2.17}$$

where f is the flow frequency, VS is the slug velocity and A, B and C are experimental constants.

Further development of the above correlation based on theoretical and experimental data became Eq. 18.

$$f = 0.0226\left[\frac{J_L}{gD}\left(\frac{19.75}{J} + J\right)\right]^{1.2}. \tag{2.18}$$

Although the correlation is given in terms of flow parameters, it is important to note that this equation is developed based on small sample sizes and for restricted flow conditions. Heywood and Richardson (1979), using numerous experimental data collected from literature, proposed similar correlation, Eq 2.19.

$$f = 0.0364\frac{J_L}{J}\left(\frac{2.02}{D} + \frac{J^2}{gD}\right)^{1.06}. \tag{2.19}$$

Zabaras (2000), extensively reviewing frequency correlations and data published in literature, proposed a quite similar correlation to those mentioned above, but taking care to explicit the influence of the inclination angle, as shown in Eq. 2.20.

$$f = 0.0226\left(\frac{J_L}{gD}\right)^{1.2}\left(\frac{212.6}{J} + J\right)^{1.2}(0.836 + 2.75sin^2\theta). \tag{2.20}$$

Embracing the struggle to develop a frequency correlation valid for all inclinations, Hernandez-Perez et al. (2010), while also extensively reviewing frequency studies, assumed that frequency could be split in horizontal and vertical components, Eq. 2.21.

$$f = f_h cos\theta + f_v sin\theta, \tag{2.21}$$

where f_h is the frequency for the horizontal case and f_v is the frequency for the vertical case.

As the authors claim that there was not a frequency correlation developed specifically for the vertical case, they proposed an equation based on experimental data, as shown in Eq. 2.22.

$$f_v = 0.8428\left[\frac{J_L}{gD}\left(\frac{19.75}{J} + J\right)\right]^{0.25}. \tag{2.22}$$

2.2.3 Phase fraction

Phase fraction is another hydrodynamic parameter used as closure relation for numerical models – liquid slug phase fraction, specifically. Furthermore, it is used by the present work as a starting point to analyze data. Usually, two different approaches are found in literature: describing average values for phase fraction in a specific structure –

liquid slug or elongated bubble – or using histograms to analyze the phase fraction time series in order to characterize the flows. While the former is usually applied as a closure relation to mechanistic models, the latter is used in order to identify flow patterns.

Costigan and Whalley (1997), analyzing vertical two-phase flows, concluded that each flow pattern had a characteristic time series histogram. For the slug flow case, specifically, the histogram was bimodal, where the peaks were characterized by the liquid slug and elongated bubble passage, indicating the intermittency of the flow. Reis and Leonardo (2010) verified that this condition holds for horizontal slug flow as well.

As a closure relation, phase fraction is usually correlated by a deterministic equation rather than statistical description. Even though it is known that phase fraction fluctuates along the flow and among structures, average values are commonly used by mechanistic models. Following the average value trail, Gregory et al. (1978) developed a simple correlation for liquid slug hold-up, as shown in Eq. 23.

$$R_{LS} = \frac{1}{1 + (\frac{J}{8.66})^{1.39}}, \tag{2.23}$$

where R_{LS} is the liquid slug hold-up.

Gomez et al. (2000), synthetizing data from different experiments, found a correlation valid for horizontal, upward inclined and vertical flows. Applying data regression, the equation was found to depend on the inclination angle and superficial liquid Reynolds number, Eq. 2.24.

$$R_{LS} = e^{-(0.45\theta + 2.48 \cdot 10^{-6} Re_{LS}}, \tag{2.24}$$

where Re_LS is the superficial liquid Reynolds number.

2.2.4 Slug length

Slug length is another key parameter in multiphase flows, being critical to designing slug catchers, which do not depend on average slug length, but must consider the maximum liquid slug length instead. Statistical analysis, therefore, becomes an invaluable tool to investigate such phenomenon.

Brill et al. (1981) used statistical tools in order to describe slug length distributions. Analyzing data from a horizontal flow in Prudhoe bay field, the authors concluded that slug lengths distribute themselves following a log-normal distribution. Sæther et al. (1990), investigating horizontal two-phase slug flow, concluded that fractal statistics may be used in order to describe slug lengths.

Deterministic correlations are also developed in literature, as slug length is often a closure relation for mechanistic models as well. While Nicholson et al. (1978) assume that liquid slugs have a fixed dimensionless length of 30 diameters, Scott et al. (1989) presents a correlation to calculate the average slug length, as shown in Eq. 25.

$$L_S = max(30D; -26.6 + 28.5[ln(D) + 3.67]^{0.1}). \tag{2.25}$$

As this correlation tends to underpredict the slug length for smaller diameters, the minimum slug length average value is set to 30D, in consonance to Nicholson et al. (1978) proposition.

Slug lengths may also be retrieved from simulations. Barnea and Taitel (1993) proposed a simple model to simulate bubble and slug evolution along the pipe, known as Slug Tracking model. Applying experimental closure relations, such as the ones described in Eq. 2.5 and 2.11, the algorithm can track bubble coalescence and the behavior of flow structures along the pipe. Several authors proposed updates to this model, including Taitel and Barnea (2000), Al-Safran et al. (2004) and Rodrigues et al. (2009).

2.3 Horizontal two-phase slug flow experimental studies

Due to its chaotic nature, slug flow is inherently unsteady. Hydrodynamic parameters, therefore, do not tend to follow a deterministic value, but rather assume a range of values instead. Statistical analysis, hence, becomes an invaluable tool in order to describe slug flow. Studies regarding statistical aspects of slug flow were chosen and are presented in this section.

Nydal et al. (1992b) investigated horizontal air-water two-phase slug flow by statistical means. Analysis were conducted through 53 mm and 90 mm internal diameter 17 m long pipes over a wide range of superficial velocities and conductance probes were used in order to measure the liquid hold-up time series. Pressure was measured along with the liquid hold-up in order to take in account the gas expansion effect.

The authors reported two types of slugs: developed – regular slugs with average length and aeration – and undeveloped slugs – which are shorter than usual and highly aerated. It was found that, even though some of these slugs decay along the pipe, on average these slugs develop into regular slugs. Furthermore, undeveloped slugs travel at the same velocity of regular slugs.

As reported previously by Brill et al. (1981), slug length distribution is observed to fit to a log-normal distribution, which is the same distribution applied by the authors to describe liquid slug void fraction. Bubble velocity data shows agreement to the normal distribution.

Bubble velocity parameter C_0 – as defined by Nicklin et al. (1961), Eq. 2.7 – was investigated as well. It was observed that this value was somewhat higher than the ratio of the average to the peak velocity, as reported by other studies, namely Gregory and Scott (1969), Dukler and Hubbard (1975) and Ferre (1981). The authors say that possible explanations to this phenomenon is that the presence of dispersed bubbles in liquid slugs may substantially disturb the liquid velocity profile, as reported by Andreussi et al. (1990 apud Nydal et al., 1992).

Following the same trail, Fabre et al. (1993) analyzed horizontal air-water two-phase slug flow using a longer 50 mm internal diameter tube – the last measuring station was located 89 m ahead of the mixing device. Void fraction data was registered using conductance probes. The experiment was carried under restricted flow conditions: three different scenarios were studied, with mixture velocity ranging from 0.87 m/s to 2.22 m/s.

Using cross-correlation to evaluate bubble and slug velocity individually, it was found that they were remarkably close and narrowly distributed around its average. Moreover, bubble velocity was found to increase slightly along the flow and the authors attribute that finding to the gas expansion effect – which slightly increases gas superficial velocity.

Slug lengths were found to be in the range of 10 to 40 diameters. Furthermore, the authors conclude that, even after 1500 diameters of tube, the flow did not seem to be fully developed. Bubble coalescence were also investigated: after a coalescence, the resulting bubble seemed to have a larger length than the sum of the former bubbles' lengths. The authors conclude that a small portion of the gas entrained in the liquid slug is captured by the bubbles during the process.

Wang et al. (2007) used conductance probes in a 50 mm internal diameter 133 m long tube to measure hydrodynamic parameters of horizontal air-water two-phase horizontal slug flow over a wide range of superficial velocities – gas superficial velocity ranging from 1 to 20 m/s and liquid superficial velocity ranging from 0.16 to 1.5 m/s. Hydrodynamic parameters were investigated in two separate measuring stations, the first one mounted at x/D = 1157 and the second one at x/D = 2609.

Bubble translational velocity was measured in different scenarios. Although it was found that the drift velocity is inexistent for Froude numbers greater than 3.5, as reported by Bendiksen (1984), these studies have a major disagreement: bubble translational velocity parameters showed significant discrepancy when compared to Bendiksen's report – agreement was only found for low mixture velocities. Moreover, translational velocity parameters are found to vary along the pipeline: when Froude number is less than 3.5, C_0 seems to dwindle and is approximately constant; when Froude is greater than 3.5, it shows the opposite behavior and rises significantly. Measured values for x/D = 2609 are shown in Fig. 6.

Figure 6 – Wang et al. (2007) measured velocities vs. Bendiksen (1984) correlation.

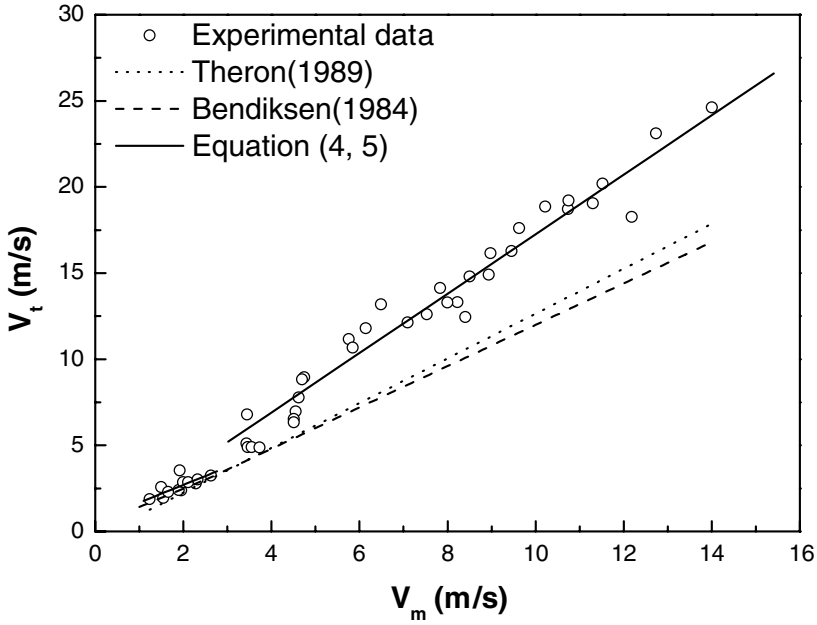

Source: adapted from Wang et al. (2007).

Even though no correlation was found for liquid slug length, as values are dispersed, their intervals limits are reported to increase along the pipeline: while slug lengths measured at the first station were in the [15D, 27D] interval, the second station exhibits slugs of [23D, 40D] length. Furthermore, the authors report that slug lengths tended to develop faster at higher mixture velocities. As for the bubble length, it was found that it increases with increasing gas superficial velocities, but decreases with increasing liquid superficial velocities.

Finally, the authors investigated unit-cell frequency, mistakenly reporting its arithmetic mean value as the average flow frequency. Unit-cell frequency was found to weakly depend on gas superficial velocity, but to have strong dependence on liquid superficial velocity. Strouhal number is used in order to report frequency correlations, following Fossa et al. (2003) methodology.

Vicencio (2013) used wire-mesh sensors (WMS) and a high-speed camera to monitor horizontal air-water two-phase slug flow hydrodynamic parameters in a 9.2 m long tube with 25.8 mm internal diameter. Agreement was found between the velocity measured from the image processing and the WMS data analysis. Furthermore, correlations were developed using the retrieved data for bubble and slug lengths, as well as for frequency and bubble velocity. Not only average values were analyzed, but their standard deviation as well, in order to provide sufficient information to fit a statistical distribution – a major concern to numerical simulations initial conditions. A summary of the analyzed parameters, as well as their correlations and correlation coefficient are presented in Table 2.

Table 2 – Summary of correlations presented by Vicencio (2013).

Parameter	Statistic	Correlation	R^2
Velocity	Average	$Fr_{V_{TB}} = 1.19Fr_J + 0.4$	0.99
	Standard deviation	$\frac{\sigma_{V_{TB}}}{\sqrt{gD}} = 0.0357Fr_J^2$	0.81
Frequency	Average	$Sr_L = exp\left(6.31\frac{J_L}{J} - 5.75\right)$	0.98
	Standard deviation	$\sigma_f = 0.502f^{0.956}$	0.89
Bubble length	Average	$\frac{L_B}{D} = 1.34exp\left(5.68\frac{J_G}{J}\right)$	0.95
	Standard deviation	$\frac{\sigma_{L_B}}{D} = 0.331\left(\frac{L_B}{D}\right)^{1.075}$	0.93
Slug length	Average	$\frac{L_S}{D} = 2.67ln\left(\frac{4.84 \cdot 10^5}{Re_J Sr}\right)$	0.69
	Standard deviation	$\frac{\sigma_{L_S}}{D} = 2.152exp\left(1.89\frac{J_G}{J}\right)$	0.63
Bubble void fraction	Average	$R_{GB} = 0.748\left(\frac{J_G}{J}\right)^{0.5}$	0.83
	Standard deviation	0.036	–

Source: Adapted from Vicencio (2013).

Most correlations presented fair agreement to experimental data, notwithstanding the fact that the tube was relatively short – consequently, the flow might have not been fully developed at the test section.

Recently, Rodrigues et al. (2020) investigated the effect of superficial velocities on histogram distributions for bubble translational velocity and slug frequency in horizontal air-water slug flow. Qualitative description about the influence of the former on the latter were given. The authors reported that changes in liquid superficial velocity were responsible for noticeable changes in the bubble translational velocity probability density function; gas superficial velocity, however, was found to play a minor role in the process. Liquid slug void fraction, on the other hand, did not seem to change significantly with liquid superficial velocity changes, while bubble void fraction was reported to decrease with its increase. Furthermore, velocity histograms were found to fit to a Weibull distribution, whereas slug frequency histogram was represented by a log-normal distribution.

2.4 Summary and final words

In this chapter, two-phase horizontal slug flow studies were reviewed and characteristic hydrodynamic parameters were investigated, as well as the phenomena behind some of the findings. The studies reviewed are summarized by subject in Tables 3-5. As slug length is usually treated as a statistical distribution, it is unusual to find deterministic correlations for average slug length; therefore, a table for this hydrodynamic parameter will not be provided.

Two-phase horizontal slug flow is extensively researched in literature. Yet, it is not fully understood and there are still some points open to discussion and further investigation. While experimental studies tend to focus on Eulerian referential, as the data analyzed is usually separated by measuring stations, numerical models usually require information from a Lagrangian referential, e.g. the behavior of unit cells across different stations. Furthermore, insightful information about flow phenomena may be obtained from Lagrangian referential analysis, such as the changes of individual unit cells' hydrodynamic parameters, which could be used in order to deeper understand the involved phenomena – often obfuscated by average values.

The present work aims to provide a novel methodology to analyze data in order to supply the required information of the flow. Data reported in literature does not often exceed one thousand diameters of pipeline length; on the other hand, data used in the present work goes over 1400D, allowing a more embracing description of the flow. Another major concern of this work is to provide accurate data from modern measuring systems, as most of the reference works in literature used equipment which would be far outdated nowadays.

Table 3 – Summary of slug liquid hold-up correlations analyzed.

Author	Correlation	Applicability
Gregory et al. (1978)	$R_{LS} = \frac{1}{1 + (\frac{J}{8.66})^{1.39}}$	$\theta = 0°$
Malnes (1983)	$R_{LS} = 1 - \frac{J}{83(\frac{g\sigma}{\rho_L})^{0.25} + J}$	$\theta = 0°$
Marcano et al. (1998)	$R_{LS} = \frac{1}{1.001 + 0.0179J + 0.0011J^2}$	$\theta = 0°$
Gomez et al. (2000)	$R_{LS} = exp(-(0.45\theta + 2.48 \cdot 10^{-6} Re_{LS})$	$0° \leq \theta \leq 90°$

Source: The author.

Table 4 – Summary of velocity correlations analyzed.

Author	C_0	C_∞	Applicability
Dumitrescu (1943)	–	0.351	$\theta = 90°$
Nicklin et al. (1961)	$\begin{cases} 2, & Re_L < 8000 \\ 1.2, & Re_L \geq 8000 \end{cases}$	0.351	$\theta = 90°$
Benjamin (1968)	–	0.54	$\theta = 0°$
Gregory and Scott (1969)	1.35	0	$\theta = 0°$
Dukler and Hubbard (1975)	$1.022 + 0.021 \ln(Re_S)$	0	$\theta = 0°$
Collins et al. (1978)	$\frac{V_{avg}}{V_{max}}$	–	$\theta = 90°$
Weber (1981)	–	$0.54 - 1.76Eo^{-0.56}$	$\theta = 0°$
Bendiksen (1984)	$\begin{cases} 1.05 + 0.15sin^2\theta, & Fr_L < 3.5 \\ 1.2 & Fr_L \geq 3.5 \end{cases}$	$\begin{cases} 0.54cos\theta + 0.35sin\theta, & Fr_L < 3.5 \\ 0.35sin\theta & Fr_L \geq 3.5 \end{cases}$	$-30° \leq \theta \leq 90°$
Marcano et al. (1998)	1.201	0.532	$\theta = 0°$
Wang et al. (2007)	$x/D = 1157$: $\begin{cases} 1.096, & Fr_J < 3.5 \\ 1.373, & Fr_J \geq 3.5 \end{cases}$ $x/D = 2609$: $\begin{cases} 1.028, & Fr_J < 3.5 \\ 1.726, & Fr_J \geq 3.5 \end{cases}$	$x/D = 1157$: $\begin{cases} 0.342, & Fr_J < 3.5 \\ 0, & Fr_J \geq 3.5 \end{cases}$ $x/D = 2609$: $\begin{cases} 0.927, & Fr_J < 3.5 \\ 0, & Fr_J \geq 3.5 \end{cases}$	$\theta = 0°$

Source: The author.

Table 5 – Summary of frequency correlations analyzed.

Author	Correlation	Applicability
Gregory and Scott (1969)	$f = 0.0226\left[\frac{J_L}{gD}\left(\frac{19.75}{J} + J\right)\right]^{1.2}$	$\theta = 0°$
Greskovich and Shrier (1972)	$f = 0.0226\frac{J_L}{J}\left[\left(\frac{79.5276}{D} + \frac{J^2}{gD}\right)\right]^{1.2}$	$\theta = 0°$
Heywood and Richardson (1979)	$f = 0.0364\frac{J_L}{J}\left(\frac{2.02}{D} + \frac{J^2}{gD}\right)^{1.06}$	$\theta = 0°$
Trononi (1990)	$f = 0.61\frac{\rho_G}{\rho_L}\frac{V_G}{h_G}$	$\theta = 0°$
Hill and Wood (1990)	$\frac{fD}{J} = 0.275 \cdot 10^{2.68H_{Le}}$	$\theta = 0°$
Jepson and Taylor (1993)	$\frac{fD}{J_L} = 7.59 \cdot 10^{-3} + 0.01$	$\theta = 0°$
Marcano et al. (1998)	$f = -0.089 + 0.214J_L$	$\theta = 0°$
Zabaras (2000)	$f = 0.0226\left[\left(\frac{J_L}{gD}\right)\left(\frac{212.6}{J} + J\right)\right]^{1.2}(0.836 + 2.75sin^2\theta)$	$0° \leq \theta \leq 11°$
Al-Safran (2009)	$ln(f) = 0.8 + 1.53ln(V_L) + 0.27\left(\frac{V_{slip}}{J}\right) - 34.1D$	$\theta = 0°$
Gokcal et al. (2010)	$f = 2.623\frac{1}{N_f^{0.612}}\frac{J_L}{D}$	$\theta = 0°$
Hernandez-Perez et al. (2010)	$f = f_h cos\theta + f_v sin\theta,\ where:$ $f_v = 0.8428\left[\frac{J_L}{gD}\left(\frac{19.75}{J} + J\right)\right]^{0.25}$	$0° \leq \theta \leq 90°$
Abed (2015)	$f = 0.0478\left[\frac{J_L}{gD}\left(\frac{19.75}{J} + J\right)\right]^{1.2}$	$\theta = 0°$
Al-Safran (2016)	$ln(f) = 1.51 - 17.04D + 0.77ln(J_L) - 0.181ln\left(\frac{V_G}{V_L}\right)$	$\theta = 0°$

Source: The author.

3 Materials and Methods

The current chapter will briefly introduce the experimental technique used to retrieve time series data, since it is not the main concern of the present study. Data analysis technique, on the other hand, is thoroughly discussed and documented, since it is the purpose of the current work. Furthermore, different methods for unit cell velocity calculation are presented and compared.

3.1 Experimental apparatus

The methodology applied to this research aims to answer to specific objectives: acquiring hydrodynamic parameters – such as bubble and slug length – and to fit statistical distributions to the obtained data. Data was retrieved by Barros et al. (2019) using an experimental circuit of 35m long and 0,026m diameter at NUEM experimental facilities. The circuit is divided in two main sections: the test section – made of acrylic in order to visualize the flow – and the return pipeline, which aims to recirculate the liquid used in the study. A schematic representation of the experimental apparatus is shown in Fig. 7.

Figure 7 – Experimental loop schematic representation.

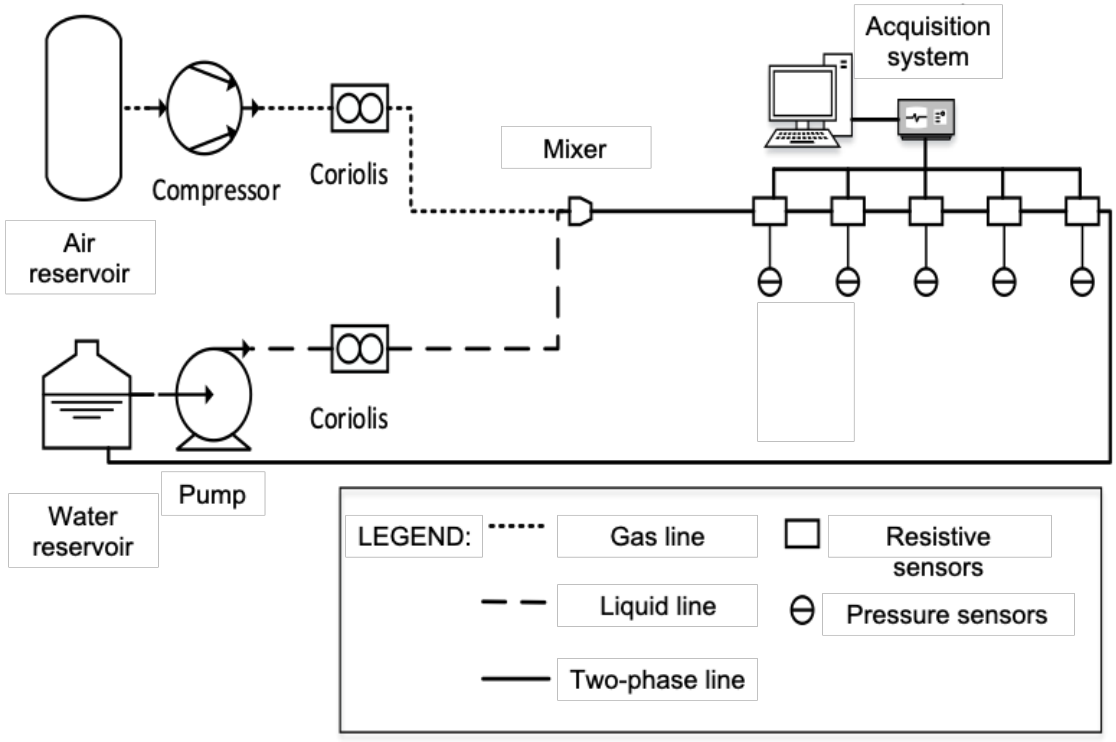

Source: adapted from Barros et al. (2019)

The experimental loop has five measuring stations – positioned at 390D, 538D, 615D, 807D and 1154D – equipped with two-wire sensors and pressure transducers. Two-wire sensors measure the liquid height in order to acquire the void fraction time series and the pressure is recorded in order to fix gas superficial velocity due to gas expansion. Coriolis flow meters are used to measure the air and water mass flow at the loop inlet. Both fluids are mixed using a parallel plate device in order to promote stratified flow at the tube entrance, as stratified flow tends to quickly develop to slug flow. Details of the experimental procedure and uncertainties are found in Barros et al. (2019).

The experimental test matrix is defined in order to ensure slug flow regime in the testing section. The flow map used as standard is proposed by Taitel and Dukler (1976). Superficial liquid and gas velocities are chosen respecting operational limitations of the experimental apparatus, both for the lower (accuracy) and upper (maximum flow) limits. The experimental matrix used is shown in Table 6 and the experimental points are marked on the Taitel and Dukler (1976) flow map, as shown in Fig. 8.

Table 6 – Experimental test matrix.

P	J_G [m/s]	J_L [m/s]	J [m/s]	P	J_G [m/s]	J_L [m/s]	J [m/s]
P01	0.3	0.7	1.0	P10	1.3	0.7	2.0
P02	0.5	0.5	1.0	P11	1.5	0.5	2.0
P03	0.7	0.3	1.0	P12	1.0	2.0	3.0
P04	0.5	1.0	1.5	P13	1.5	1.5	3.0
P05	1.0	0.5	1.5	P14	2.0	1.0	3.0
P06	0.5	1.5	2.0	P15	1.0	3.0	4.0
P07	0.75	0.75	1.5	P16	1.5	2.5	4.0
P08	1.0	1.0	2.0	P17	2.0	2.0	4.0
P09	0.7	1.3	2.0	P18	2.5	1.5	4.0

Source: Adapted from Barros et al. (2019).

3.2 Data analysis

Time series retrieved is given in terms of voltage. The conversion to liquid height depends on the calibration of the sensor, which is made measuring single-phase flow voltage. It is assumed that voltage registered in two-phase flow varies linearly between two extremes – liquid and gas single phase flow –, as shown in Eq. 3.1.

$$h_L = \frac{U - U_{gas}}{U_{liq} - U_{gas}}, \tag{3.1}$$

in which U is the sensor voltage registered and h_L is the liquid height.

Figure 8 – Experimental points in Taitel and Dukler (1976) flowmap.

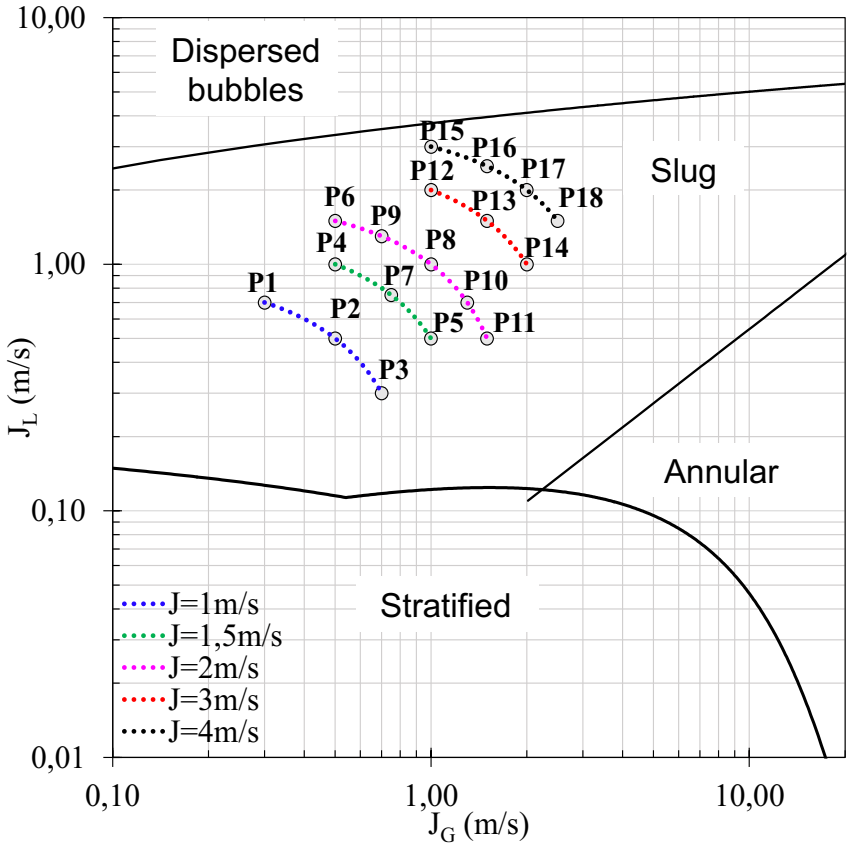

Source: Barros et al. (2019)

In order to convert liquid height to void fraction, geometrical parameters are used to develop further relations. Figure 9 represents the parameters used, namely liquid height (h_L), contact angle (γ), interface perimeter (S_i) and tube diameter (D).

Figure 9 – Geometrical parameters for stratified flow.

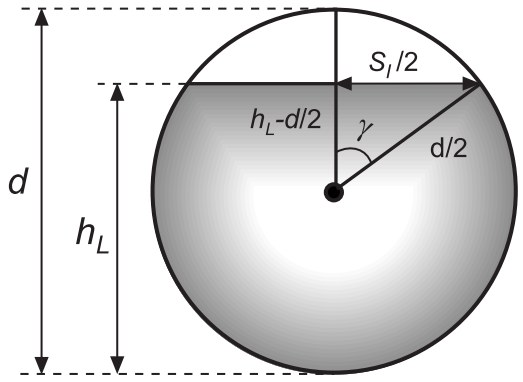

Source: adapted from Shoham (2006)

Conversion between liquid height and void fraction is given by Eq. 3.2, after Taitel

and Dukler (1976).

$$R_G = \frac{1}{\pi}\left[cos^{-1}\left(\frac{2h_L}{D} - 1\right) - \left(\frac{2h_L}{D} - 1\right)\sqrt{1 - \left(\frac{2h_L}{D} - 1\right)^2}\right] \tag{3.2}$$

where R_G is the void fraction and D is the tube diameter.

With void fraction time series, the analysis may proceed. The algorithm is organized in four common routines for both approaches – unit cell detection, velocity calculation and subsequent parameters calculation – and one specific routine for each method. Due to the method chosen to calculate velocity, unit cell match – a routine developed to measure the time displacement between sensors – will not be necessary.

3.2.1 Unit cell detection

The first step towards flow analysis is to detect unit cells and to determine whether these detections are true or false positives. The detection itself is divided in six steps: coarse void fraction cutting factor, fine void fraction cutting factor, derivative sign change, minimum average void fraction, minimum length and detection fix.

In order to determine both coarse and fine void fraction cutting factors, the void fraction histogram is analyzed. Two-phase slug flow exhibits a bimodal histogram, where the first peak characterizes low void fraction flow, i.e. liquid slugs, and the second peak characterizes high void fraction flow, i.e. elongated bubbles. The histogram is divided in two and the fine cutting factor is defined as the first peak of the histogram. The coarse cutting factor is defined as the average between the fine cutting factor and the half of the histogram. Figure 10 depicts the applied procedure.

Figure 10 – Void fraction histogram. Left and right stars represent fine and coarse factors, respectively.

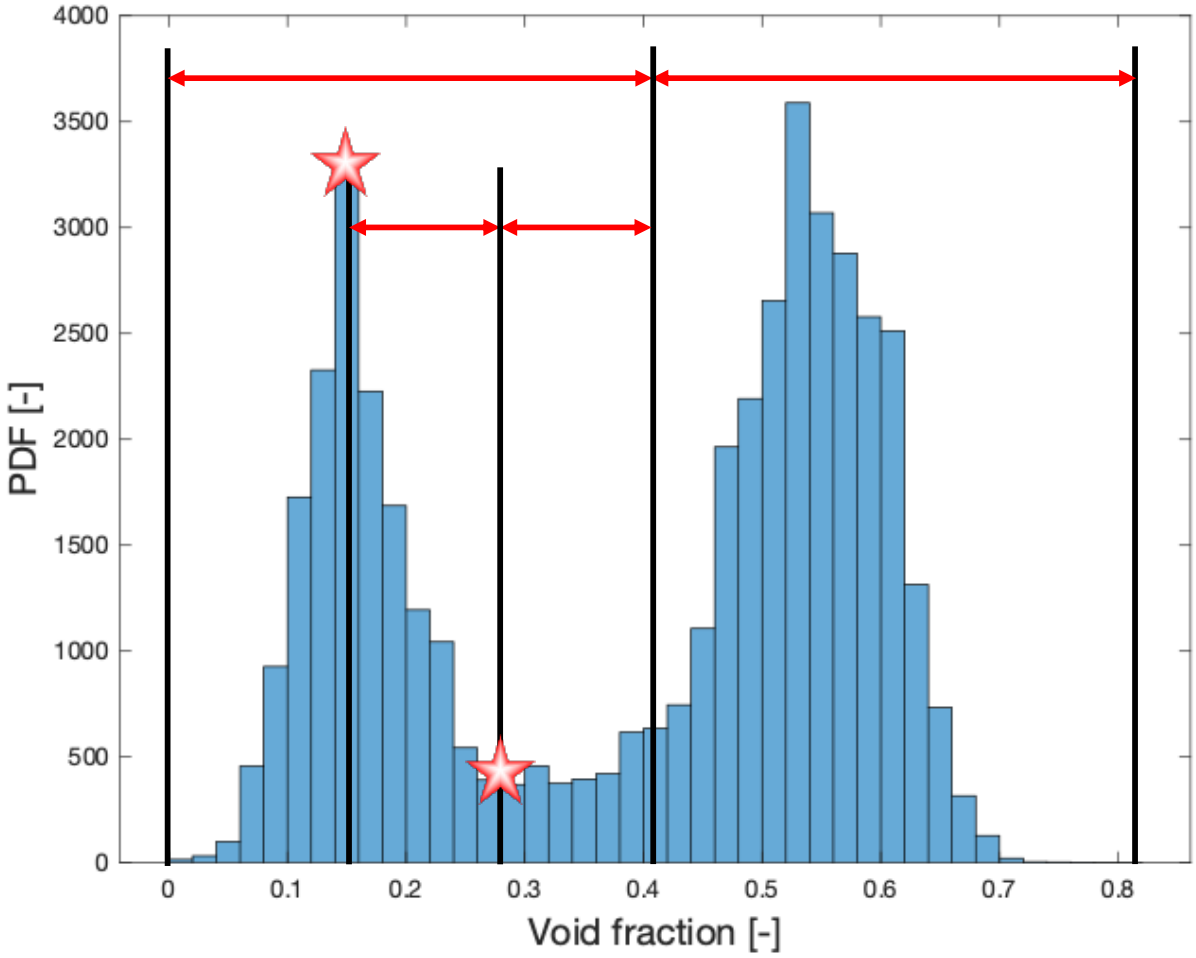

Source: The author.

The coarse void fraction cutting factor is applied in order to differentiate bubbles and slugs. Bubbles are defined as the data above the coarse cutting factor and liquid slugs as the data below it. After applying the coarse cutting factor, the algorithm searches for the first correspondence before (for bubble start) or after (for bubble tail) equal or lower than the fine cutting factor, improving the accuracy of the detection.

The next step in unit cell detection is to analyze the void fraction time series derivative. Whenever a bubble nose touches the sensor, void fraction tends to increase substantially up from a lower value. Similarly, whenever the bubble tail last touches the sensor, void fraction is expected to decrease substantially. The algorithm, hence, searches for the first detection before (for bubble start) or after (for bubble tail) where the derivative change its sign or is equal to zero. This step is the last effort to improve detections.

After detecting unit cells, additional procedures are applied in order to eliminate false positives, namely, fake bubbles. The first additional procedure searches for bubbles

with low average void fraction. An intermediate value between the two histogram peaks – the void fraction corresponding to the half of the histogram – is chosen, as a less restrictive value in order to delete as few real bubbles as possible. Bubbles with average void fraction equal or less than this value are considered fake bubbles and summarily deleted, being, therefore, incorporated to the adjacent slugs.

Shoham (2006) reports that very small bubbles (L < 1.2D) tend to break into smaller bubbles along the flow. Since the bubble length is calculated using the velocity, it is not possible, at this time, to determine the true length of the structures. One approximation used in order to evaluate lengths is to consider that every bubble in the flow has the velocity as proposed by Bendiksen (1984), Eq. 2.8. Lengths are, thus, approximated and bubbles with length equal or less than one tube diameter are considered false positives and deleted.

One last step to unit cell detection is to find incongruousness. The algorithm searches for bubble nose detections which happened at the same time or even after its tail. These are considered bad detections and are summarily deleted. Also, it is checked whether a bubble nose is registered at the same time or before its leading bubble tail. These detections are deleted in order to unify both bubbles.

3.2.2 Velocity calculation

In order to calculate velocity, the goal is to find the passage time of a bubble between two sensors, since the distance between them is known. Different methods were used to compare results and are briefly described ahead.

A first approach is to simply subtract the times of the bubble nose detection, henceforth called naive method. Aeration and oscillation in detection may substantially influence the accuracy of this method, which is summarily discarded. In order to overcome the setbacks, bubble nose is defined as a small interval in time series – which takes in account the void fraction upper ramp – rather than just a point. Mao and Dukler (1989), investigating vertical flows, claim that, because the bubble oscillates as it rises, this is not a straightforward method to measure its true velocity; rather, cross-correlation is used. The bubble oscillation along the pipe is also observed in horizontal flow and may, therefore, lead to wrong results when small samples of the bubble are analyzed.

A simple method to evaluate bubble velocity is to assume that every bubble has the same velocity – evaluating an average delay of the whole signals rather than comparing structures. Although this hypothesis is physically inconsistent, this velocity may be used as standard to compare with velocities calculated using other methods, given that velocities are narrowly distributed around their average, but has little value when evaluating hydrodynamic parameters.

Another approach widely used in literature is to use cross-correlation for the whole bubble to estimate its average delay between both sensors. Known problems of this method are: bubble tail velocity may slightly diminish and bubble tail detection may not be as good as the front because of the wake region. Given that the velocity difference between bubble nose and tail is irrisory and often lower than the experiment precision, it is reasonable to assume that the bubble has a constant velocity along its interface.

Even though the velocity is assumed to be constant along the whole bubble, the tail detection may still vary substantially. In order to surmount this issue, one more approach is used: to use cross-correlation for the whole unit cell, given that the bubble nose detections are usually better than the tail because of the already mentioned wake behind the bubble tail. One major flaw of this approach is the assumption that the whole unit cell has the same velocity, which may not hold for every structure. Fabre (2003) reports that the unit cell method is a good approximation for two-phase slug flow, as bubble and slug velocities are narrowly distributed around their average and differ slightly.

There is still one more method applicable to the velocity calculation which does not deal with time delay itself – being this the great difficulty of the velocity calculation. It is possible, stating some assumptions, to evaluate the velocity of a bubble using mass conservation. This method heavily relies on the accuracy of the detection and the precision of the sensor used, but ensures that mass conservation is achieved – which is a major concern for numerical models. Assuming that the liquid slug travels at mixture velocity, bubble translational velocity may be calculated as per Eq. 3.3.

$$V_{TB} = \frac{N_U[J_L - J(1 - R_{GS})]}{R_{GS}N_F - \int_0^{N_F} R_{GB}dN} \tag{3.3}$$

where N_U is the length of the unit cell in number of acquisitions and N_F is the length of the film region in number of acquisitions.

As the mass conservation method is strongly dependent on the detection and the quality of the signal, this is a major difficulty to apply it. As two-wire sensors are primarily used to measure liquid height, the measuring of dispersed bubbles in the liquid slug may not be as accurate as needed because the wires are positioned in the center of the tube, which would culminate in discrepant void fraction measures.

Similar methodology is applied by Fossa et al. (2003), whose compared the phase continuity calculation with measurements from video frames. A maximum deviation of about 15% was observed, which is a satisfactory accuracy to the present work, given the limitations of the other methods. Since mass conservation must be achieved in order to use the retrieved data to validate numerical models, the continuity method is applied to velocity calculations in this work.

3.2.3 Subsequent parameters calculation

The velocity retrieved for single bubbles is assumed to be the same for the whole unit cell, assumption that will affect bubble and liquid slug length only, but has no effect in frequency, average void fraction or intermittence factor. The calculation of subsequent parameters is straightforward.

The unit cell frequency is defined as the inverse of the period of the given unit cell, which can be calculate directly from the number of acquisitions using the acquisition frequency, Eq. 3.4.

$$f_U = \frac{f_s}{N_U}, \tag{3.4}$$

where f_s is the sensor acquisition frequency.

Slug and bubble lengths may be retrieved from the velocity and number of acquisitions as per Eq. 3.5.

$$L_k = \frac{V_{TB} N_k}{f_s}, \tag{3.5}$$

where L is the length, N is the length in number of acquisitions and k represents the phase – bubble or slug.

The intermittence factor, although defined as the ratio of slug length per unit cell length, may be calculated without using the unit cell velocity, as shown in Eq. 3.6.

$$\beta = \frac{N_F}{N_U} \tag{3.6}$$

where N_F is the elongated bubble length in number of acquisitions.

The average void fraction for bubble and liquid slug is calculated as the average of the average void fraction in each structure, Eq. 3.7.

$$R_{Gk} = \frac{1}{n} \sum_{i=1}^{n} \bar{R}_{Gk,i} \tag{3.7}$$

where R_{Gk} is the phase k – liquid or gas – average void fraction, n is the number of structures and $\bar{R}_{Gk,i}$ is the i-th phase k structure average void fraction.

After calculating the hydrodynamic parameters, which is a common routine for both methodologies, the analysis may be conducted through Eulerian (or stationary) reference frame or Lagragian (or moving) reference frame. These methodologies are detailed up next.

3.2.4 Eulerian reference frame (ERF) analysis

After retrieving every hydrodynamic parameter, the first step to the Eulerian analysis is to fit statistical distributions using the results. Even though there is enough literature background regarding statistical distributions for specific parameters, it is up to the analyst to choose the distribution which better fits the data retrieved. The chi-square method is a quantitative criterium to evaluate, given the significance level, whether the statistical distribution fits well to results. Details of the method are found in Appendix A.

The next step in Eulerian analysis is to evaluate average values of the hydrodynamic parameters, as well as their standard deviations. Retrieving these values allows the search for correlations of these variables as a function of given parameters, such as superficial velocities or mixture velocity, for example. Engineering correlations of this kind may be used in field operations as well as in numerical simulations. Once more, it is up to the analyst to choose the correct parameters in order to obtain useful engineering correlations.

3.2.5 Lagrangian reference frame (LaRF) analysis

The goal of LaRF analysis is to follow unit cells along the flow in order to analyze changes in their hydrodynamic parameters, rather than analyzing average values and their standard deviations. The first step to this approach, therefore, is to track the same unit cell across different stations.

Bubble and liquid slugs may not keep their characteristic parameters, such as length and void fraction, along the pipe. As bubbles may coalesce, liquid slugs may experiment drastic reduction in their size. Fortunately, most of the structures do not deform significantly across different stations and the signals are similar enough to be aligned.

In order to align different signals, the cross-correlation is used to retrieve their average delay. Since all the stations start to gather acquisitions at the same time, it is necessary to trim the signals, as the last unit cells of the first station would not be registered in the last station and the first unit cells in the last measuring station would have passed without being registered in the first station. The final acquisitions of the first measuring stations and the initial acquisitions of the last measuring stations are, hence, trimmed out of the analysis.

With aligned time series, unit cell identification between different stations is straightforward: structures are considered to be correspondent to the nearest unit-cell present in the other signal. The process is illustrated in Fig. 11. However, it is possible that two unit-cells in the first signal correspond to a single unit-cell in the last signal, which is treated as a coalescence.

Figure 11 – Bubble and unit-cell matching using the nearest correspondent.

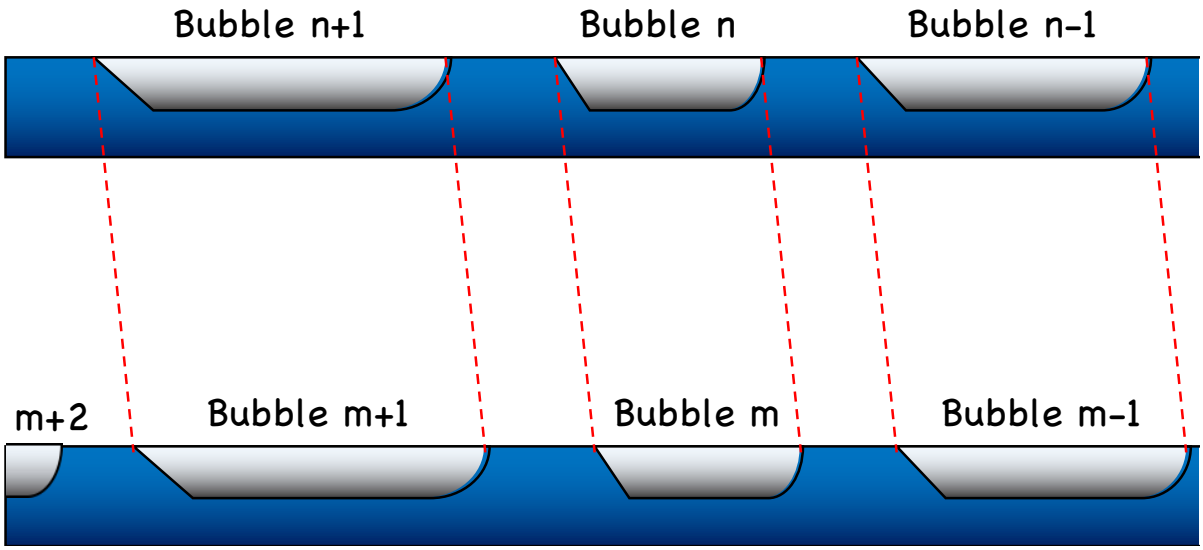

Source: The author.

After properly identified across the pipeline, a matrix of correspondence is used in order to compare the hydrodynamic parameters of the unit cell in every measuring station. Hence, evolution of hydrodynamic parameters may be retrieved for individual unit cells rather than analyzing average values. Furthermore, it is possible to analyze the behavior of unit cells after a coalescence takes place, which is a critical matter for numerical models.

3.3 Summary and final words

Along the current chapter, a briefly explanation about the experimental methodology was given, as it is not the focus of this work itself. Rather, the discussion was centered around the data analysis procedure, core of this work, proposing a methodology to identify bubbles across different stations and to track differences in hydrodynamic parameters. Various methods were pondered in order to evaluate bubble velocity and the method was chosen in order to ensure mass conservation, critical matter to numerical simulations.

4 Results and Discussions

This chapter presents the results retrieved when applying the methodologies described in Chapter 3 for the data set analyzed. Results will be presented for each hydrodynamic parameter separately and divided in two categories: Eulerian Reference Frame (ERF) – histograms, average, standard deviation and correlations – and Lagrangian Reference Frame (LaRF) – analyzing individual slug units and their behavior across the pipeline, as well as after a coalescence takes place. The discussion will regard both approaches, as they are not exclusive, but complementary.

As there are many data points processed and results, sample points are chosen in order to represent different flow scenarios: P2 for low aeration, P8 for moderate aeration and P16 for high aeration, shown in Fig. 12.

Figure 12 – (a) Low, (b) moderate and (c) high aeration points.

Source: Adapted from Rodrigues et al. (2020).

Histograms and cumulative distributions will be presented for stations 1, 3 and 5 in order to facilitate visualization. A full report is given in Appendix B. For LaRF analysis, results will be presented between stations 1 and 5 in order to magnify the differences. A full report of LaRF results is given in Appendix C. Correlations for average values and standard deviation for various hydrodynamic parameters are condensed and reported in Table 7, found at the end of this chapter.

4.1 Cumulative analysis

Before presenting average results, it is important to check whether the analyzed data set is enough to describe the flow; in other words, data must be statistically independent to effectively represent the studied phenomena. Therefore, cumulative average values and standard deviations are investigated, as statistical independence is attained when the average value converges. Cumulative analysis should be carried for every experimental point. P16 results are chosen to represent the analysis, as it has a high number of samples – and, therefore, further investigation on whether average and standard deviation converged may be conducted.

Figures 13-18 present results for the cumulative average and standard deviation analysis for bubble translational velocity, slug and bubble length, bubble void fraction, frequency and intermittence factor.

Figure 13 – Bubble velocity cumulative average and standard deviation.

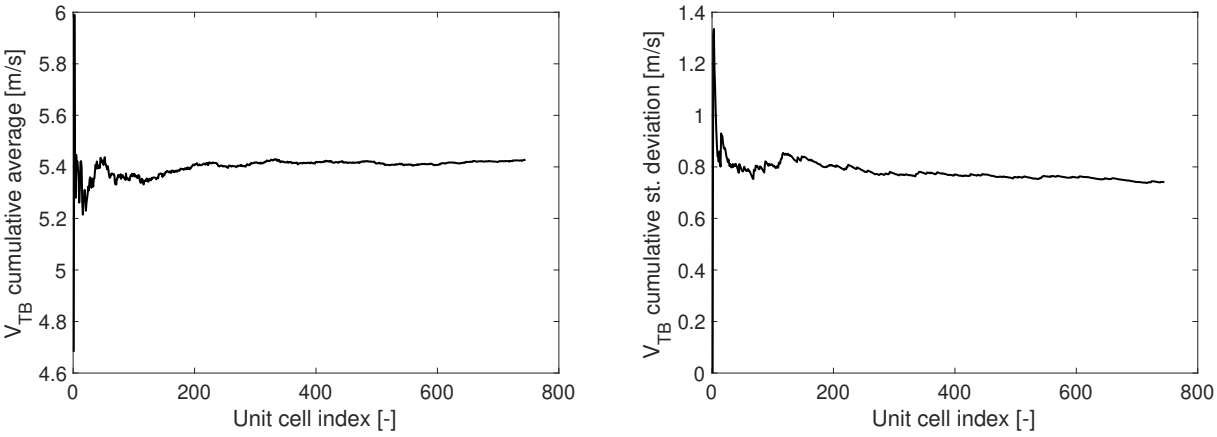

Source: The author.

Figure 14 – Slug length cumulative average and standard deviation.

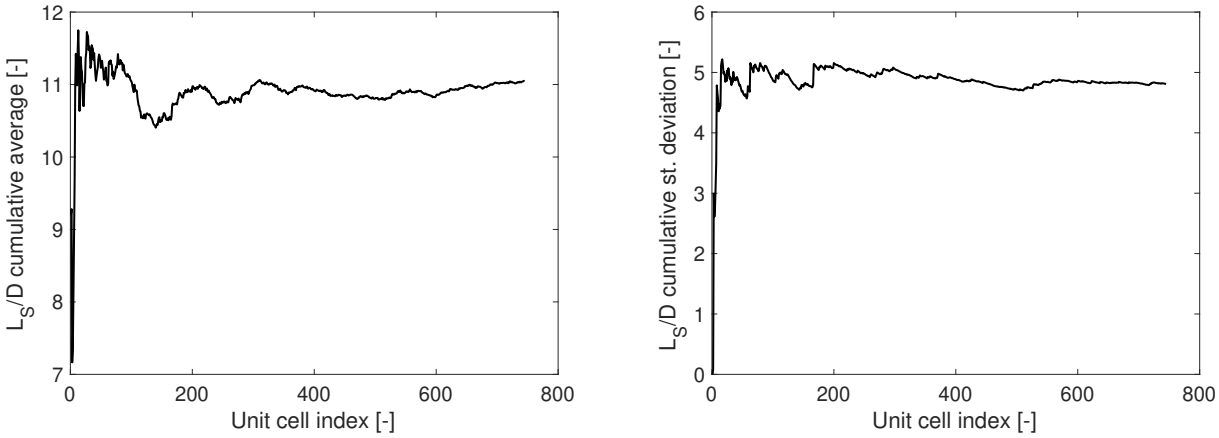

Source: The author.

Figure 15 – Bubble length cumulative average and standard deviation.

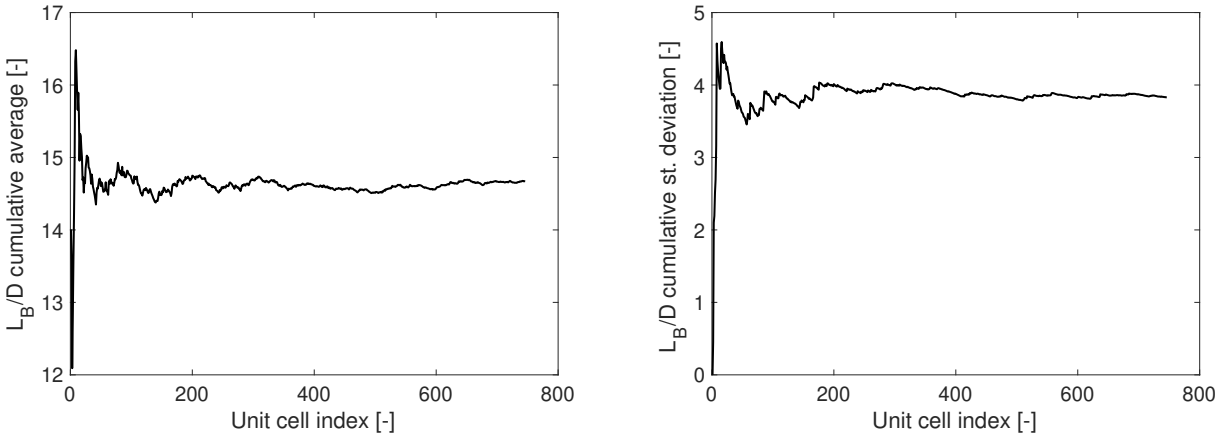

Source: The author.

Figure 16 – Bubble void fraction cumulative average and standard deviation.

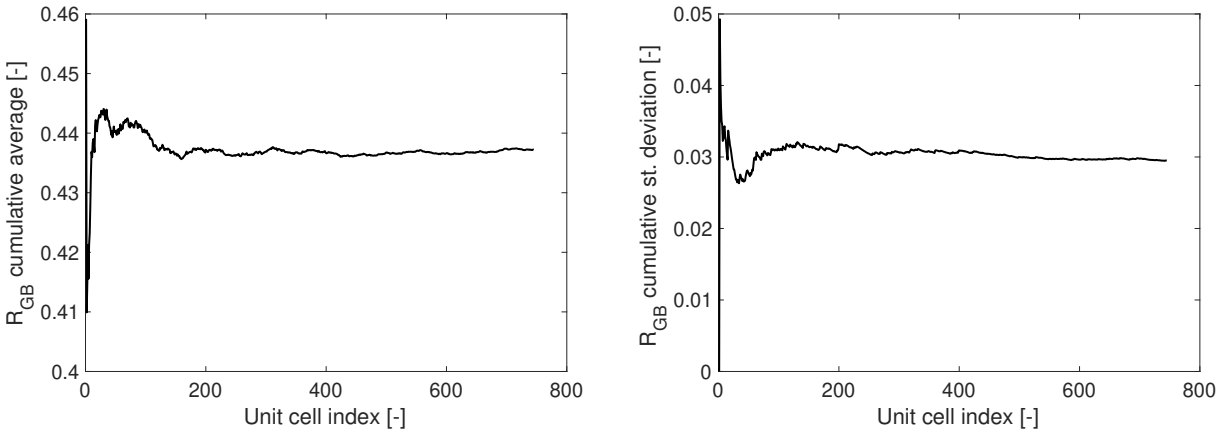

Source: The author.

Figure 17 – Flow frequency cumulative average and standard deviation.

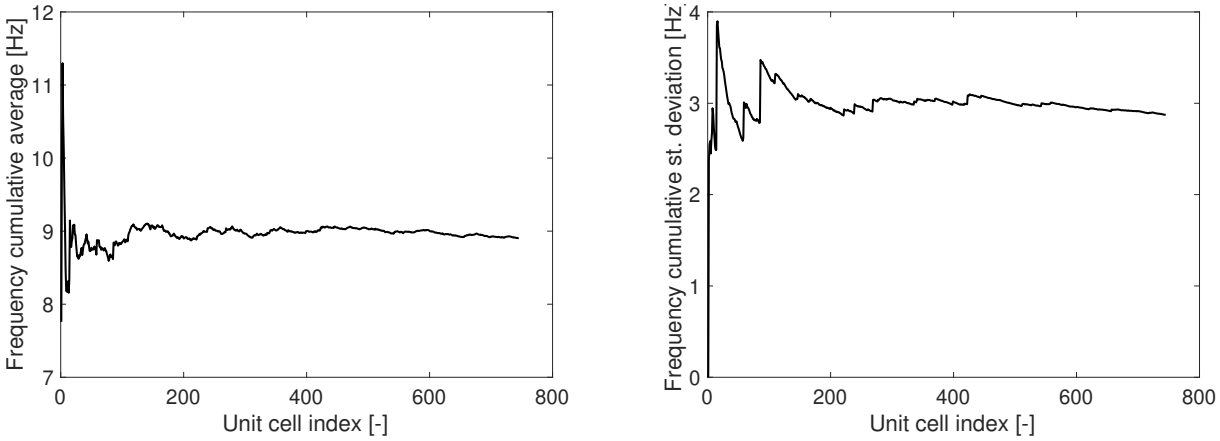

Source: The author.

Figure 18 – Intermittence factor cumulative average and standard deviation.

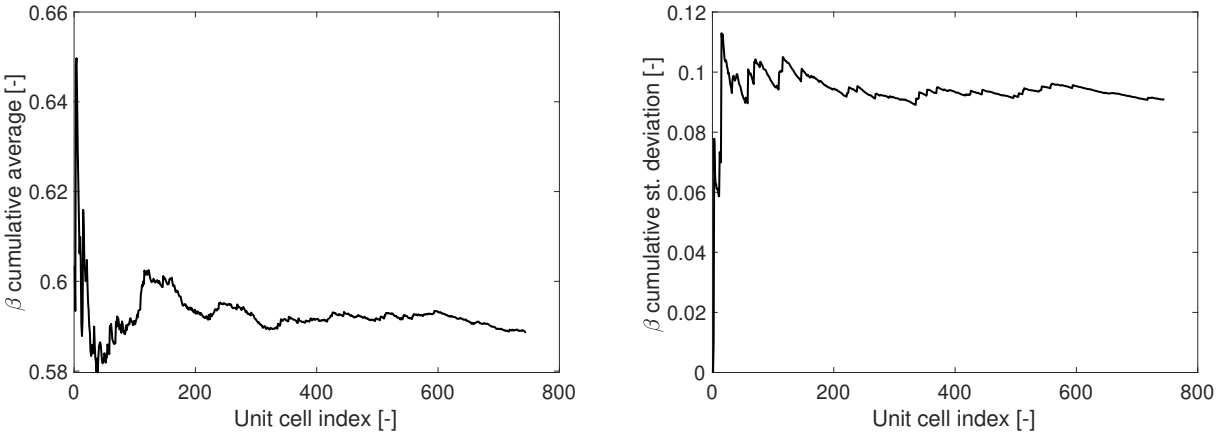

Source: The author.

Noticeable spikes are found when the number of samples is low. With increasing samples, however, it can be seen that average values and standard deviations tend to converge and does not vary significantly, specially after 400 unit-cell samples. Aside from ensuring data validation and statistical independence, this result may be used by researchers going for image processing and analysis, which may reduce the total processing time by picking only enough samples to process and analyze.

4.2 Bubble translational velocity

Translational velocity histograms along with fitted probability density functions (PDF) and cumulative density functions (CDF) are shown in Fig. 19, Fig. 20 and Fig. 21. Even though literature suggests a normal distribution for this hydrodynamic parameter, log-logistic distribution was chosen to represent velocity distribution, as it was found to better suit the analyzed data. While average velocity seems to oscillate back and forth – varying 1.9% between stations 1 and 3 and -3.62% betwen stations 3 and 5 – for low aeration – P2, Fig. 19 –, an increasing trend is found for higher aeration – P8, Fig. 20, presented 5.59 % change betwwen stations 1 and 3 and 3.58 % between stations 3 and 5, and P16, Fig. 21, with 4.35 % change between stations 1 and 3 and 28.8 % between stations 3 and 5.

Figure 19 – Histograms, PDFs, CDFs and log-logistic fits for P2 bubble velocity.

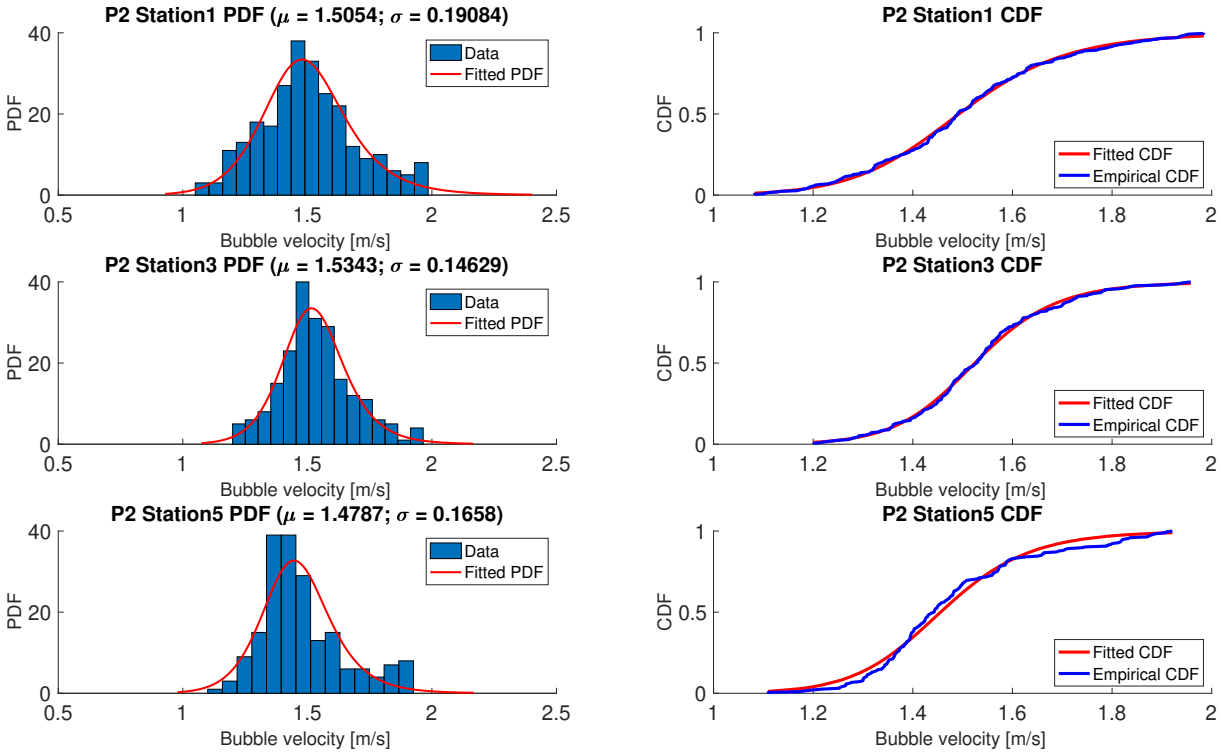

Source: The author.

Figure 20 – Histograms, PDFs, CDFs and log-logistic fits for P8 bubble velocity.

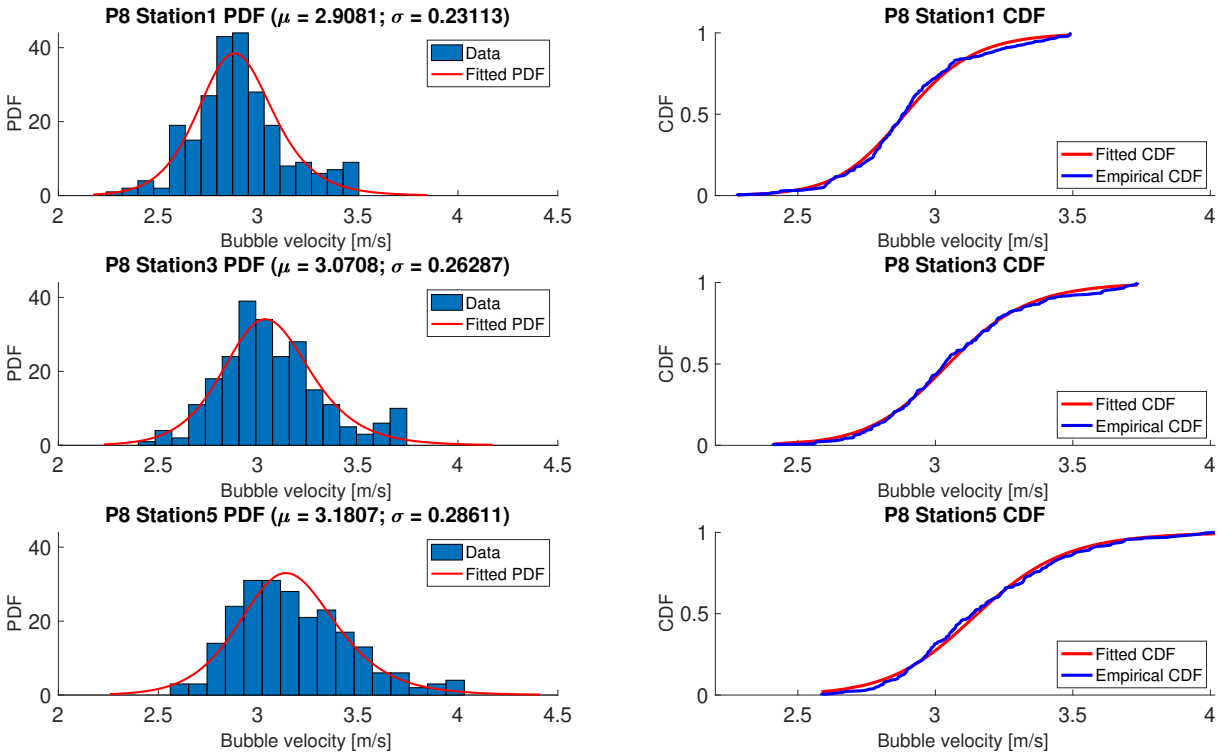

Source: The author.

Figure 21 – Histograms, PDFs, CDFs and log-logistic fits for P16 bubble velocity.

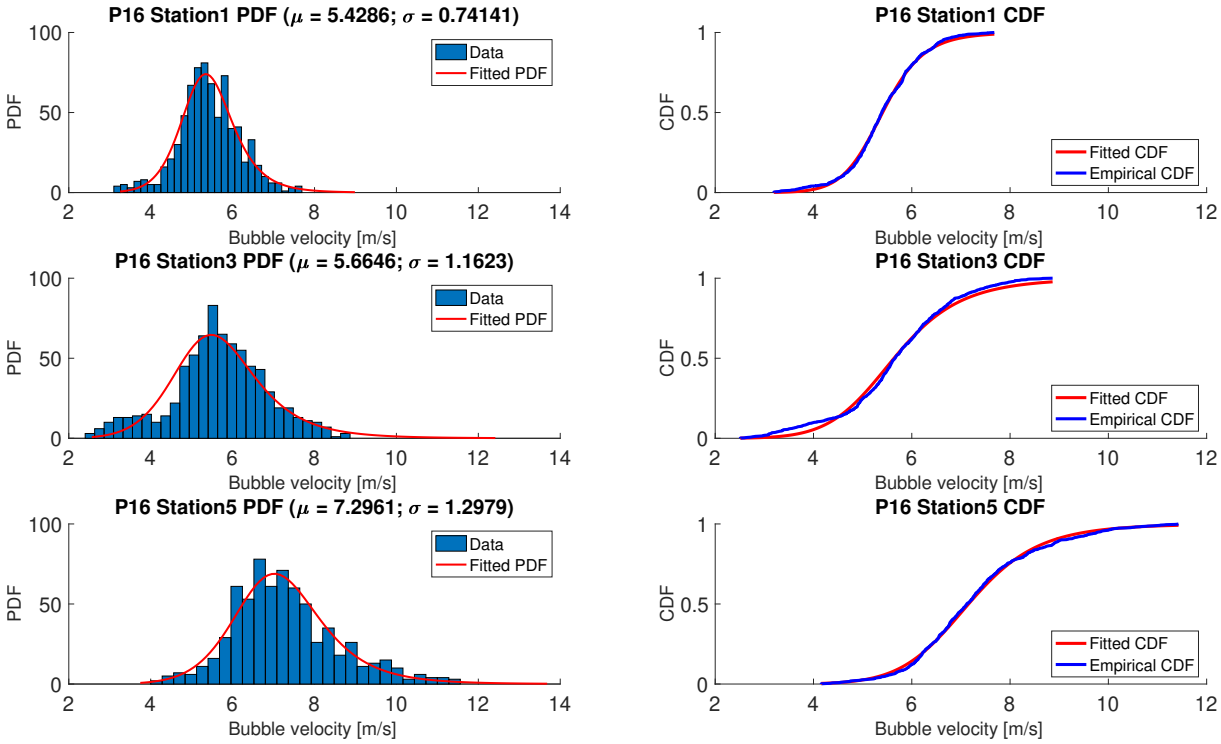

Source: The author.

The mechanism behind bubble velocity fluctuation is proposed as follows. Two major sources of bubble fluctuation are expected: net changes in bubble mass, which would alter bubble inertia and, ultimately, its velocity; and slug void fraction and gas expansion effects. Since low aerated points are expected to have little to no slug void fraction and bubbles are expected to have lower void fraction, net changes in bubble mass seem to be the driver mechanism for velocity fluctuation. Bubbles in plug flow – characterized by low aeration in liquid slugs – are usually followed by a relatively long tail, since the flow turbulence is not strong enough to tear it. Often, though, the tail becomes unstable and sheds, diminishing bubble mass and inertia, promoting a bubble acceleration. Wake effect also seems to play an important role in pressure drop – and its severity scales with flow turbulence.

When mixture velocity is increased, aeration becomes more noticeable in liquid slugs. Since the liquid has dispersed gas bubbles in it, the liquid velocity profile is disturbed, as reported by Nydal et al. (1992a), culminating in higher bubble velocities. Gas expansion is also remarkable for mid-high aeration points (P8 and P16), since there is more gas to expand. Its effects, hence, are potentialized and much more pronounced than bubble mass change – since bubble tails cease to exist because the turbulence will not allow them to grow stable.

Velocity changes reported for the low aeration case are, indeed, supported by LaRF data analysis. Results are presented in Fig. 22, suggesting that roughly half of the bubbles experiment a velocity decrease.

Figure 22 – Bubble velocity percent difference, histogram and normal fit for P2 between stations 1 and 5.

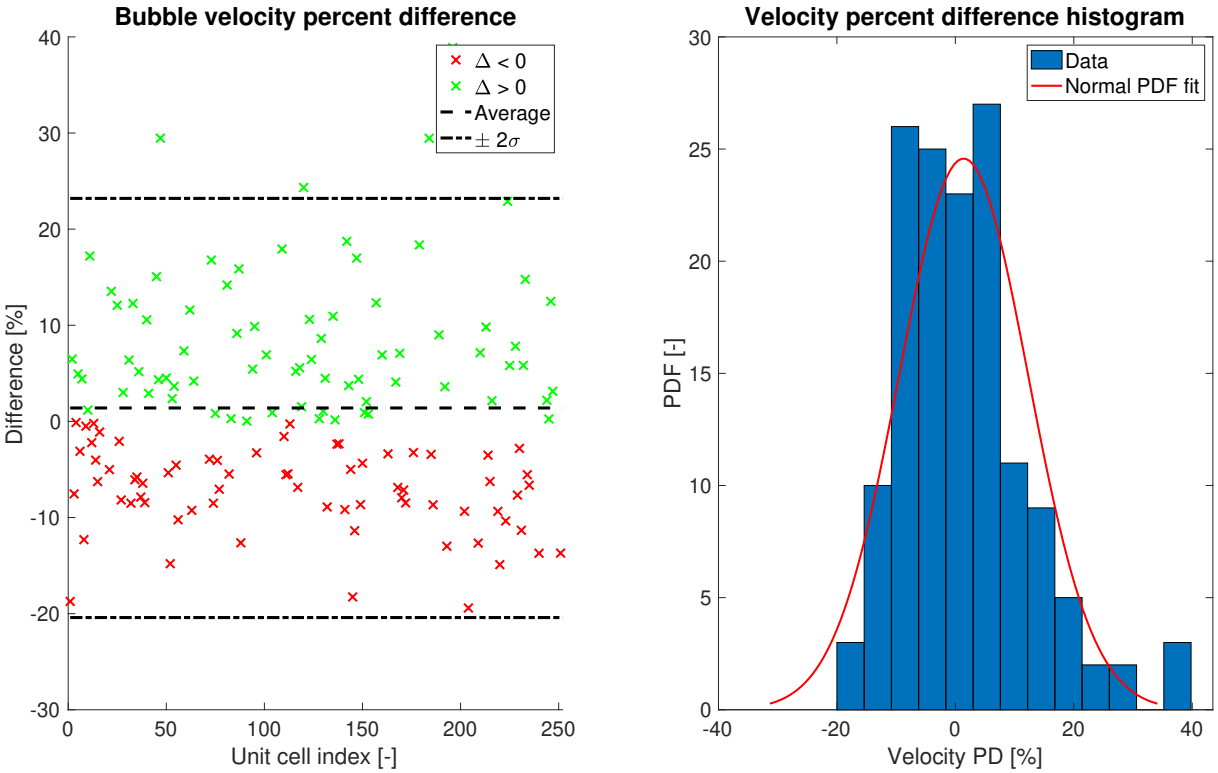

Source: The author.

Figure 23, however, exhibits a slightly different trend: even though some of the bubbles still experiment a velocity decrease, most bubbles accelerate. Velocity changes, though, are the minimum when compared to the other experimental conditions, supporting the proposed mechanism for bubble velocity fluctuation.

Figure 23 – Bubble velocity percent difference, histogram and normal fit for P8 between stations 1 and 5.

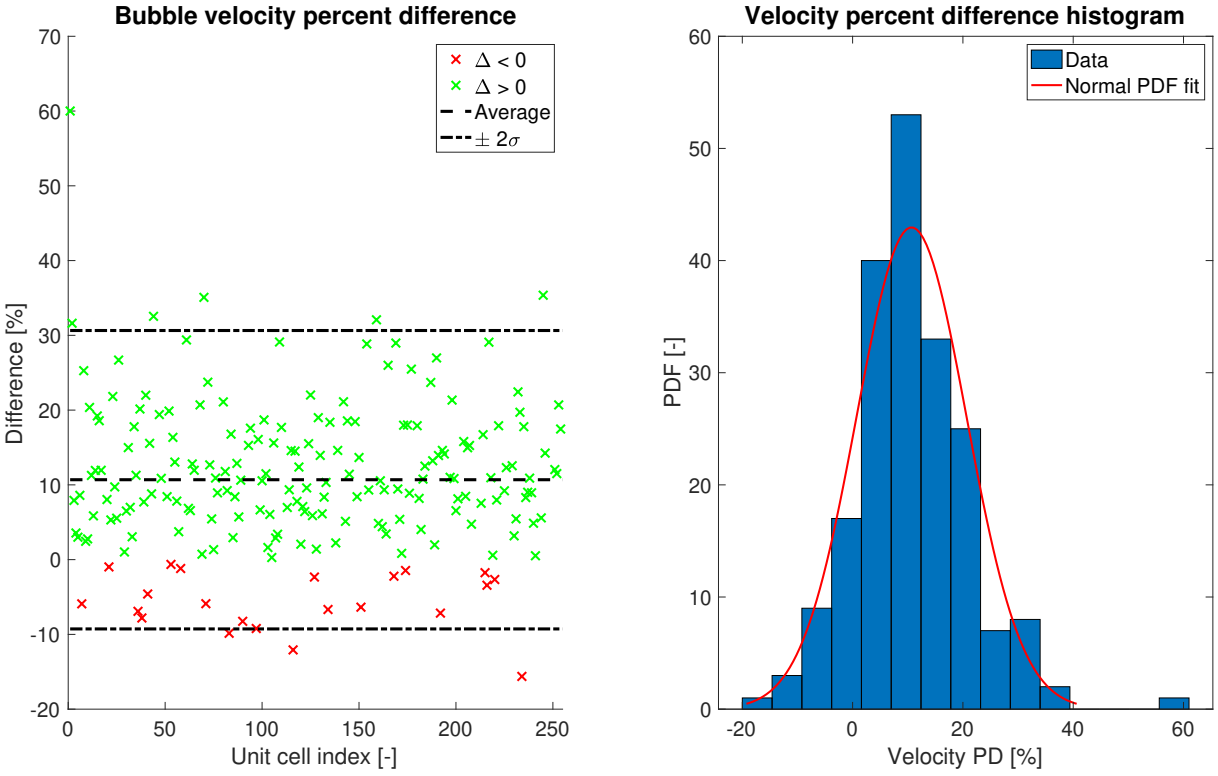

Source: The author.

As aeration increases, the velocity is expected to increase as well. Indeed, Fig. 24 reports a sharp velocity increase for most bubbles, although some still exhibit deceleration. Even though bubble deceleration is not usually expected to happen, it is possible to happen: whenever a bubble is accelerating, it gets closer to its leading bubble and the liquid slug between them is shortened; the liquid, however, does not simply vanish, as mass conservation should be satisfied at all times. Rather, it is accommodated in the trailing liquid slug, which is elongated. The wake effect, responsible for bubble accelerating, is now mitigated due to the longer liquid slug ahead of the bubble, ultimately culminating in bubble deceleration.

Figure 24 – Bubble velocity percent difference, histogram and normal fit for P16 between stations 1 and 5.

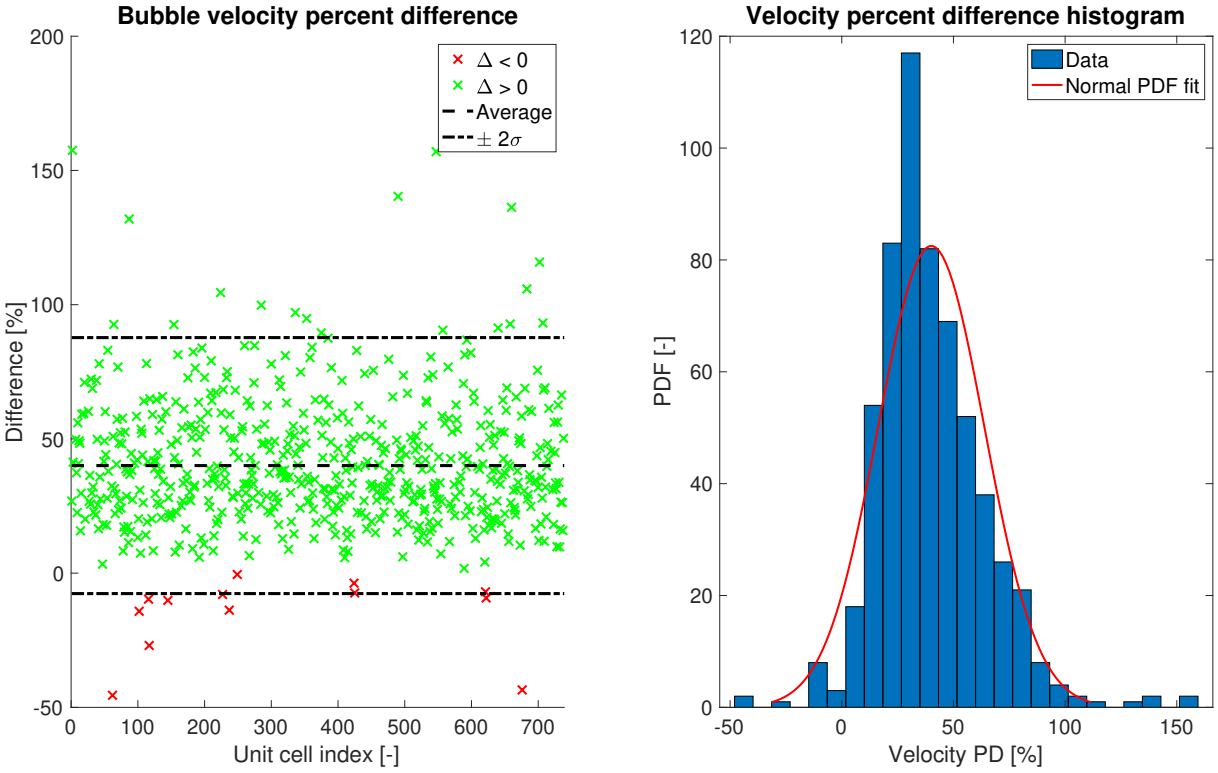

Source: The author.

Measured data and fitted curves for velocity average and standard deviation are shown in Fig. 25. As reported by several authors, such as Nicklin et al. (1961) and Bendiksen (1984), bubble velocity and mixture velocity are correlated by a straight line. It must be stressed that most data fall over the bubble centering interval – $Fr_L \geq 3.5$ – and, therefore, drift velocity should be roughly equal to zero. Albeit the linear model considered a linear coefficient term (C_∞), it was found that it is indeed not significantly different than zero (considering a 95% confidence level), in agreement with literature.

The angular coefficient (C_0) – which takes in account the contribution of the mixture velocity –, on the other hand, has a relatively wide range of values reported. Although the findings of the present work report a slightly higher value than the wide accepted correlation proposed by Bendiksen (1984), it still falls between extrema published in literature. As reported by Nydal et al. (1992b), spread can occur due to liquid velocity profile disturbance caused by dispersed gas bubbles, as well as by the wake region. Furthermore, the two-wire sensor – which gives a rough approximation to the liquid void fraction – may be responsible for minor divergence, as well as signal noise, since velocity calculation heavily depends on the quality of the measures.

For higher mixture velocities, the flow turbulence does not allow bubbles to carry

long tails across the pipeline; they are quickly broken into smaller bubbles and often trapped in bubble wake. The higher the aeration, the higher the liquid velocity profile disturbance, as reported by Andreussi et al. (1990 apud Nydal et al., 1992), and, therefore, velocities tend to fluctuate just as much as in the plug flow case. The minimum velocity variation – therefore, the minimum standard deviation – takes place when turbulence is not high enough to produce highly aerated slugs, but still considerable in order to break bubble tails. The proposed correlations are retrieved from the best fit over measured experimental data and are shown in Eq. 4.1 and 4.2.

$$V_{TB} = 1.492J - 0.066\sqrt{gD}. \tag{4.1}$$

$$\sigma_V = -0.0048J^3 + 0.1074J^2 - 0.5479J + 1.235. \tag{4.2}$$

Figure 25 – Velocity Froude number average and standard deviation data and fitted curves.

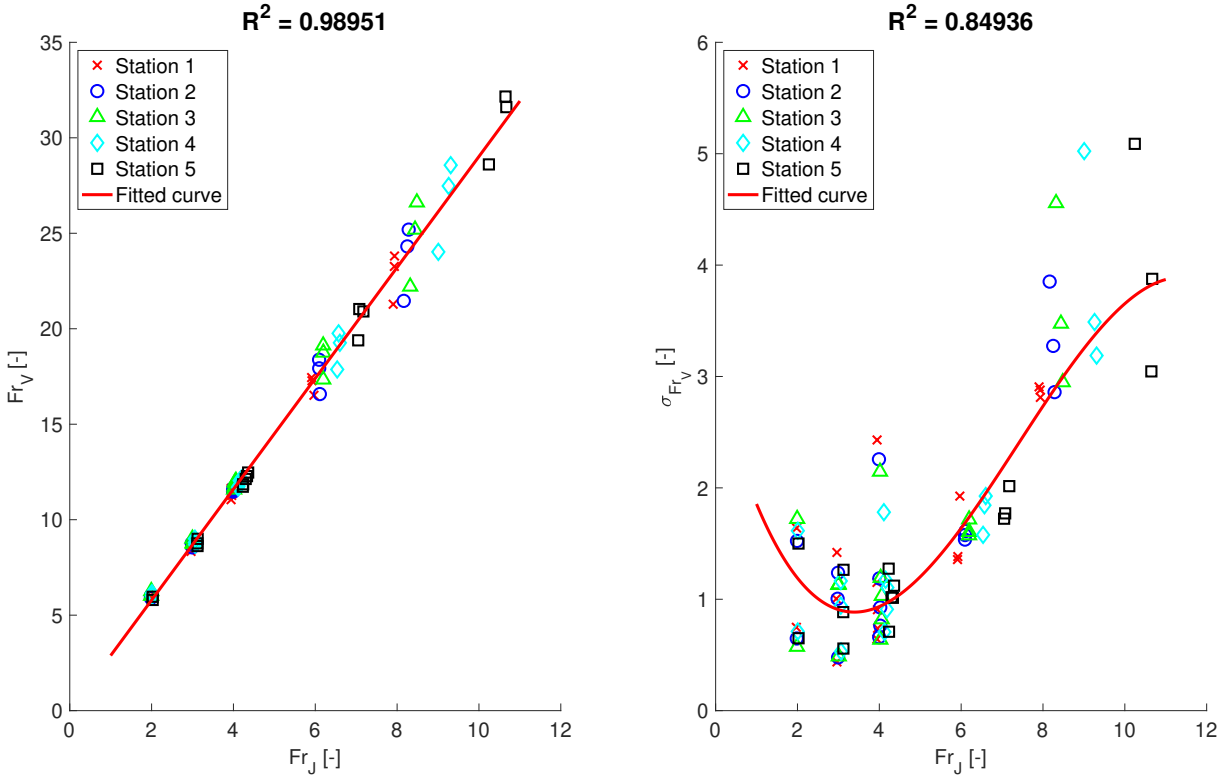

Source: The author.

Comparison between measured velocity data and selected correlations are found in Fig. 26.

Retrieved data is compared with literature correlations and shown in Fig 27. Since the presented correlation is based on measured experimental data, it is expected to better

Figure 26 – Velocity measured data vs. selected correlations.

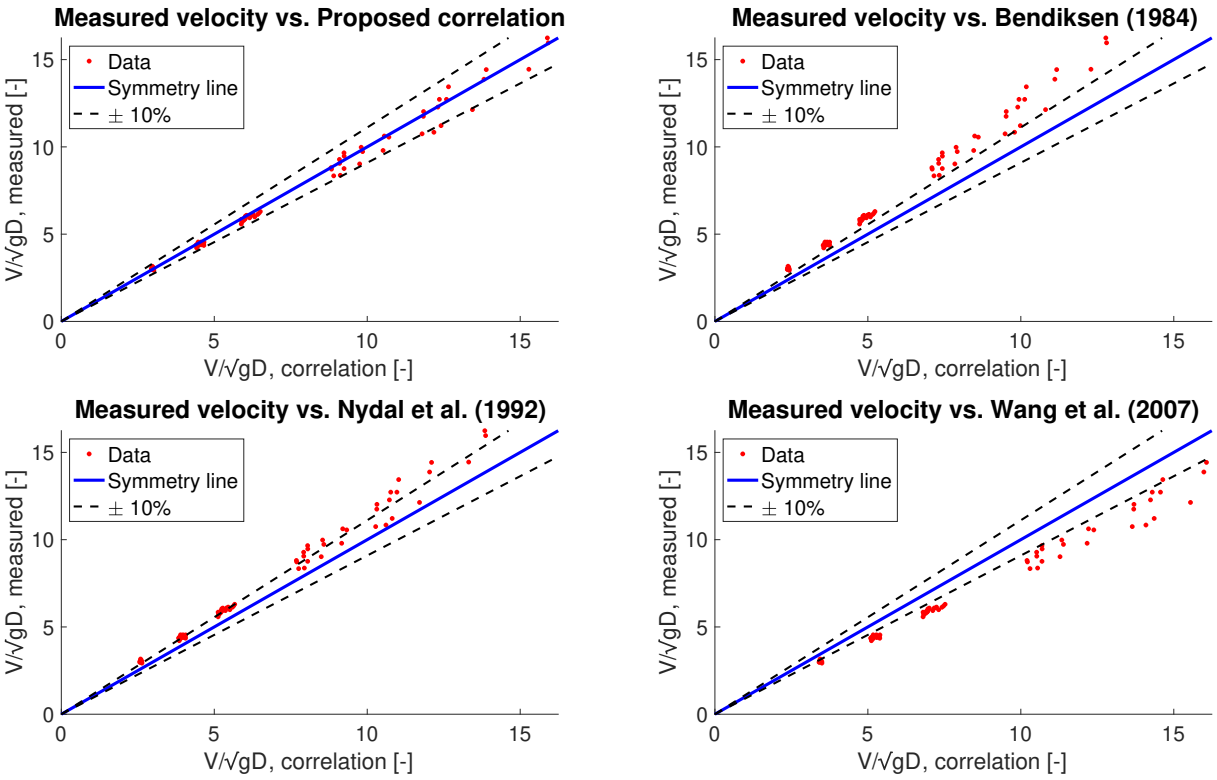

Source: The author.

represent data as well. The widely applied Bendiksen (1984) correlation seems to under predict the observed values for bubble velocity, while Wang et al. (2007) tends to over predict them. Fairly good agreement was found with the correlation proposed by Nydal et al. (1992a), with most of the data falling under the 10% difference interval.

Since most works disregard velocity standard deviation correlations, the present study will be comparing its data and correlation to the findings given by Vicencio (2013), which suggested a second-degree polynomial. Although it would suit the data, a third-degree polynomial showed better agreement to the analyzed data and was, therefore, chosen to represent the retrieved information. The correlation presented by Vicencio (2013), on the other hand, does not present good agreement with observed data, as most points fall off the 25% difference interval.

Velocity standard deviation seems to attain a minimum value when in the transition from a well-behaved (i.e., low aeration) to a moderate aeration experimental point. Very low aeration favors plug flow, which has characteristic phenomena that cannot be seen in aerated slug flow: bubbles are followed by a relatively long tail. This tail often detaches from the body, totally or partially, diminishing the air mass and liquid drag, ultimately culminating to the acceleration of the current bubble; on the other hand, the trailing bubble that absorbs the tail will have its mass increased and a possibly increased tail,

Figure 27 – Measured velocity standard deviation vs. selected correlations.

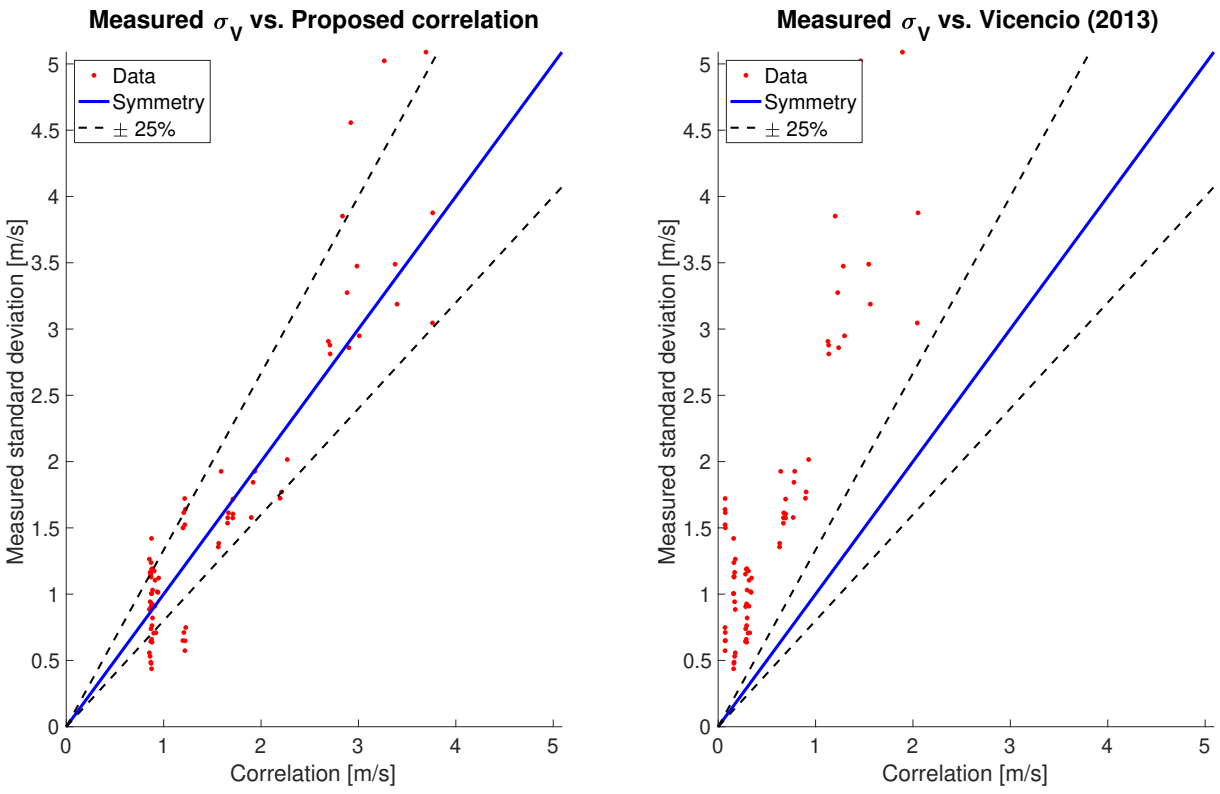

Source: The author.

favoring a velocity decrease.

4.3 Slug length

Results for slug length histograms and empirical CDF, as well as PDF and CDF log-logistic fit, are displayed in Fig. 28, Fig. 29 and Fig. 30, for P2, P8 and P16, respectively. Literature usually reports log-normal probability density function to represent slug lengths. On the other hand, the present work used the log-logistic distribution, as it has a higher peak and heavier tail – capable of representing longer slugs and better suiting the found peaks.

Figure 28 – Histograms, PDFs, CDFs and log-logistic fits for P2 slug length.

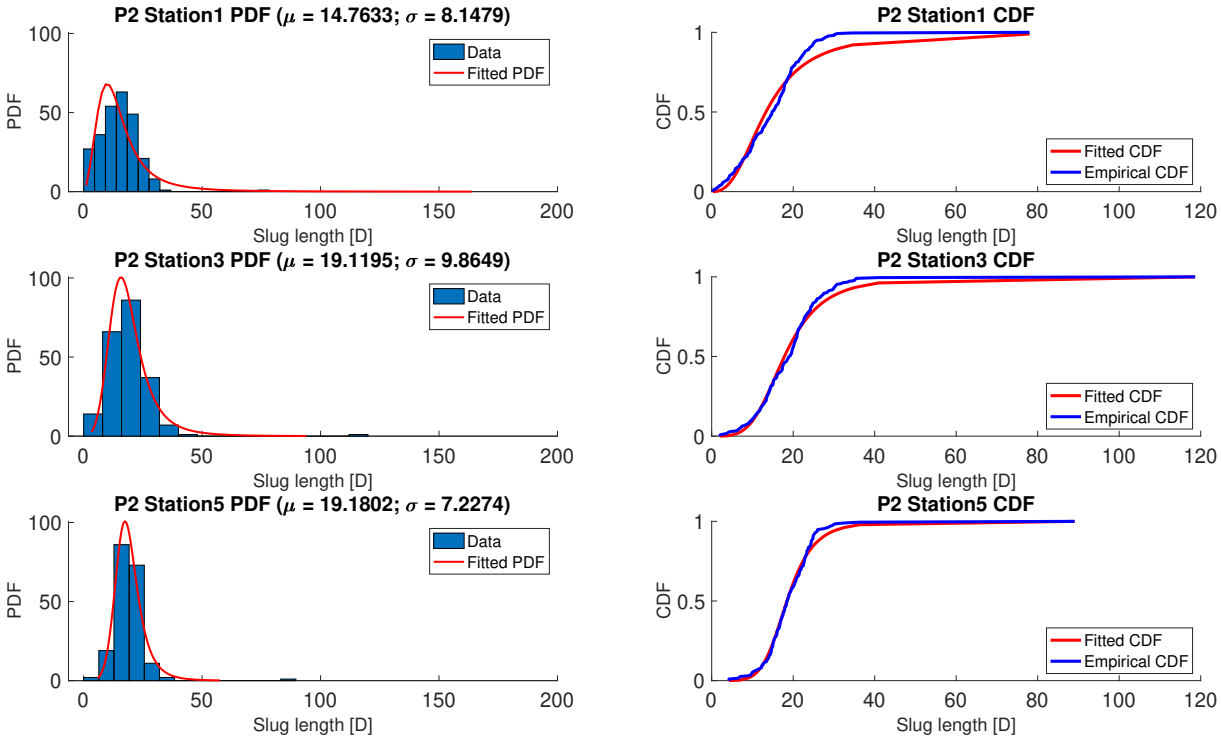

Source: The author.

Figure 29 – Histograms, PDFs, CDFs and log-logistic fits for P8 slug length.

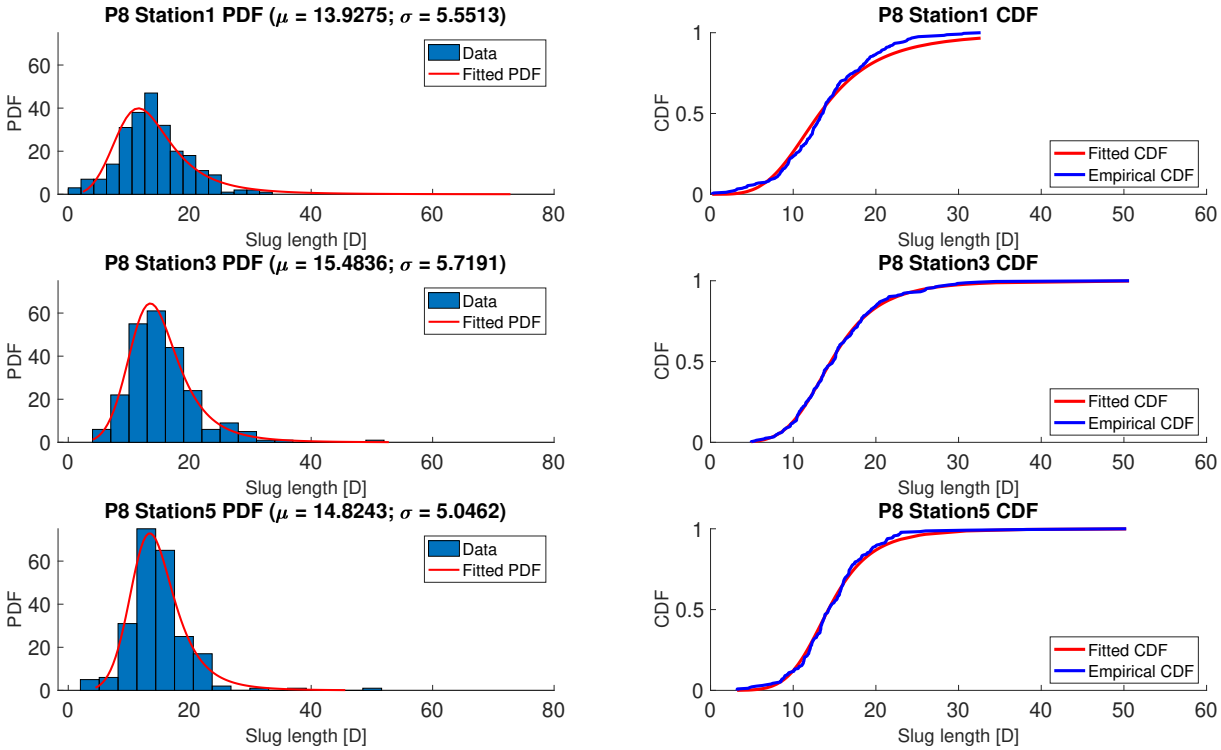

Source: The author.

Figure 30 – Histograms, PDFs, CDFs and log-logistic fits for P16 slug length.

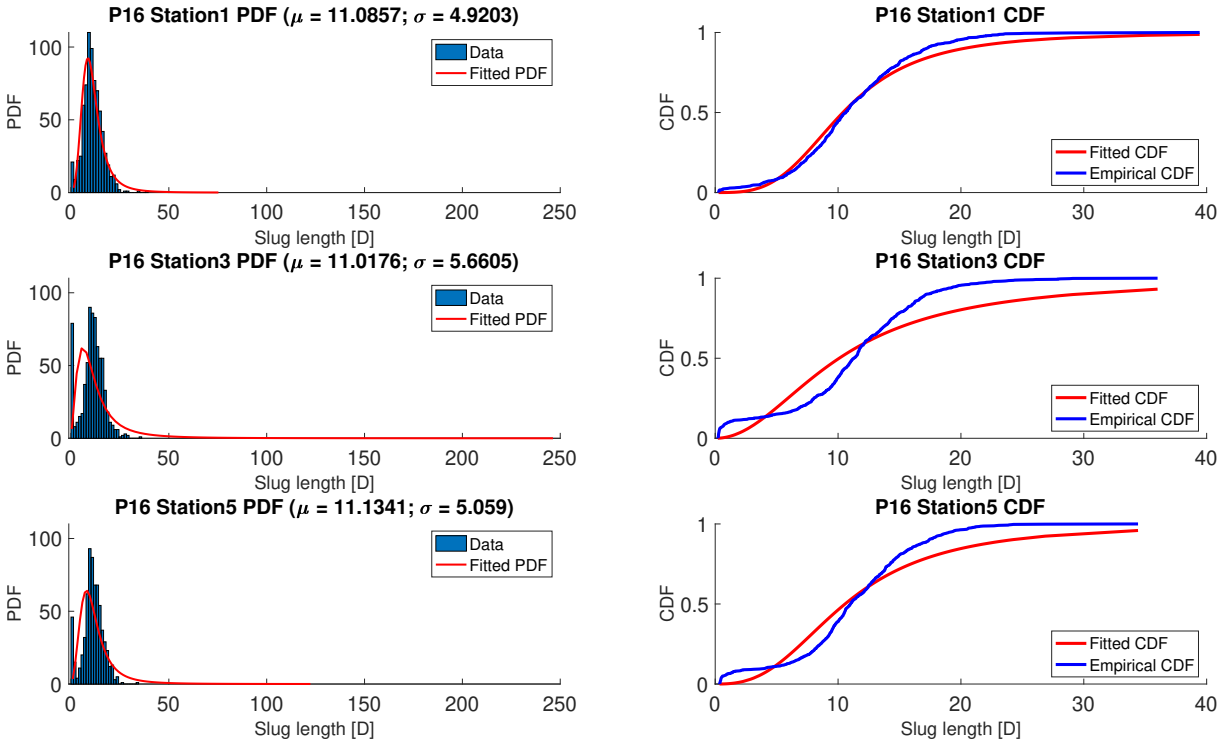

Source: The author.

Similar trend is reported for every analyzed point: even though there is a minor change in the average slug length – From 14.76D to 19.12D between stations 1 and 3 and 19.18 in station 5 –, its value stays approximately constant across the stations, suggesting that, at first glance, little change happened and the flow is developed. The standard deviation, however, seems to have a more pronounced change. Discrepancies, however, might be associated with bubble coalescence, which eliminates a small slug and add it to the trailing liquid slug, which becomes larger.

In order to better understand the behavior of liquid slugs, LaRF analysis is used. Results are found in Fig. 31, Fig. 32 and Fig. 33.

Figure 31 – Slug length percent difference, histogram and normal fit for P2 between stations 1 and 5.

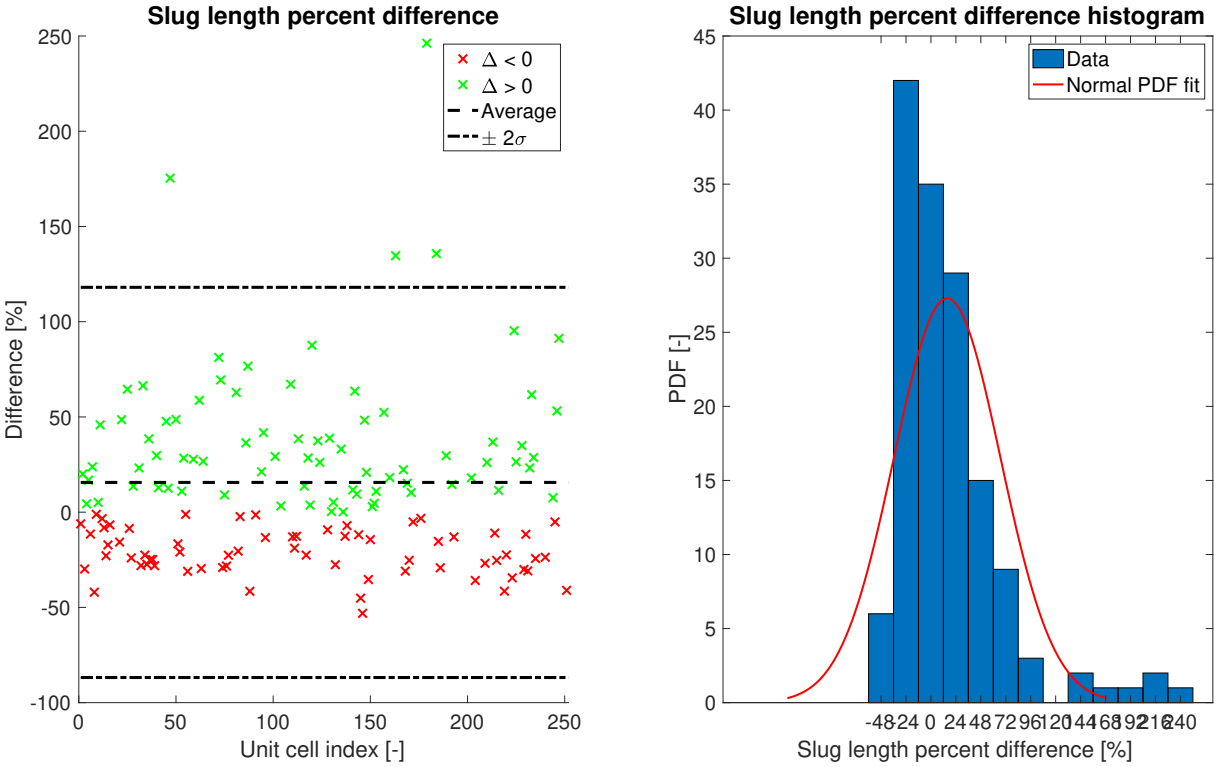

Source: The author.

Figure 32 – Slug length percent difference, histogram and normal fit for P8 between stations 1 and 5.

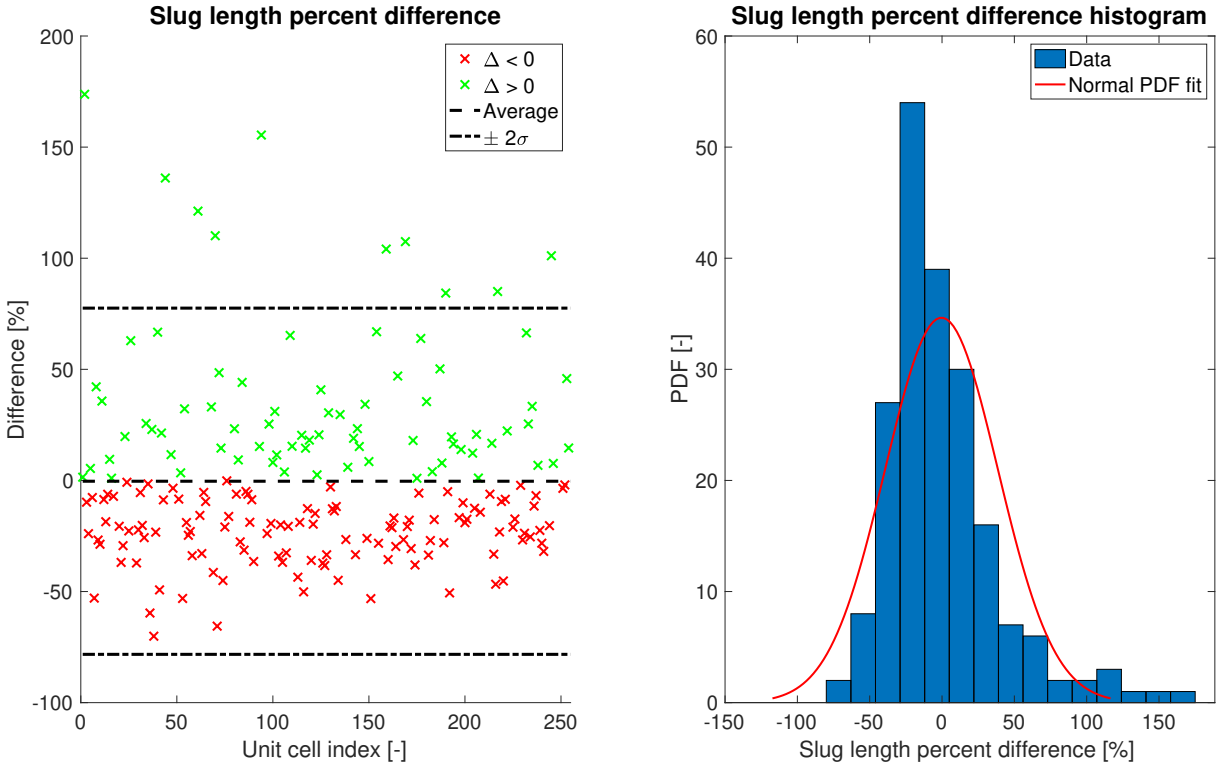

Source: The author.

Figure 33 – Slug length percent difference, histogram and normal fit for P16 between stations 1 and 5.

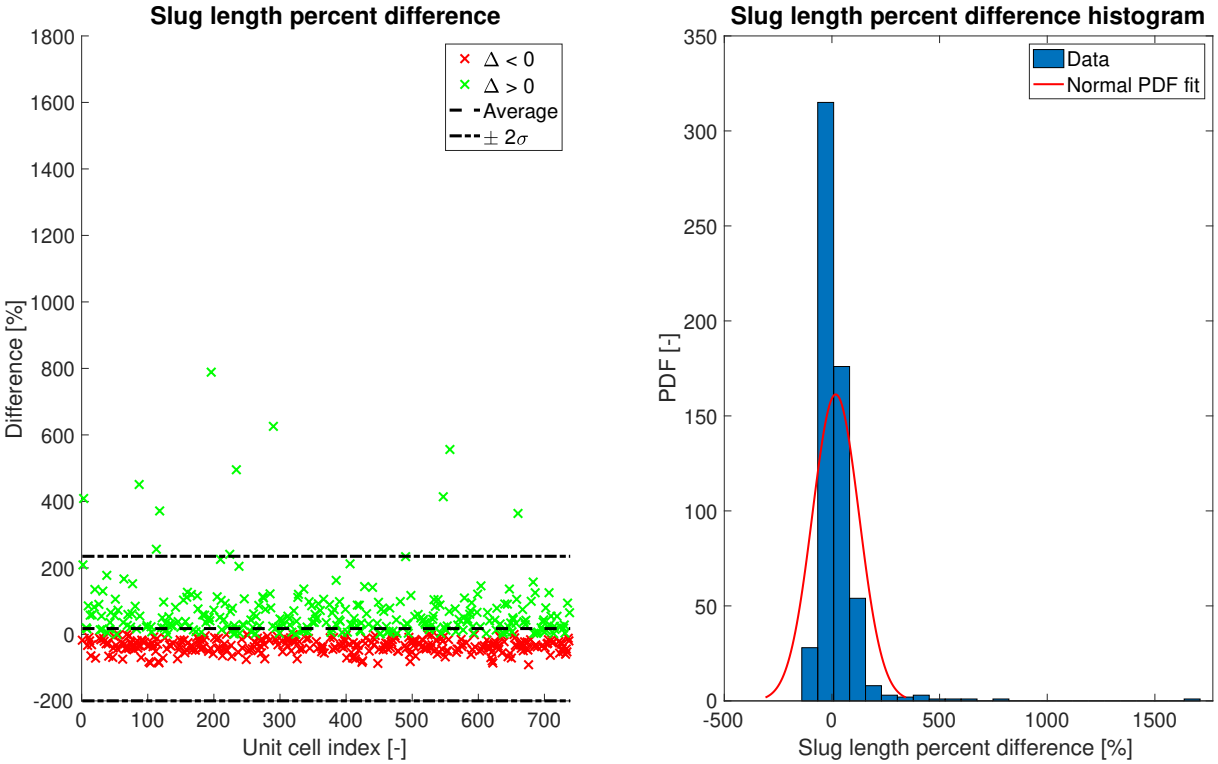

Source: The author.

Although ERF results report little change in slug length average, LaRF results – presented in Figs. 31-33 – demonstrate the ongoing changes: roughly half of the slugs have their length decreased whilst the other half experiments opposite behavior, as shown in Figs. 31-33. Mass balance is used in order to explain this phenomenon: since bubble velocities are not equal, as bubbles get closer to each other, liquid slugs tend to decrease; the liquid, though, does not disappear instantly, but is rather placed in the trailing liquid slug – hence, when a liquid slug length decreases, another liquid slug should increase by the same amount. Gas expansion, responsible for bubble expansion, can also play a minor role in the process.

Peak differences – remarkably present in higher aeration points –, although might be seen as outliers, may also be associated with coalescences. As bubble coalescence takes place, the trailing slug length is expected to substantially increase its length.

4.4 Bubble length

Histograms, empirical CDFs, fitted log-logistic PDFs and CDFs for the selected points and stations are shown in Fig. 34, Fig. 35 and Fig. 36, respectively. In order

to represent the PDFs and CDFs for bubble length, unlike most studies in literature, log-logistic is used once more – not only because it is a more versatile distribution, but also for the reasons mentioned before: a higher peak and longer tails, which makes it capable of better representing retrieved data.

Figure 34 – Histograms, PDFs, CDFs and log-logistic fits for P2 bubble length.

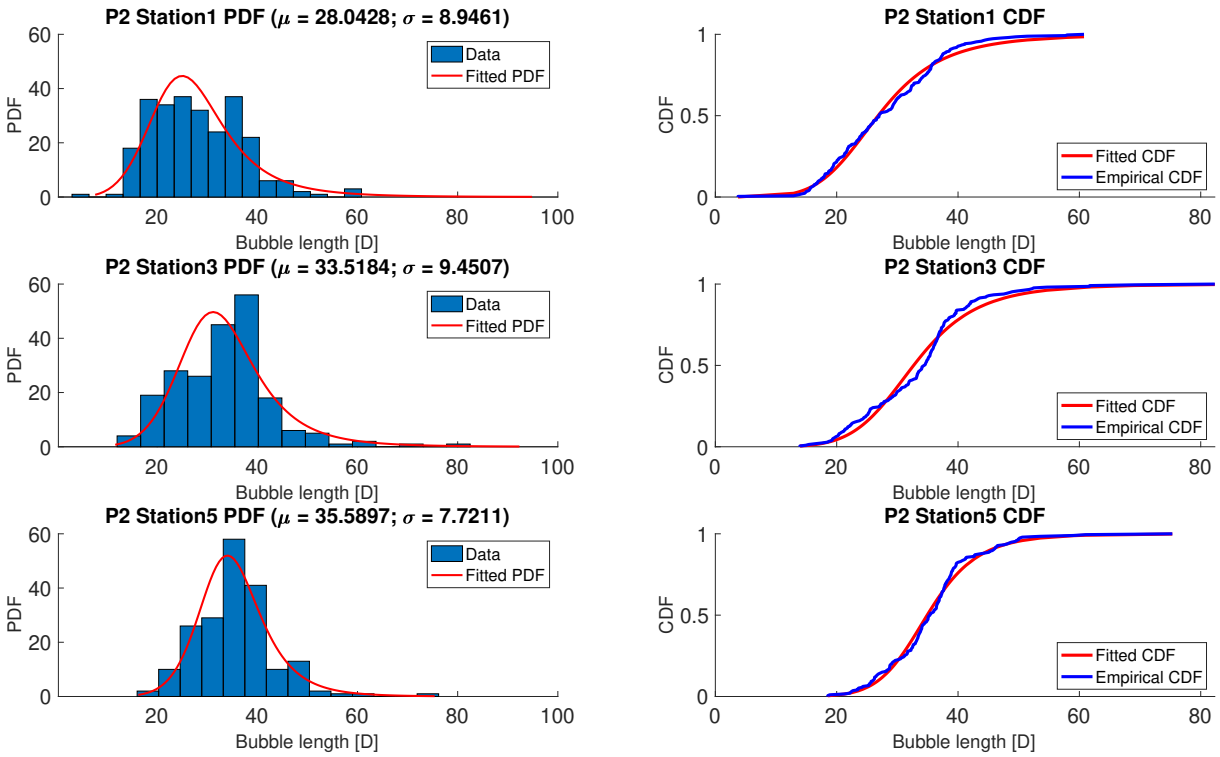

Source: The author.

Figure 35 – Histograms, PDFs, CDFs and log-logistic fits for P8 bubble length.

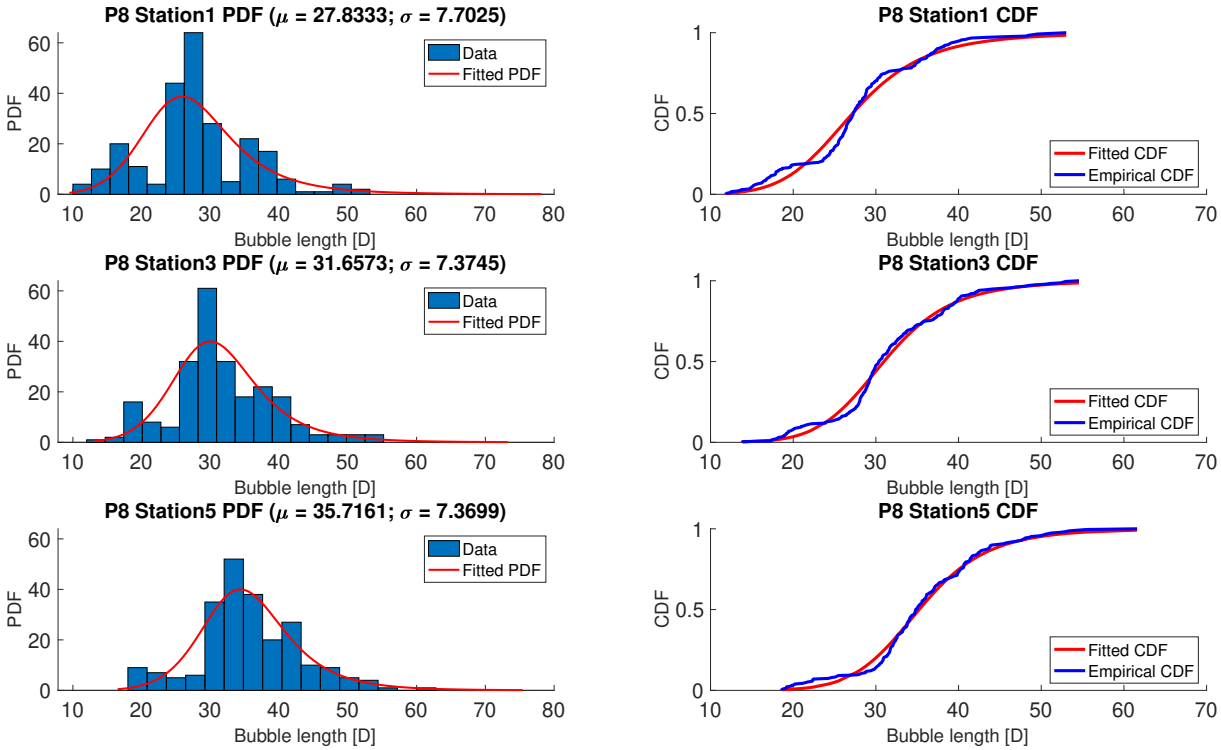

Source: The author.

Figure 36 – Histograms, PDFs, CDFs and log-logistic fits for P16 bubble length.

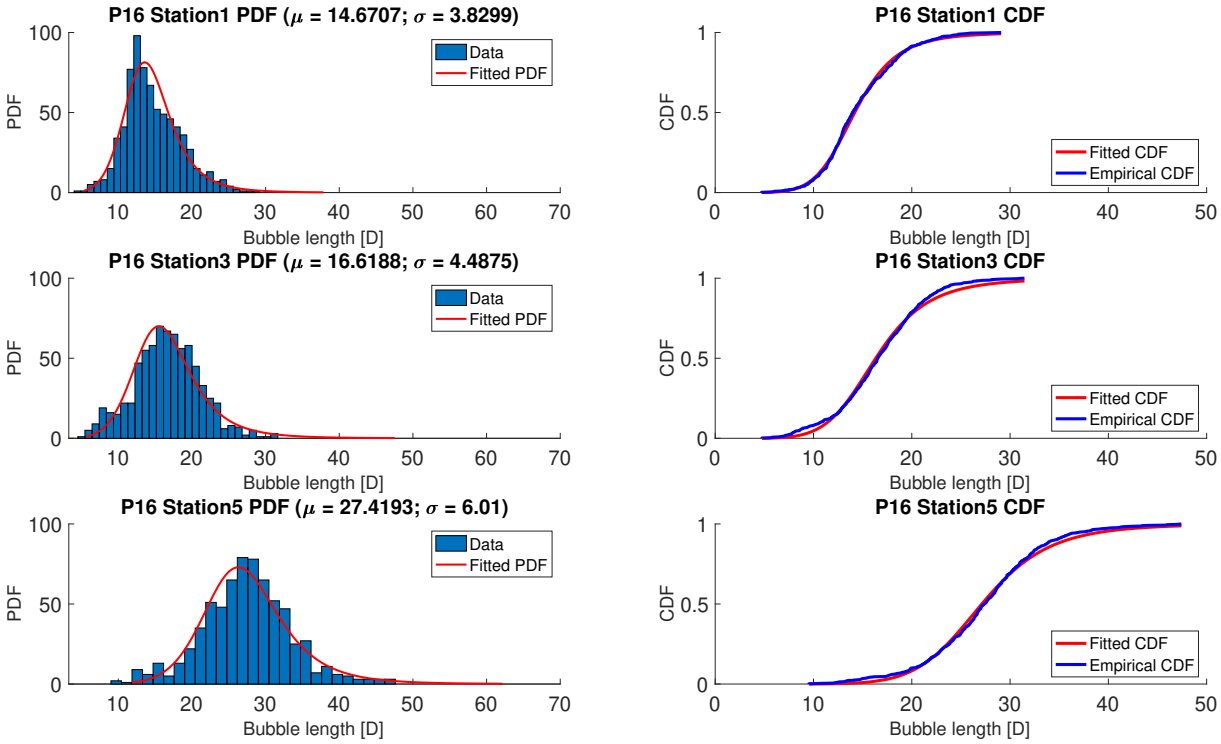

Source: The author.

Just as reported for slug lengths, a unique trend is found regardless of the experimental conditions: bubble average length tend to increase across the pipeline – 28.04D, 33.52D and 38.59D for stations 1, 3 and 5 in P2, Fig. 34; 27.83D, 31.66D and 36.72D in P8, Fig. 35; and 14.67D, 16.62D and 27.42D in P16, 36.

Gas superficial velocity is a driver parameter when it comes to bubble length. Increasing gas superficial velocity would increase the total gas mass in the flow, which would distribute itself either as elongated bubbles or dispersed bubbles in liquid slugs. Therefore, increased gas superficial velocity is expected to increase average bubble length. The pressure drop across the stations, at first glance, seems to be the major contributor to the increasing bubble length, since it promotes gas expansion – therefore, increasing gas superficial velocity.

LaRF results – shown in Fig. 37, Fig. 38 and Fig. 39 – provide complementary analyses, as follows.

Figure 37 – Bubble length percent difference, histogram and normal fit for P2 between stations 1 and 5.

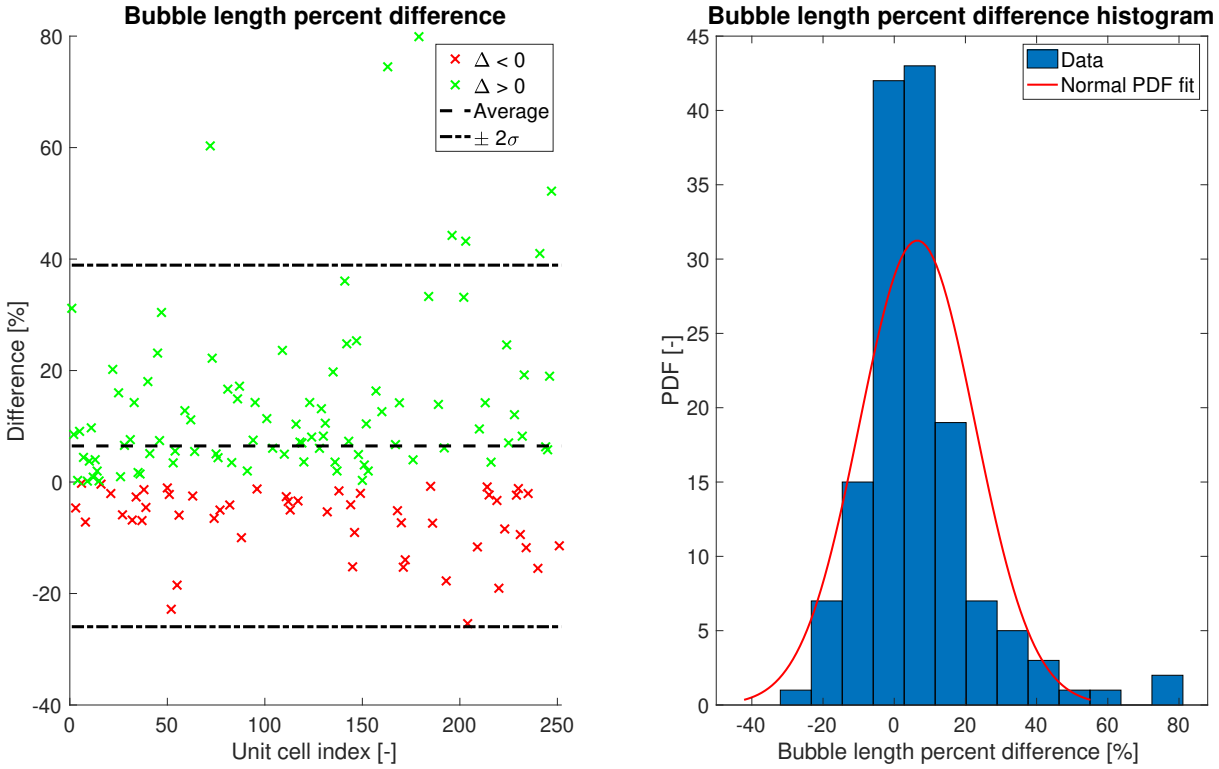

Source: The author.

Figure 38 – Bubble length percent difference, histogram and normal fit for P8 between stations 1 and 5.

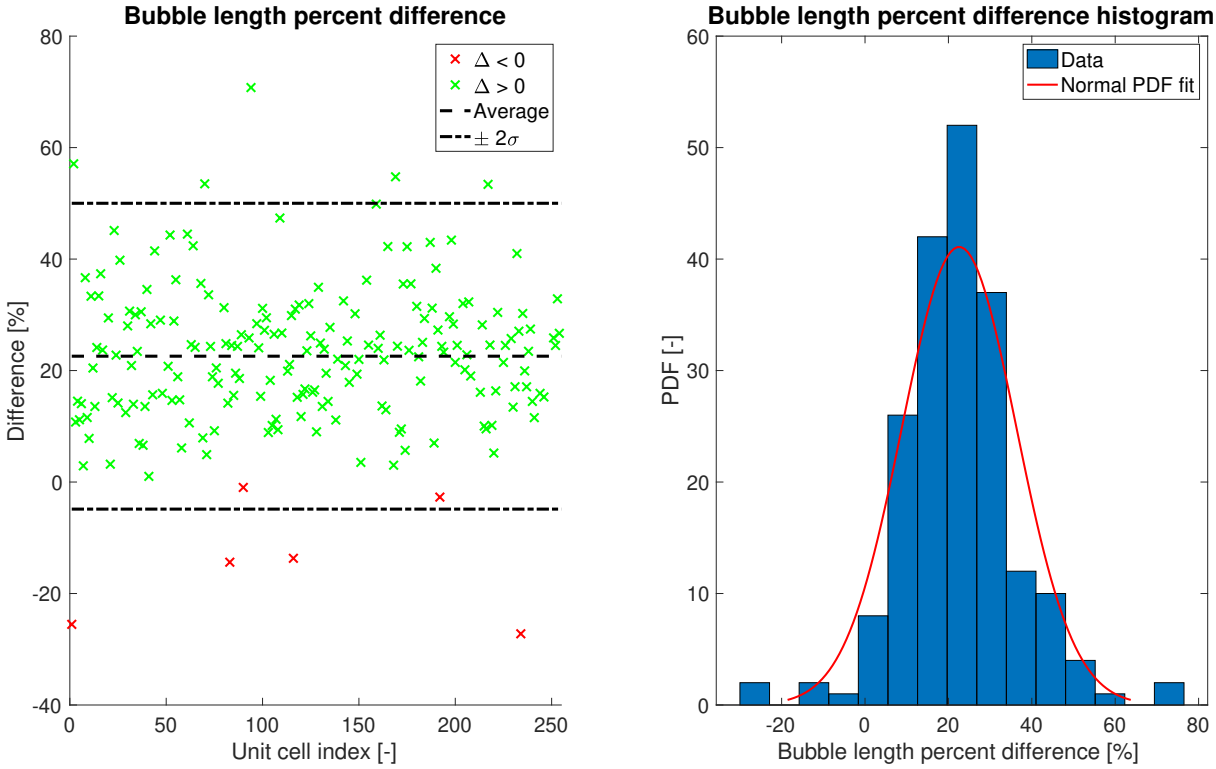

Source: The author.

Figure 39 – Bubble length percent difference, histogram and normal fit for P16 between stations 1 and 5.

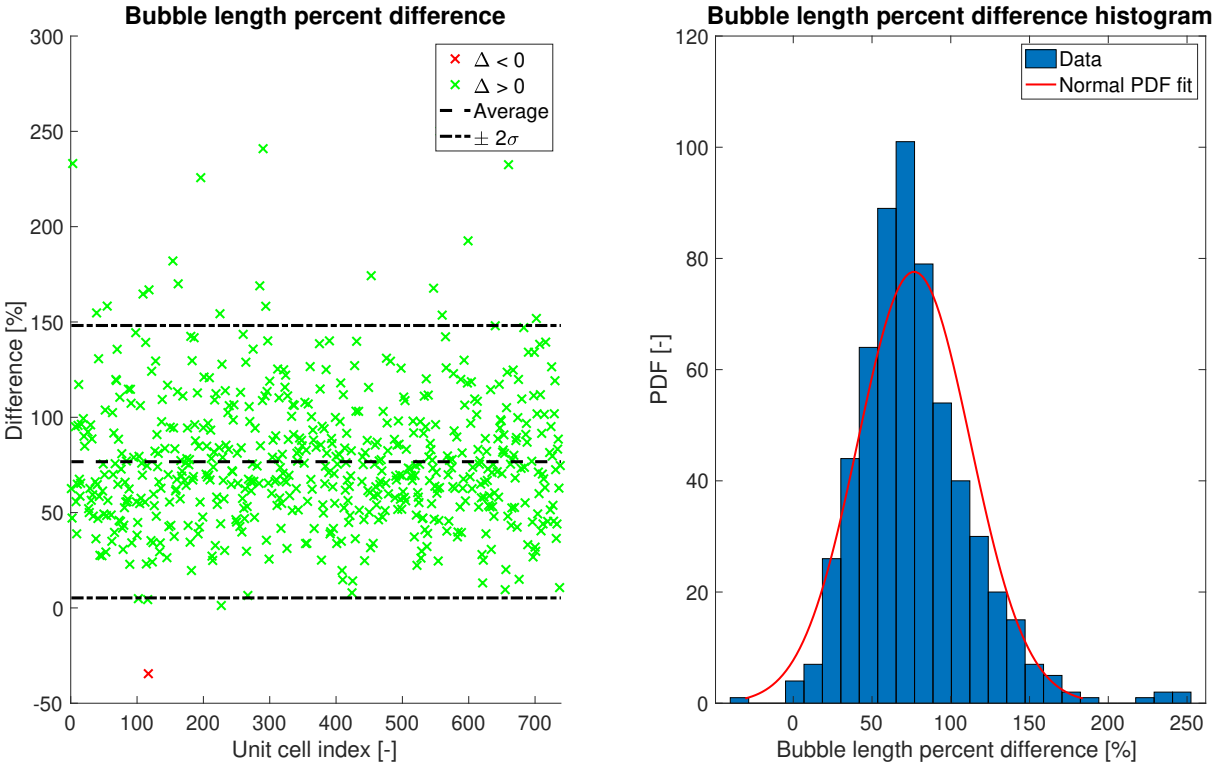

Source: The author.

While roughly half of the bubbles in P2 experiment decreasing length – shown in Fig. 37 –, Fig. 38 and Fig. 39 – P8 and P16, respectively – depict the predominance of increasing bubble lengths. The mechanism behind this phenomenon is proposed as follows.

Although still present, gas expansion does not seem to play a major role in low aerated points. Instead, what is observed is that bubble lengths are controlled by the flow dynamics, i.e., bubble tail shedding and coalescence, whereas, with higher gas superficial velocities, bubble lengths are mainly driven by gas expansion, since there is more gas to expand and it should be accommodated either as increased slug void fraction or bubble volume – which can be increased due to higher bubble void fraction, higher bubble length or both.

The correlations between bubble length and gas superficial velocity are reported by Vicencio (2013) as an exponential increase. Indeed, the same curve is observed using the current analyzed data, as shown in Fig. 40. Not only the average length shows agreement to the exponential curve, but the standard deviation as well. Correlations for average

bubble length and standard deviation are presented in Eqs. 4.3 and 4.4.

$$\frac{L_B}{D} = 2.175 exp\left(5.251\frac{J_G}{J}\right). \tag{4.3}$$

$$\sigma_{L_B} = 131.6\left(\frac{J_G}{G}\right)^{5.322} + 2.732. \tag{4.4}$$

Figure 40 – Bubble average length and standard deviation vs. J_G/J and curve fits.

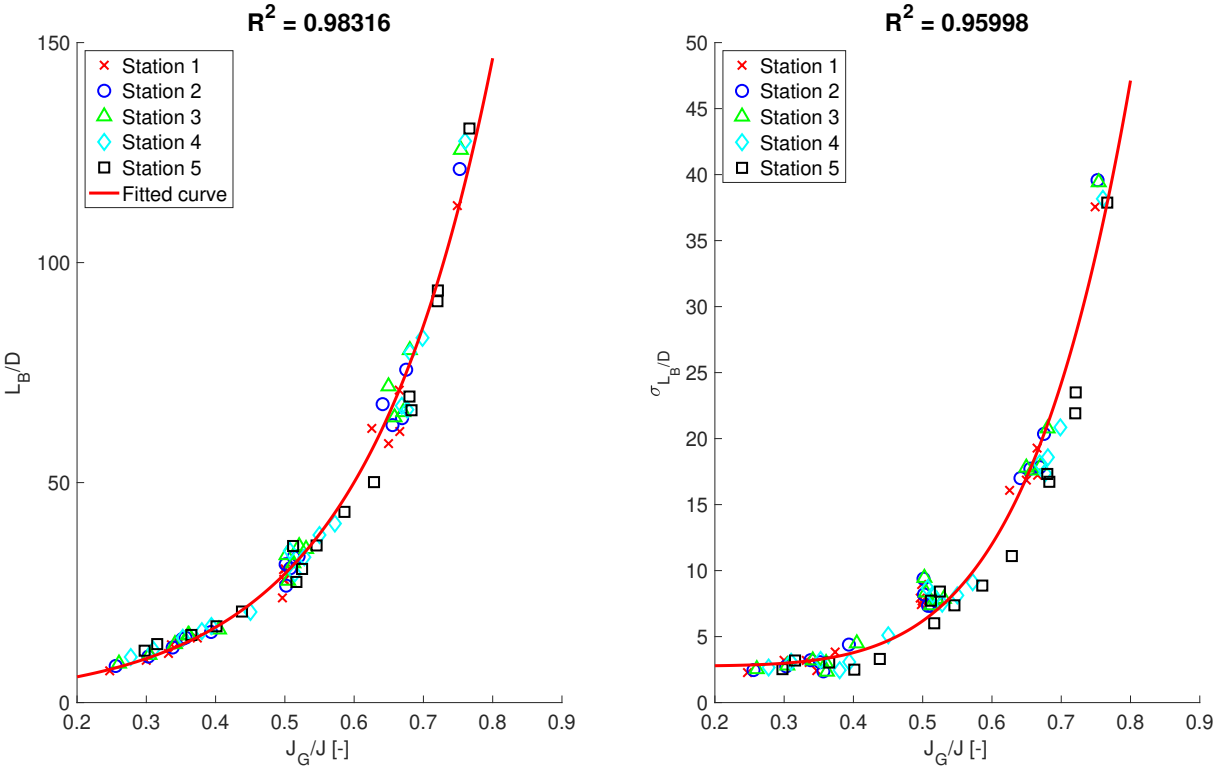

Source: The author.

As a matter of comparison, measured data is confronted to the current proposed correlation as well as to the one proposed by Vicencio (2013), as shown in Fig. 41. Both correlations seem to suit well the experimental data measured, although Vicencio (2013) equation tends to under predict bubble length by a small amount – a reasonable explanation is to consider that velocity measured by Vicencio (2013) was slightly lower when compared to the measurements of the present work. Since bubble length is calculated using bubble velocity, discrepancies regarding the latter would be directly propagated to the former.

Figure 41 – Bubble average length vs. selected correlations.

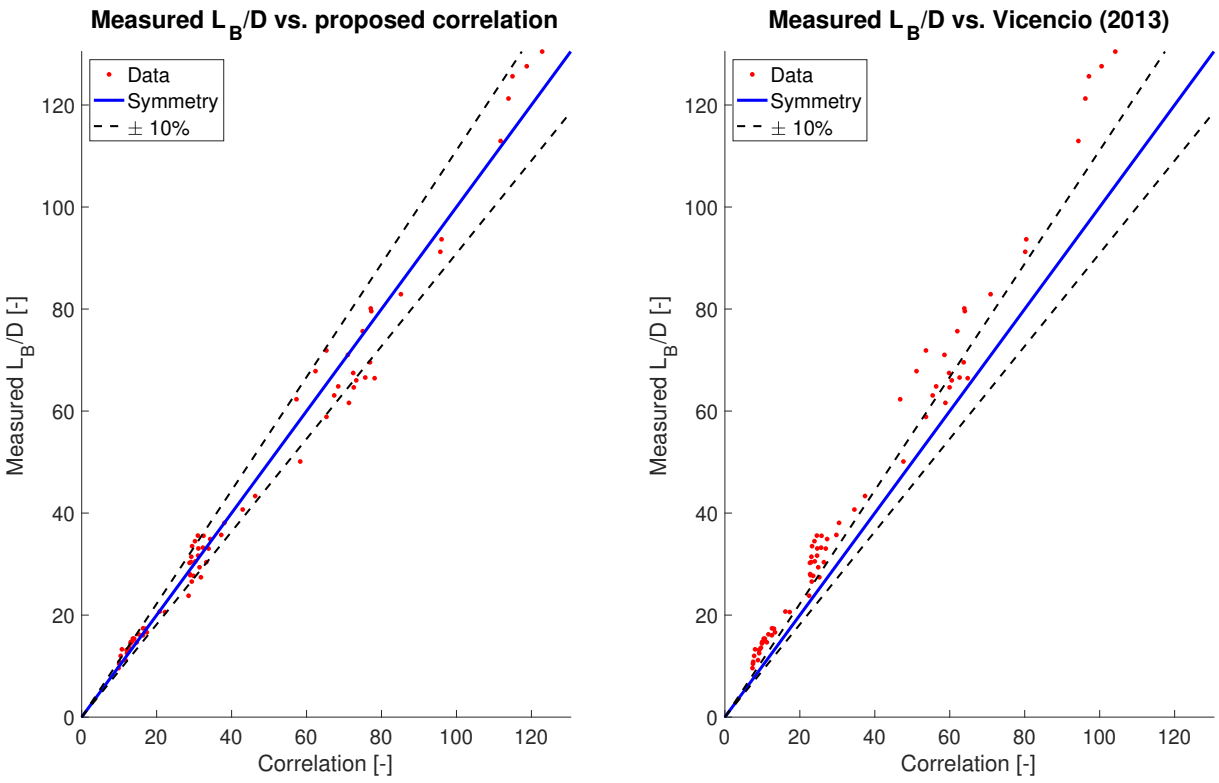

Source: The author.

4.5 Bubble void fraction

Just as bubble length, bubble void fraction is strongly dependent on gas superficial velocity, as the latter controls gas total mass in the flow. Since there is more mass, it should be accommodated either as increased bubble volume, increased bubble count or increased dispersed bubbles in liquid slug in order to attain mass conservation. Regarding bubble volume, two mechanisms may be responsible for its increasing: either bubble length or cross-sectional area – void fraction – should be increased (or both). Therefore, with increasing gas superficial velocity, bubble void fraction is expected to increase as well.

Figure 42 – Histograms, PDFs, CDFs and log-logistic fits for P2 bubble void fraction.

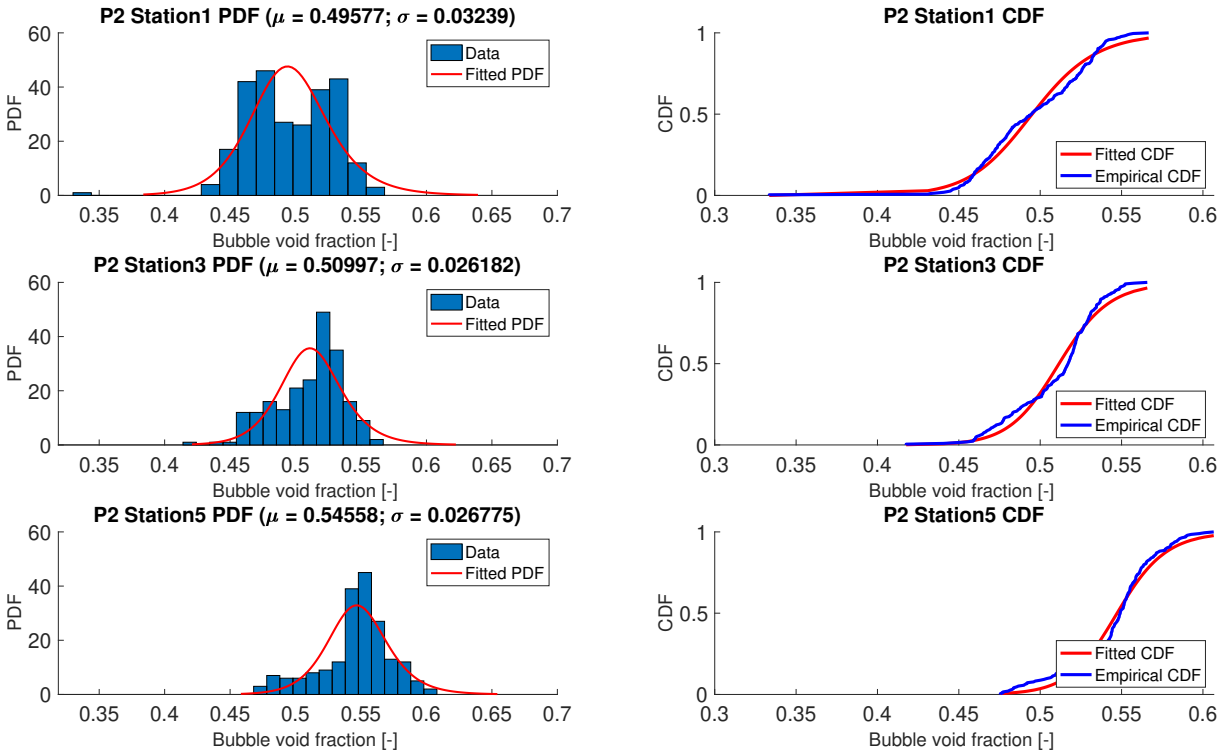

Source: The author.

Figure 43 – Histograms, PDFs, CDFs and log-logistic fits for P8 bubble void fraction.

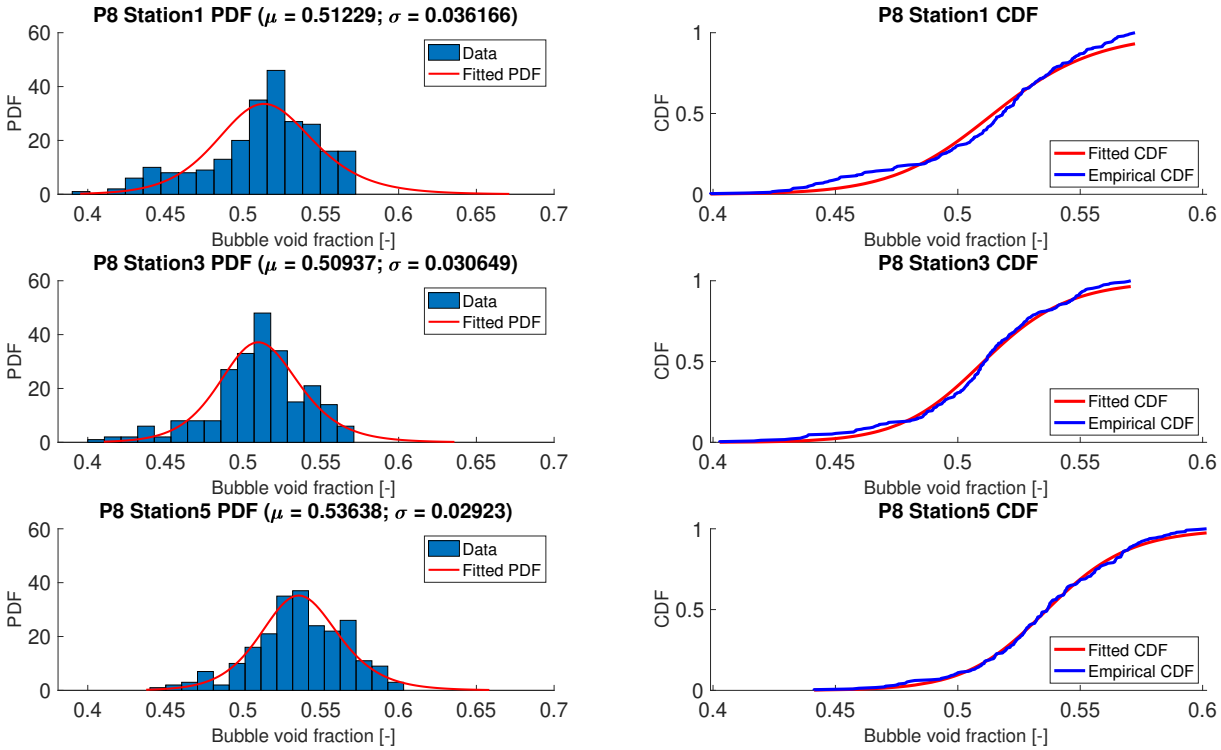

Source: The author.

Figure 44 – Histograms, PDFs, CDFs and log-logistic fits for P16 bubble void fraction.

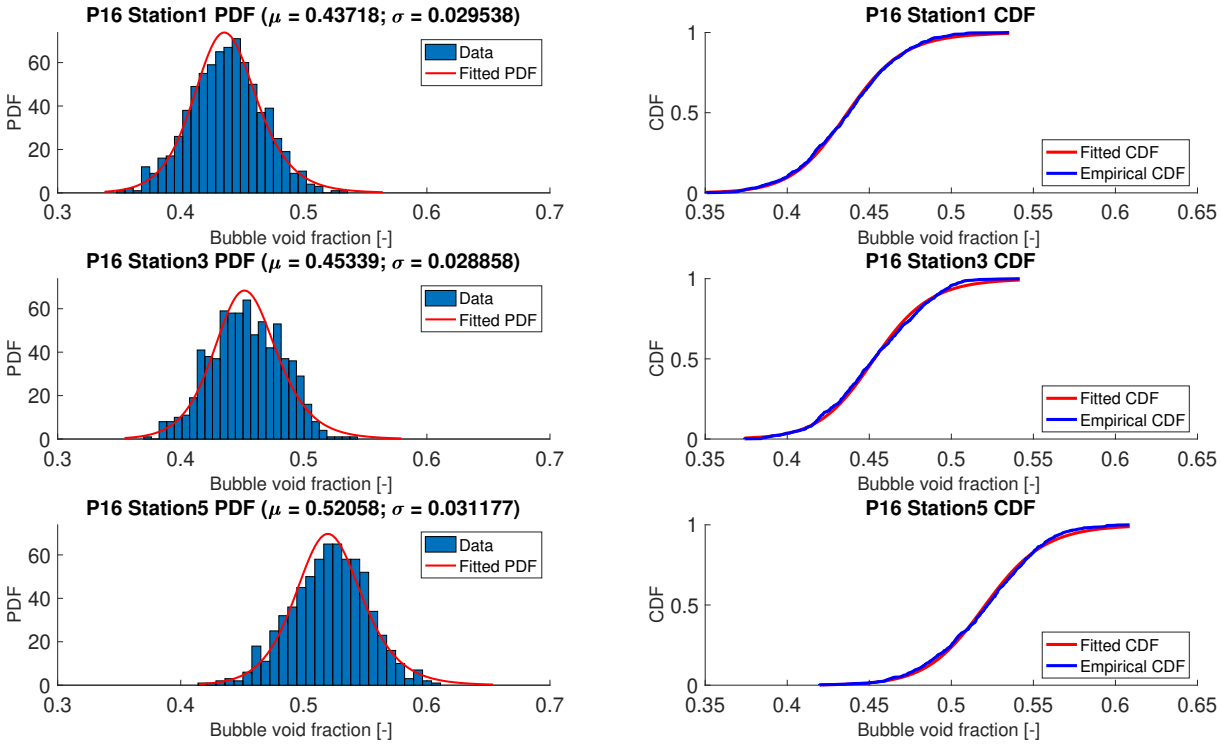

Source: The author.

Although P2, Fig. 34, and P16, Fig. 36, clearly follow this trend, P8, Fig. 35, seems to oscillate and LaRF analysis – Fig. 37, Fig. 38 and Fig. 39 – is used in order to deep investigate this behavior.

Figure 45 – Bubble void fraction percent difference, histogram and normal fit for P2 between stations 1 and 5.

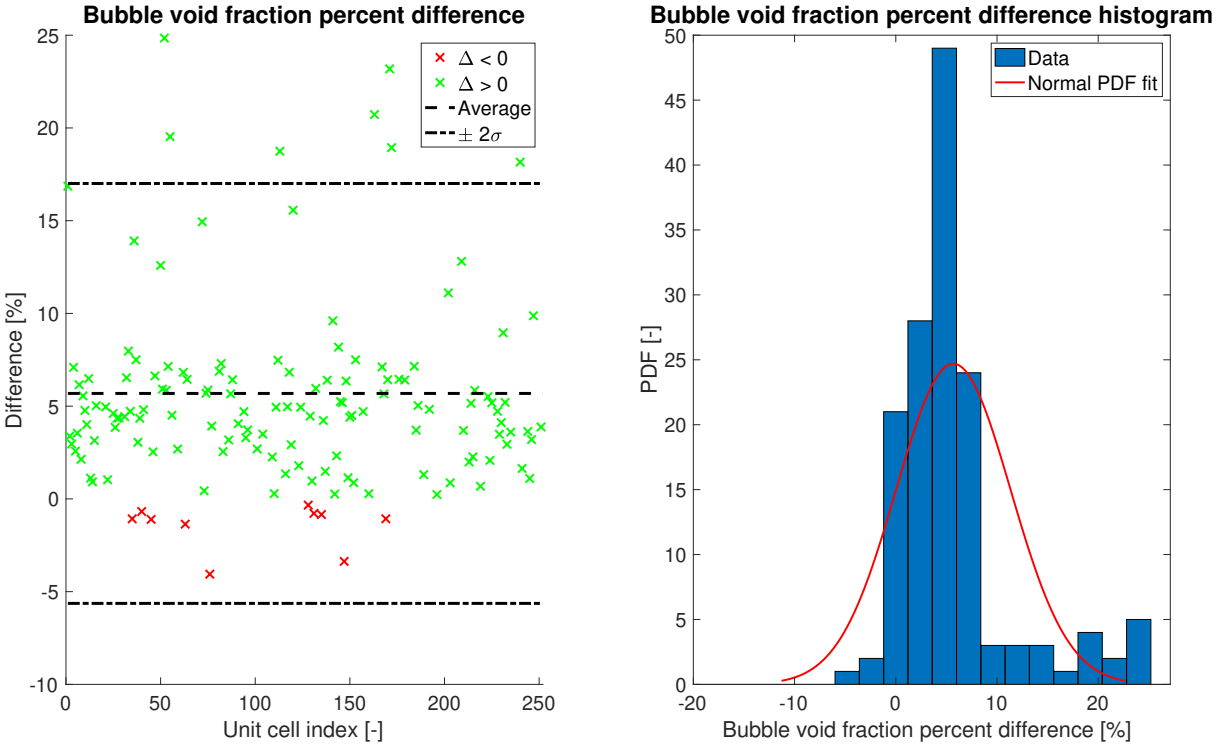

Source: The author.

Figure 46 – Bubble void fraction percent difference, histogram and normal fit for P8 between stations 1 and 5.

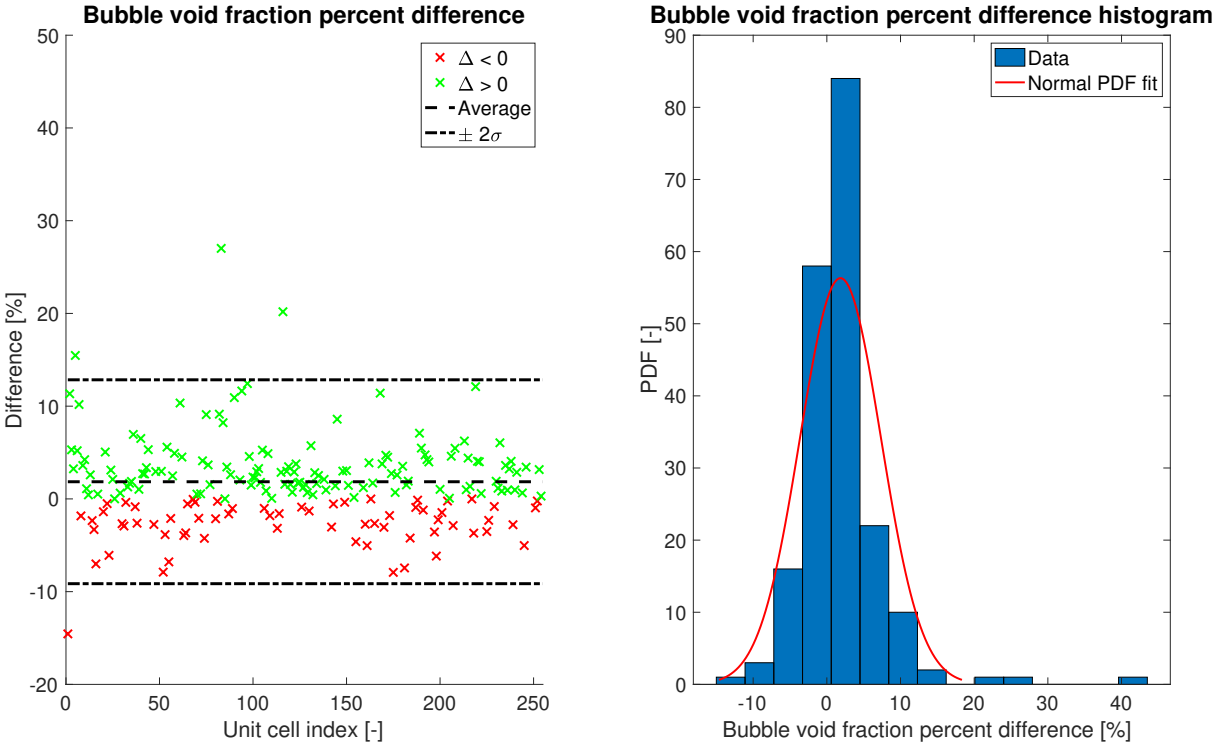

Source: The author.

Figure 47 – Bubble void fraction percent difference, histogram and normal fit for P16 between stations 1 and 5.

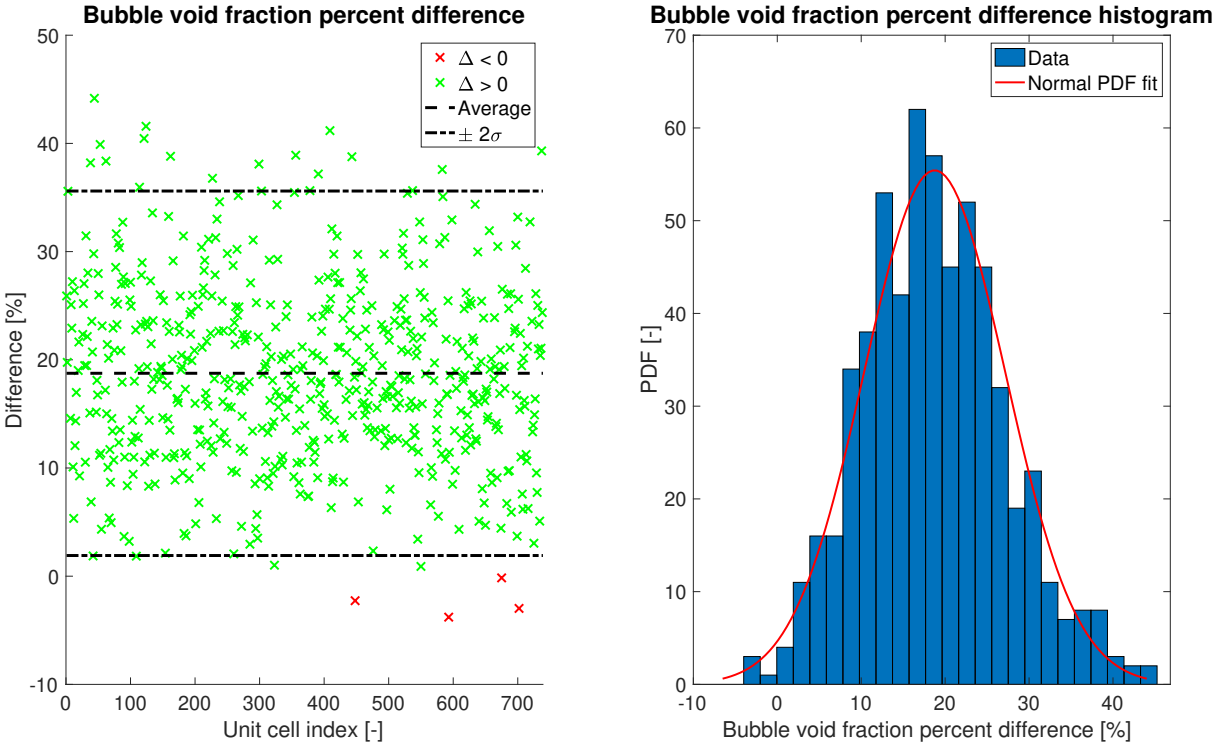

Source: The author.

Lagrangian reference frame results for P2, P8 and P16 are found in Fig. 45, Fig. 46 and Fig. 47, respectively. When it comes to analyze the void fraction change in a bubble across different stations, two phenomena should be considered: bubble tail shedding and gas expansion. As it can be seen in P2, there is a predominance tendency of increasing bubble void fraction. As turbulence is relatively low, bubbles are often followed by a long tail. When tails are long enough, they become unstable and break away from the bubble. When a bubble tail shed takes place, the resulting bubble will be smaller in length, but the average void fraction will be increased, since the tail is accounted as part of the bubble and has a low void fraction.

P16, on the other hand, shows the opposite situation: bubbles with no tail, since the turbulence would not allow long tails to stabilize and follow bubbles. In this case, due to the increased gas flow, the mass of the gas phase is substantially higher when compared to a plug flow – not only in elongated bubble, but as dispersed bubbles in liquid slug as well. Again, in order to attain mass conservation, the expanded gas should be accommodated either as increased bubble volume – bubble length or void fraction – or increased slug void fraction. What is seen in a two-phase flow is not one phenomenon or another alone, but a combination.

P8, though, exhibits an alternating behavior, where, again, roughly half of the bubbles experiment increasing bubble void fraction while the other half have it decreased. As discussed earlier, this experimental point has enough turbulence to keep bubbles from developing a long tail, but not enough gas superficial velocity to have a noticeable gas expansion effect. It must be stressed that these variations are considerably small and signal noise may be playing a significant role there. Besides, the flow turbulence may be dragging gas out of the elongated bubble, which, as there is not enough gas to a considerable gas expansion effect, may have its void fraction slightly decreased.

Figure 48 presents the fitted correlations for average bubble void fraction and standard deviation. Void fraction is ultimately controlled by the quantity of gas in the flow. Therefore, it is expected that bubble void fraction is intimately related to the gas superficial velocity (corrected for expansion effects). Experimental evidence supports that, indeed, average bubble void fraction is correlated with gas superficial velocity; moreover, a simple linear correlation is found. Vicencio (2013), on the other hand, reports a power model to represent bubble average void fraction.

Unlike average void fraction, the standard deviation does not seem to have a clear functional relation with gas superficial velocity. It must be stressed, though, that its values are small when compared to the measured average, indicating that bubble void fraction does not vary significantly among bubbles. Average bubble void fraction and its standard deviation correlations are presented in Eqs. 4.5 and 4.6.

$$R_{GB} = 0.4469\left(\frac{J_G}{J}\right) + 0.2716. \tag{4.5}$$

$$\sigma_{R_{GB}} \approx 0.035. \tag{4.6}$$

Figure 48 – Bubble average void fraction and standard deviation vs. gas superficial velocity and curve fit.

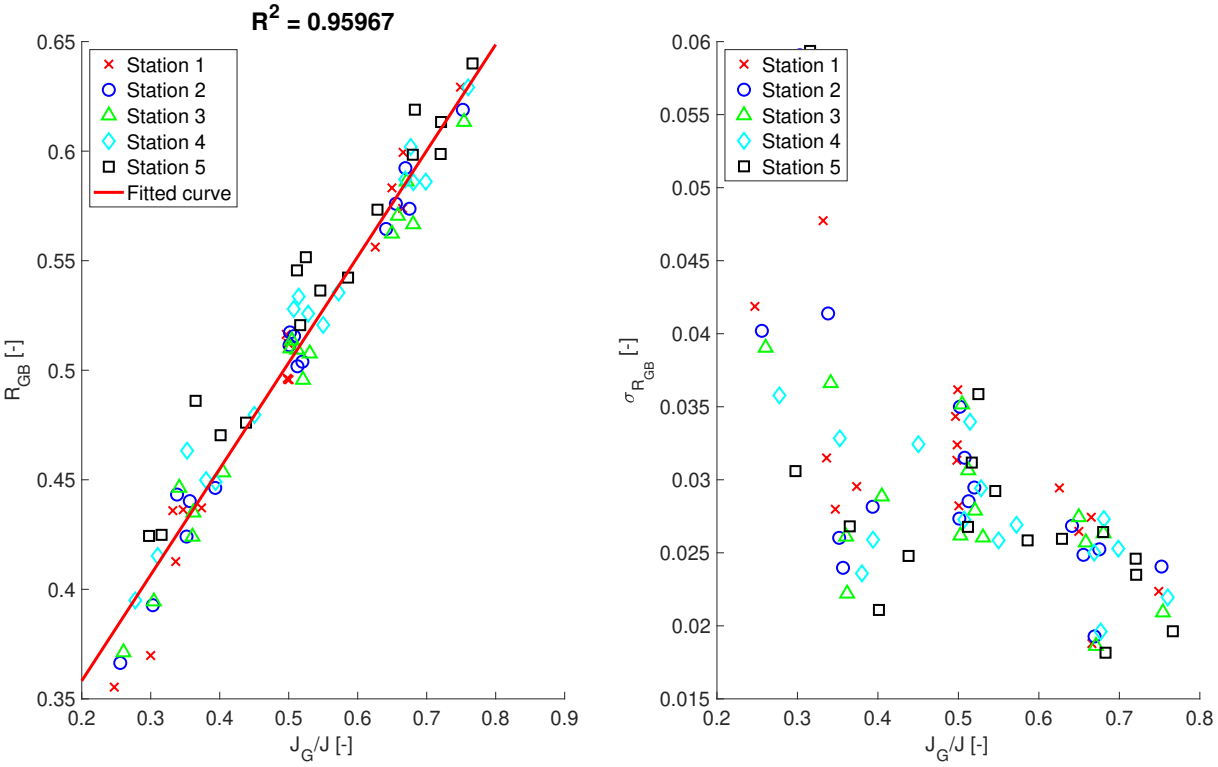

Source: The author.

4.6 Frequency

Log-logistic distribution is used to represent unit-cell frequency distribution. Histograms, PDFs, CDFs and log-logistic fits are depicted in Fig. 49, Fig. 50 and Fig. 51, for P2, P8 and P16, respectively.

Figure 49 – Histograms, PDFs, CDFs and log-logistic fits for P2 unit-cell frequency.

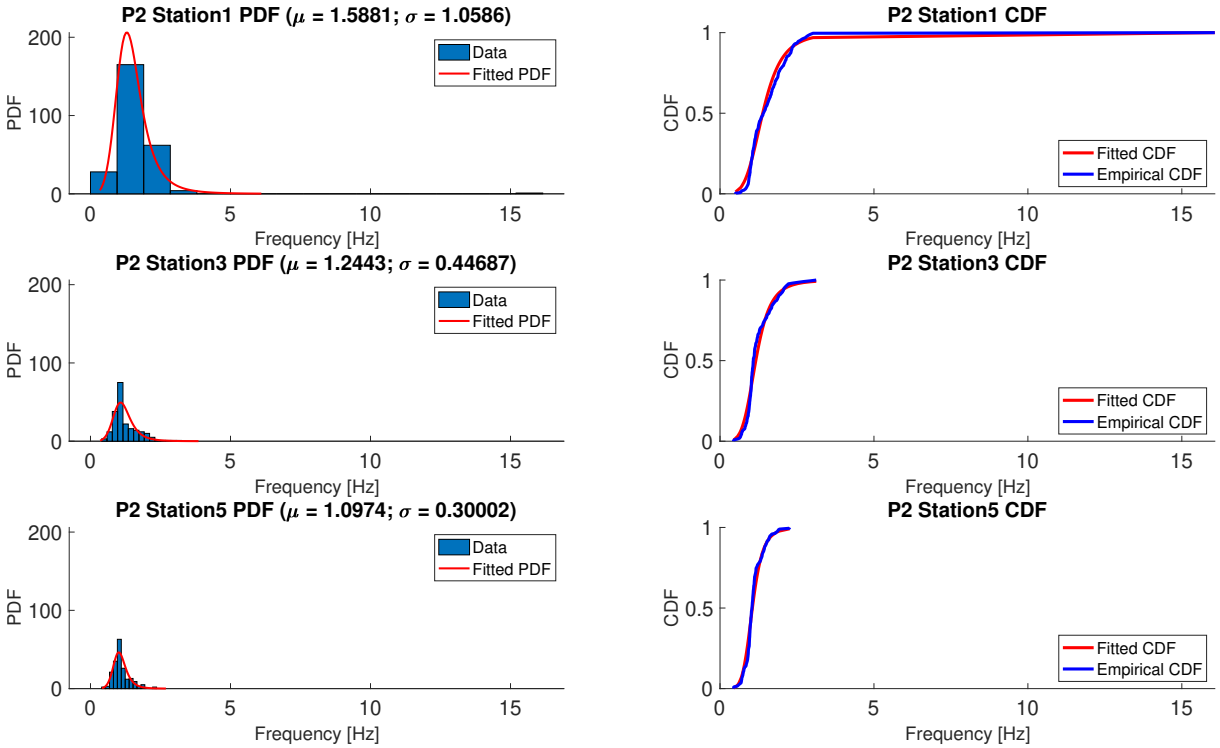

Source: The author.

Figure 50 – Histograms, PDFs, CDFs and log-logistic fits for P8 unit-cell frequency.

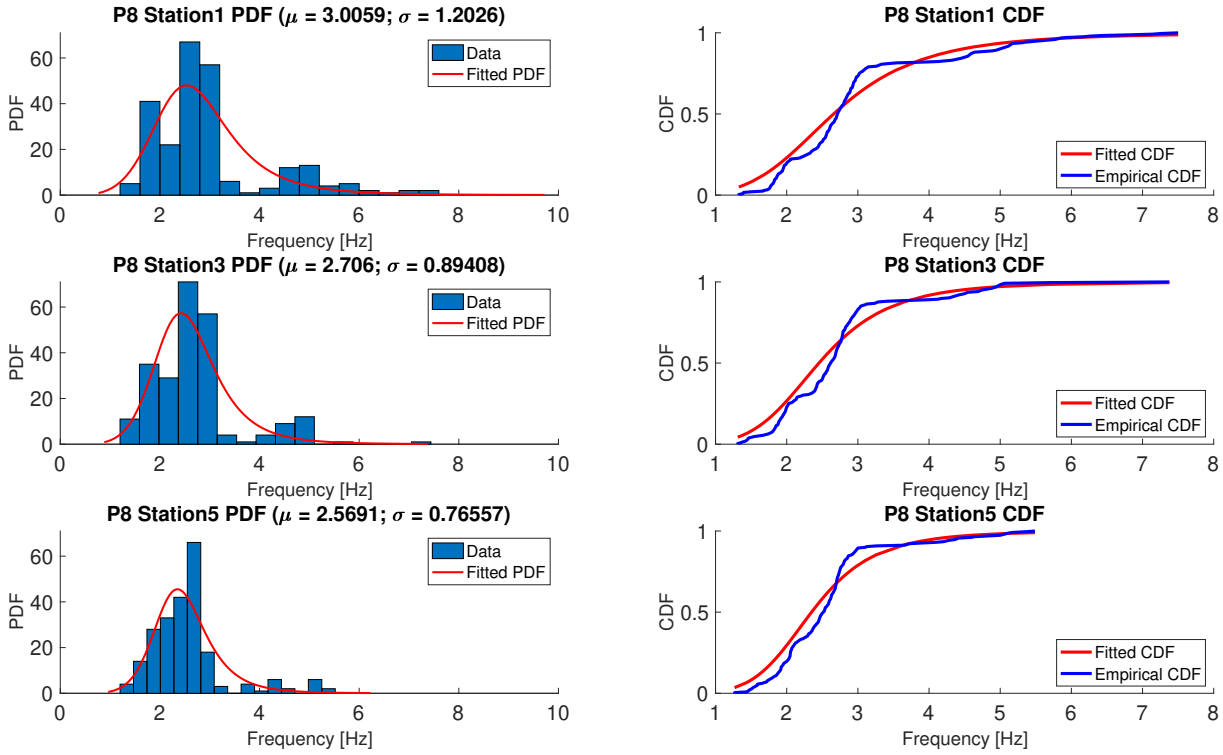

Source: The author.

Figure 51 – Histograms, PDFs, CDFs and log-logistic fits for P16 unit-cell frequency.

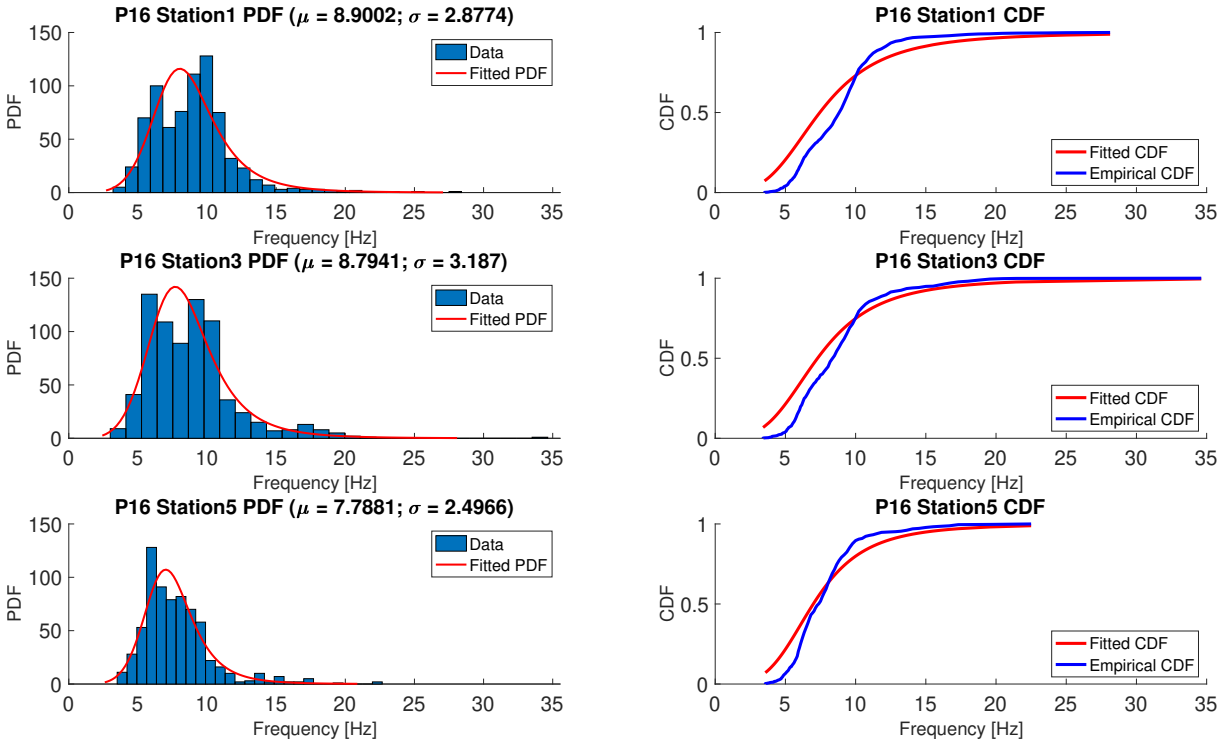

Source: The author.

As mixture velocity increases, the average bubble velocity increases as well. The passage time of these bubbles, hence, decreases significantly, substantially increasing flow frequency. Across stations, though, even as the number of bubbles decrease a little due to coalescences, gas expansion plays a major role, culminating in increased bubble lengths. As bubbles get longer, so do the unit cells and the frequency is expected to decrease, since the passage time is increased.

Figure 52, Fig. 53 and Fig. 54 depict the LaRF results for frequency, which are used to better understand the dynamics of the flow and how it affects the unit-cell frequency.

Figure 52 – Unit-cell frequency percent difference, histogram and normal fit for P2 between stations 1 and 5.

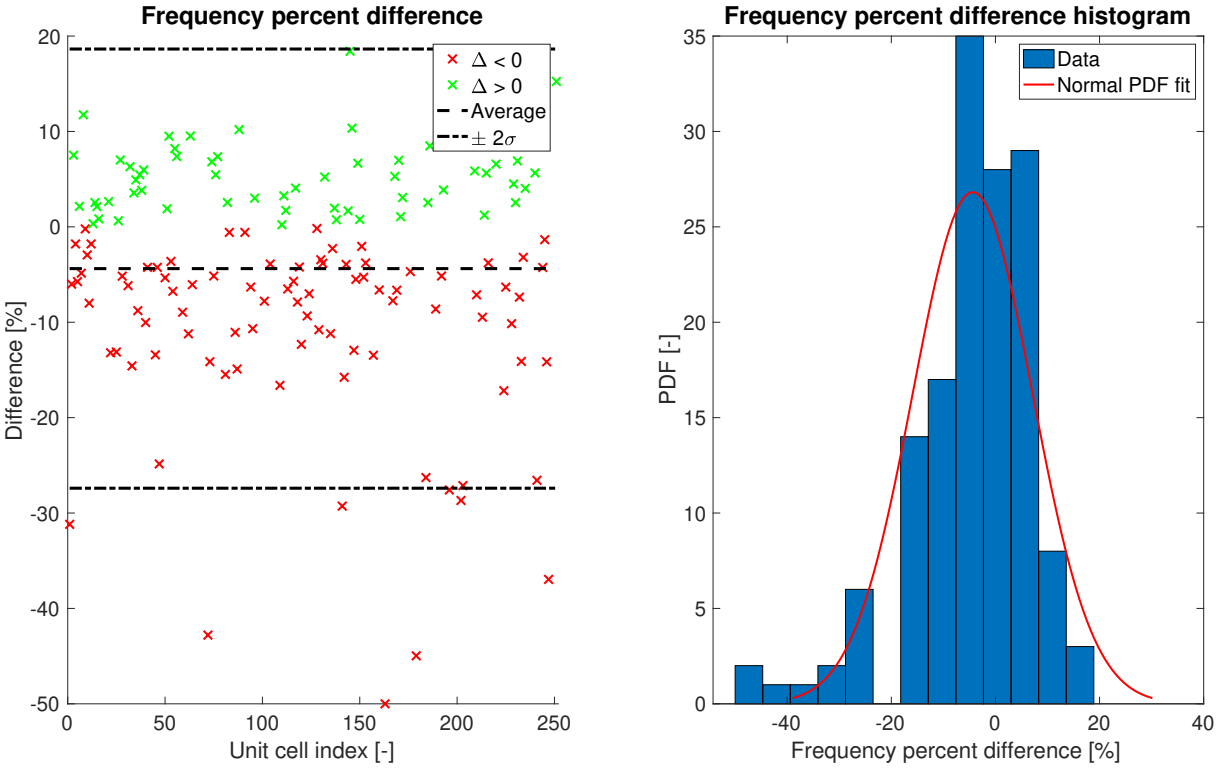

Source: The author.

Figure 53 – Unit-cell frequency percent difference, histogram and normal fit for P8 between stations 1 and 5.

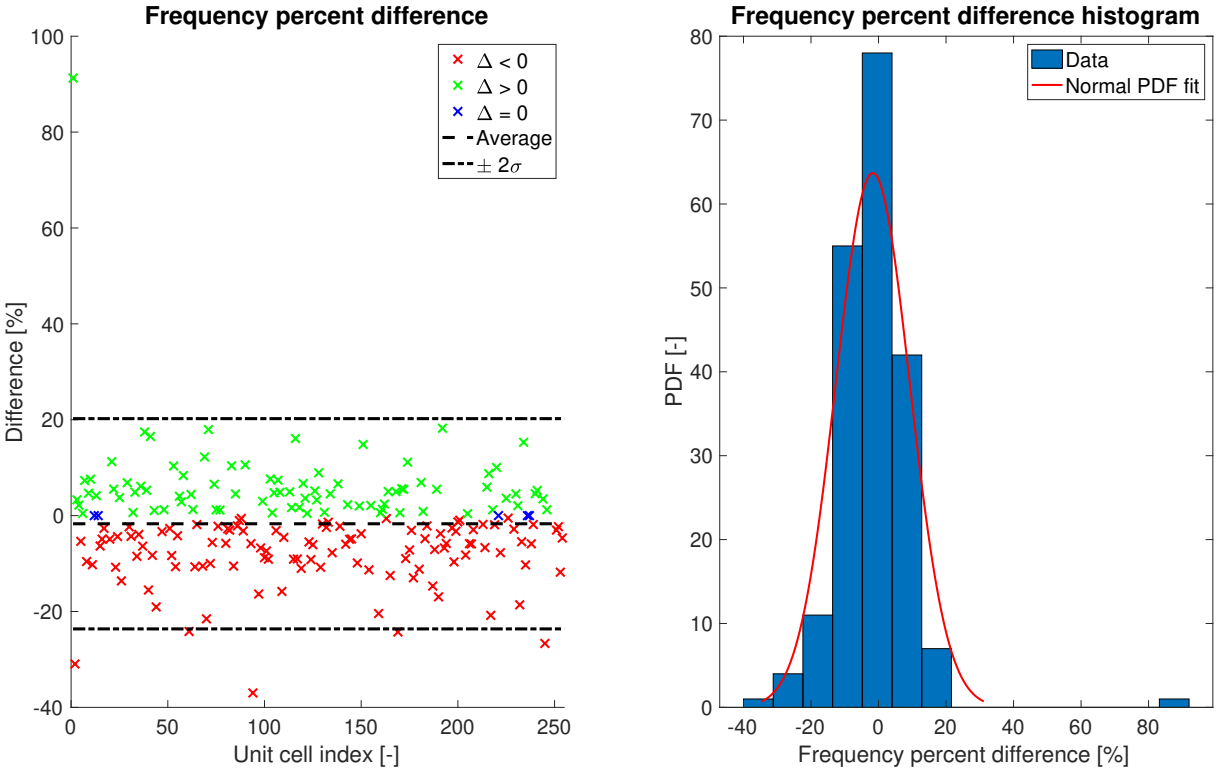

Source: The author.

Figure 54 – Unit-cell frequency percent difference, histogram and normal fit for P16 between stations 1 and 5.

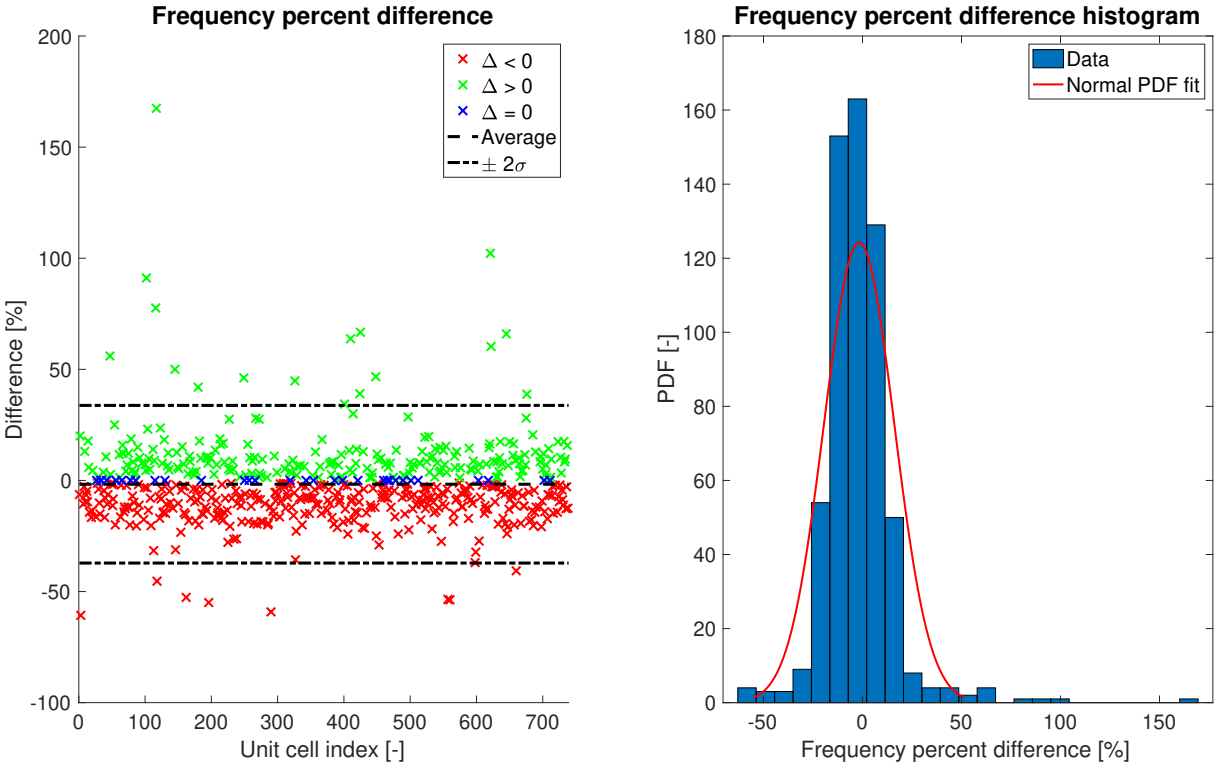

Source: The author.

An oscillating trend is found for every experimental point. Since unit-cell frequency is strongly constrained to the unit-cell length and unit-cell velocity, frequency should exhibit a behavior that ponders these variables.

When gas expansion takes place, bubbles are increased, but so is the velocity: while the former decreases frequency, the latter tends to increase it. Slug lengths oscillate across stations, as shown before. Since there are concurrent phenomena happening, an alternative behavior is expected and, indeed, observed.

Results and curve fits for dimensionless flow average frequency and standard deviation are found in Fig. 55. Increased gas flow is expected to primarily increase the average bubble length and, hence, decrease flow frequency, while increased liquid velocity favors a velocity increase, raising the flow frequency. Therefore, a functional relation is investigated between these parameters. Mixture velocity Strouhal number is used as a dimensionless frequency in order to generalize findings. Correlations for average flow frequency and standard deviation are presented in Eqs. 4.7 and 4.8.

$$Sr_J = 0.0735\left(\frac{J_G}{J_L}\right)^{-0.3687} - 0.03779. \tag{4.7}$$

$$\sigma_{Sr} = 0.003241\left(\frac{J_G}{J_L}\right)^{-1.91} + 0.006405. \tag{4.8}$$

Figure 55 – Dimensionless flow average frequency, standard deviation and curve fits.

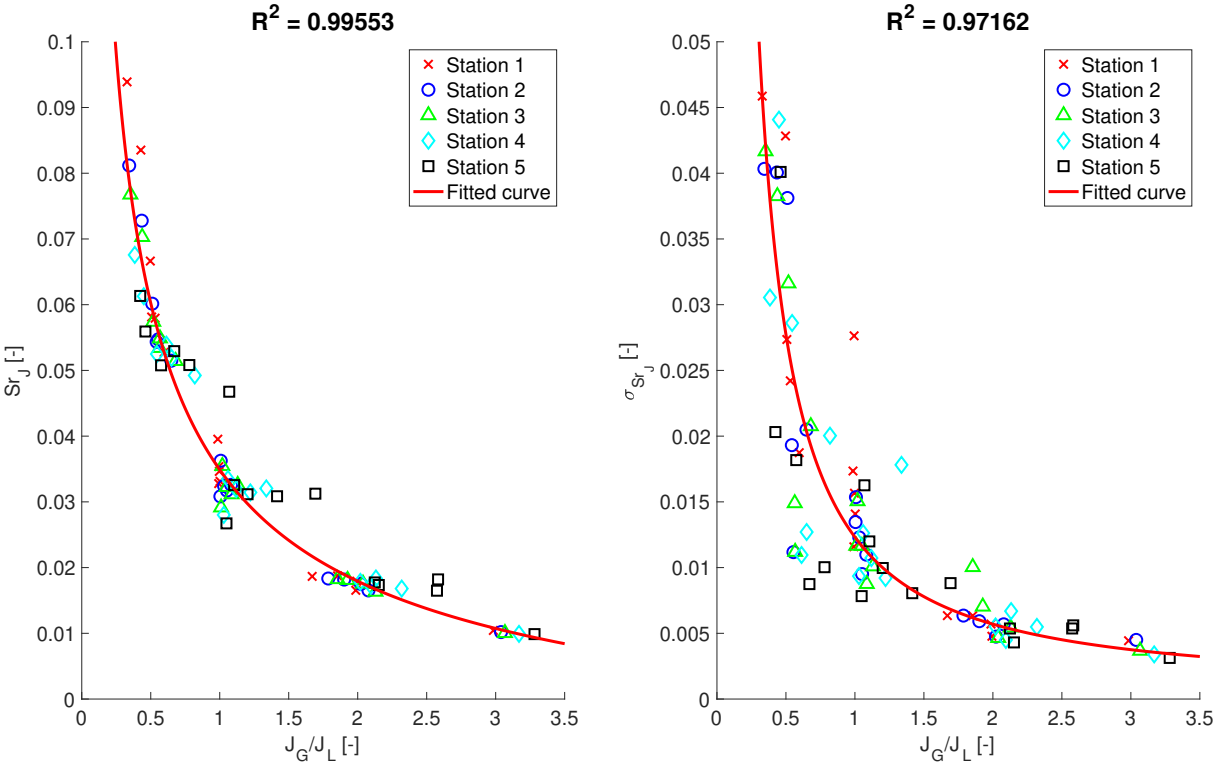

Source: The author.

Dimensionless frequency seems to decrease as the superficial velocities' quotient rises, a scenario that would happen either when gas superficial velocity is high or liquid superficial velocity is low – which would, indeed, favor the formation of slower and longer bubbles, ultimately culminating in a lower frequency. The proposed mechanism does apply to the other direction as well, since greater liquid superficial velocities would favor faster bubbles and lower gas superficial velocities would create shorter bubbles. As for standard deviation, the same trend is reported. As liquid superficial velocity increases, the flow seems to become more chaotic and turbulent, supporting more heterogeneous structures and a higher standard deviation.

4.7 Intermittence factor

Histograms, PDFs and CDFs are depicted in Fig. 56, Fig. 57 and Fig. 58, for P2, P8 and P16, respectively. Once more showing its versatility, log-logistic distribution was

chosen to represent intermittence factor probability density function – and the agreement of the experimental and fitted data is noticeable, even better than lengths alone.

Figure 56 – Histograms, PDFs, CDFs and log-logistic fits for P2 intermittence factor.

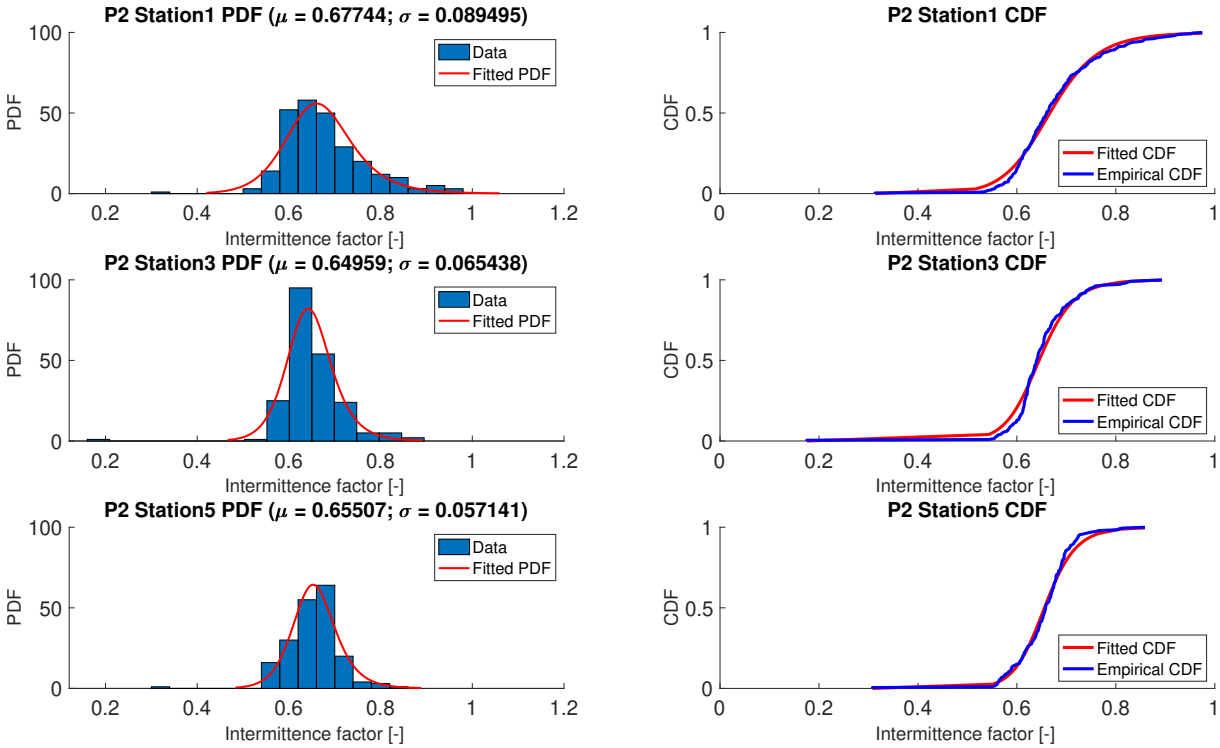

Source: The author.

Figure 57 – Histograms, PDFs, CDFs and log-logistic fits for P8 intermittence factor.

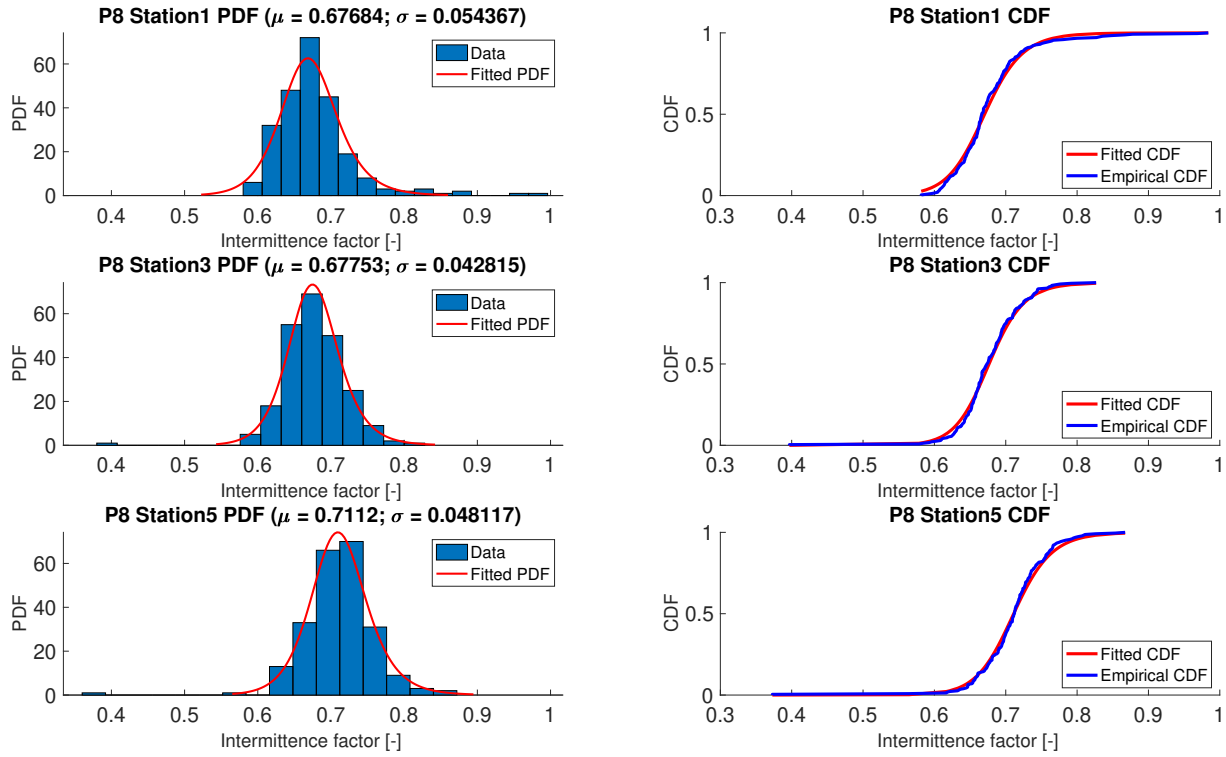

Source: The author.

Figure 58 – Histograms, PDFs, CDFs and log-logistic fits for P16 intermittence factor.

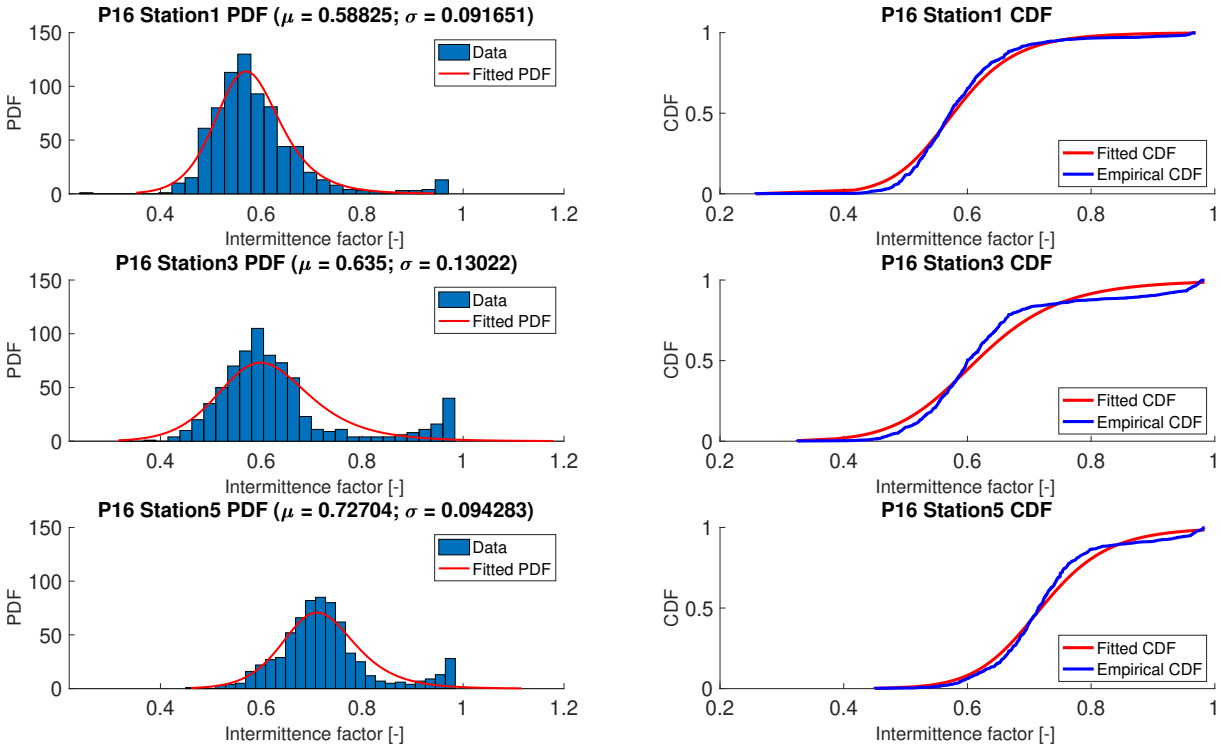

Source: The author.

Since intermittence factor is defined as a ratio of the bubble length to the unit-cell length, and the former is defined as the sum of bubble and slug lengths, the trend of this hydrodynamic parameter is expected to behave similarly as the aforementioned lengths. Indeed, an increasing average trend is noted, just as the trend reported for bubble lengths – and, since slug average length oscillate and hardly change, intermittence factor average value should behave just like bubble length.

Results for intermittence factor are shown in Fig. 59, Fig. 60 and Fig. 61, for P2, P8 and P16, respectively. Even though a clear trend is found, LaRF analyses are used in order to deep investigate flow hydrodynamics and mechanisms.

Figure 59 – Intermittence factor percent difference, histogram and normal fit for P2 between stations 1 and 5.

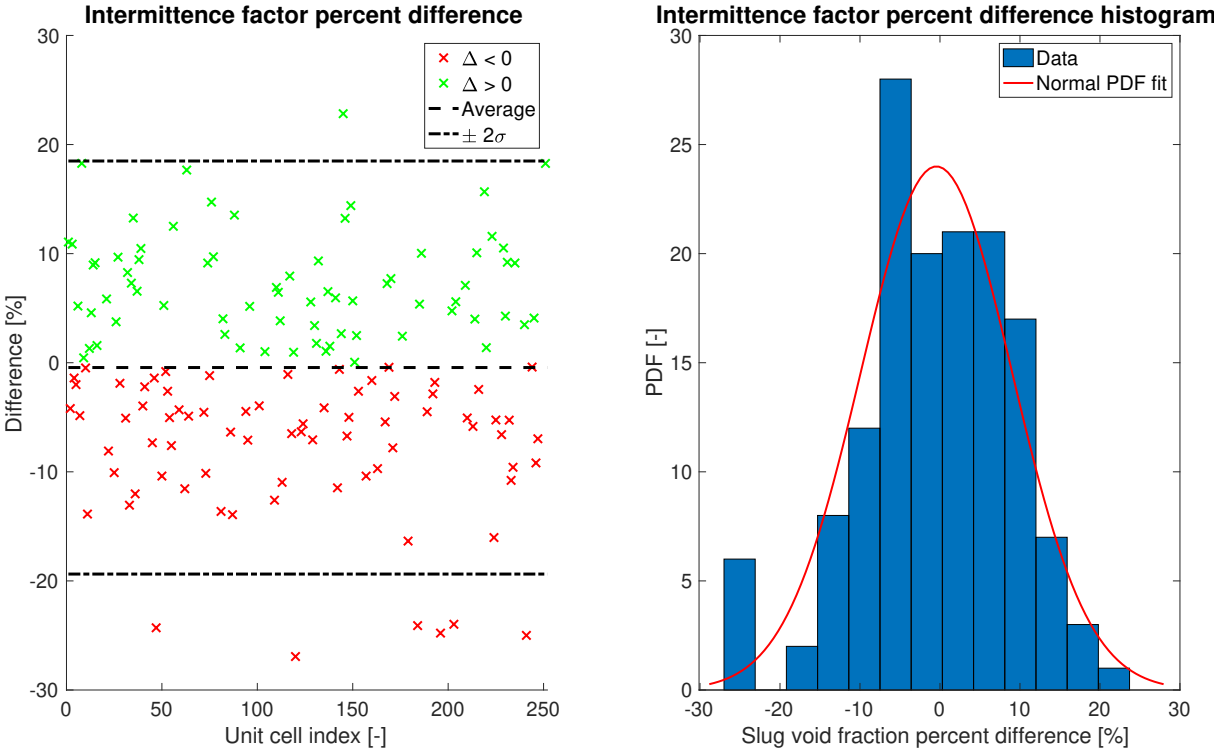

Source: The author.

Figure 60 – Intermittence factor percent difference, histogram and normal fit for P8 between stations 1 and 5.

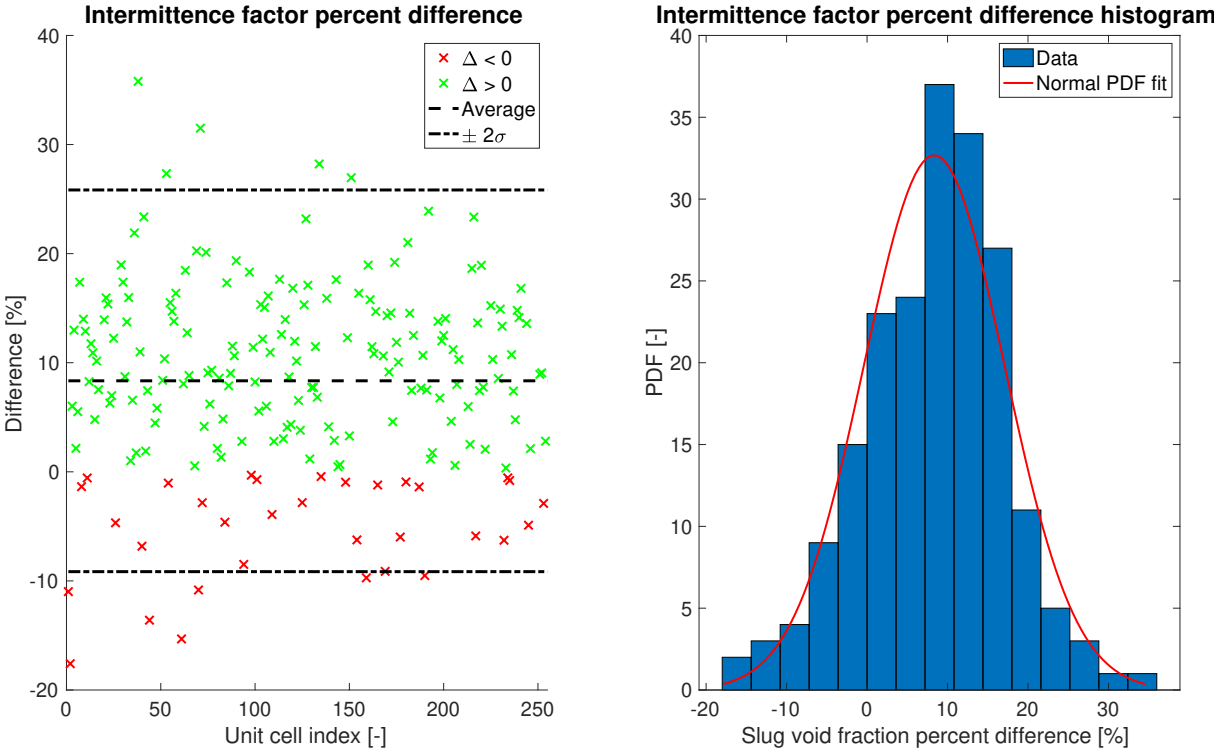

Source: The author.

Figure 61 – Intermittence factor percent difference, histogram and normal fit for P16 between stations 1 and 5.

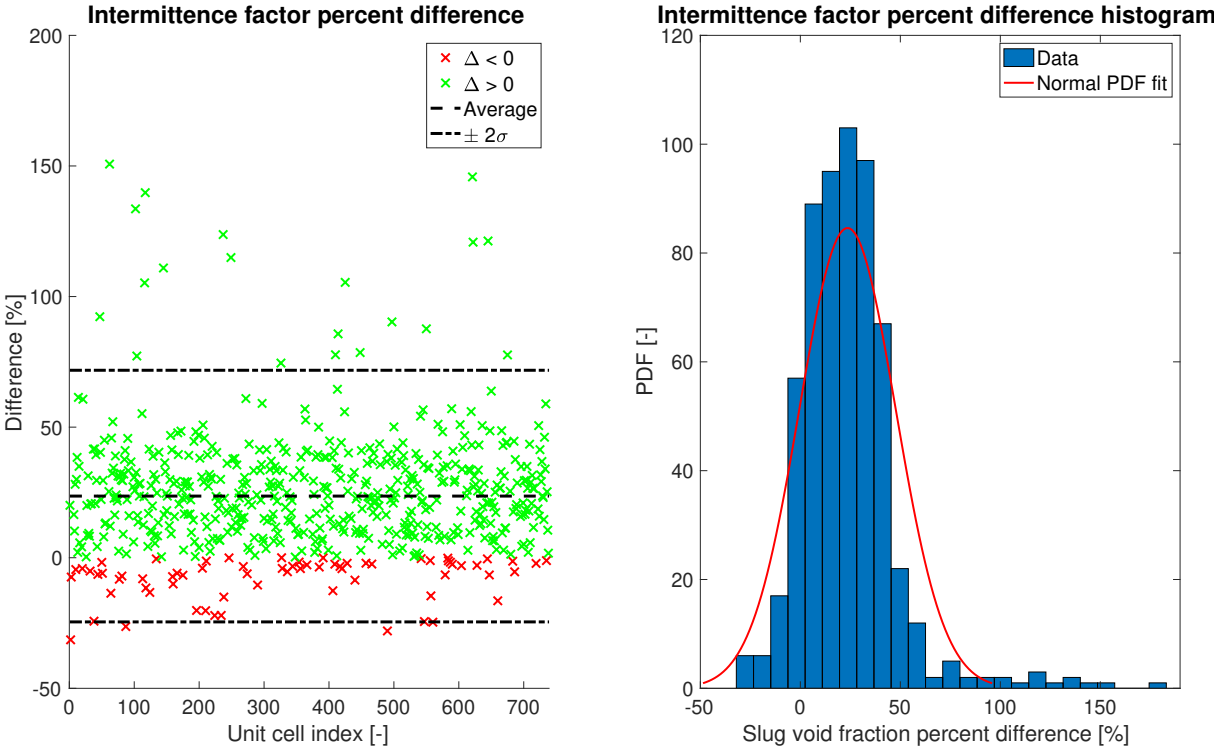

Source: The author.

When analyzing low aeration points, such as P2, both bubble and slug lengths oscillate back and forth and these oscillations are reflected in intermittence factor behavior, which shows some symmetry between positive and negative changes, as shown in Fig. 59.

When gas expansion becomes more noticeable – P8 and P16, Fig. 60 and Fig. 61, respectively –, bubble lengths increase more severely and similar trend is found in intermittence factor, drastically reducing – but not eliminating – negative changes in this hydrodynamic parameter. However, some of the cells still experience decreasing intermittence factor – which may be explained by the other trend followed: slug lengths. Since roughly half of the slug lengths increase, some of these changes are enough to overcome increasing bubble lengths and culminate to a negative intermittence factor variation.

Figure 62 presents the found correlations for intermittence factor average and standard deviation as a function of gas superficial velocities. As discussed before, since intermittence factor is a ratio of lengths, it is expected to behave according to the quantity of gas present in the flow – and, therefore, correlated to the gas superficial velocity (corrected to the gas expansion effect). Correlations for average intermittence factor and

standard deviation are presented in Eqs. 4.9 and 4.10.

$$\beta = -5.126\left(\frac{J_G}{J}\right)^{-0.07274} + 6.079. \tag{4.9}$$

$$\sigma_\beta = 1.223 \cdot 10^{-7}\left(\frac{J_G}{J}\right)^{-11.26} + 0.05452. \tag{4.10}$$

Figure 62 – Intermittence factor average values, standard deviation and curve fits.

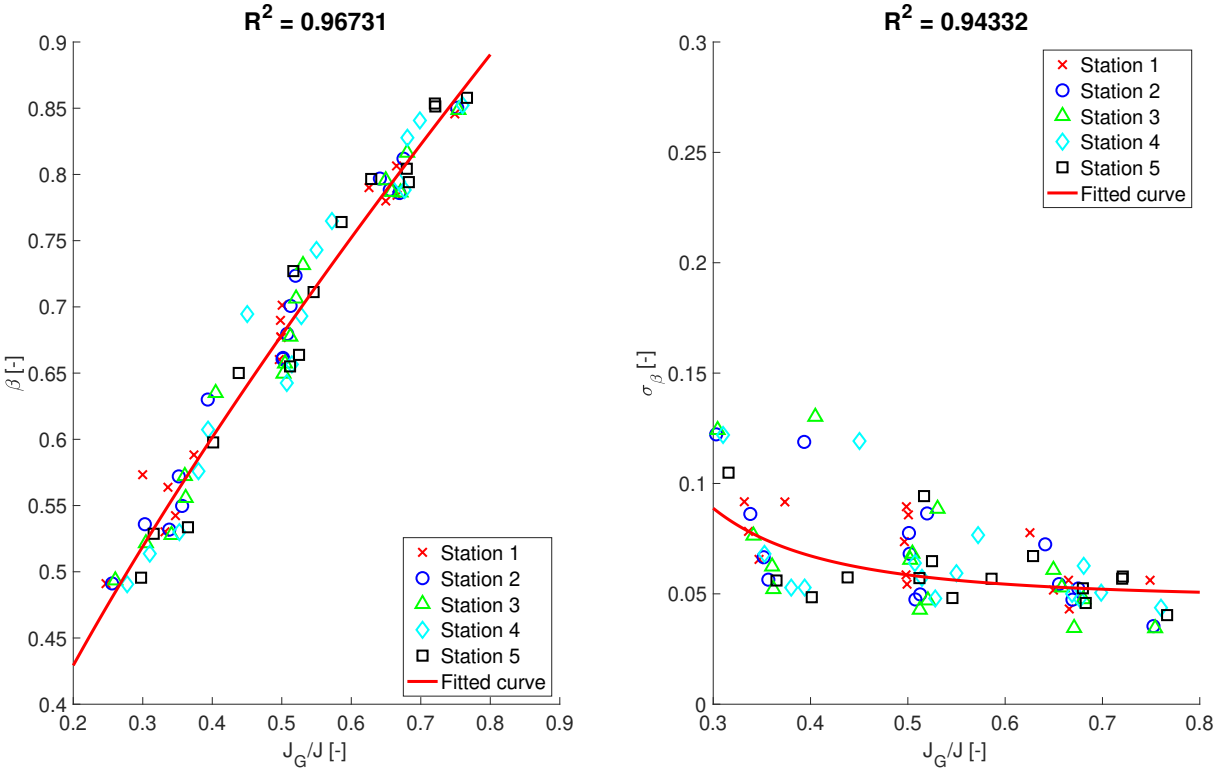

Source: The author.

As gas superficial velocity rises, bubbles become larger and intermittence factor, due to the nature of its definition, goes up as well. When it comes to the standard deviation, though, the rise in liquid superficial velocity – which elevates the mixture velocity and decreases the ratio of the gas superficial velocity to mixture velocity – seems to produce a disordered and turbulent flow, contributing to a wider range of values to this hydrodynamic parameter and, therefore, increasing its standard deviation.

4.8 Summary and final words

In the present chapter, sample results for both ERF and LaRF data analysis were presented. Samples were chosen in order to represent data – fully reported in Appendix B

and Appendix C –, as many experimental points were processed. The new methodology proposed retrieved results that could not be obtained otherwise, since a moving (or Lagrangian) reference frame is needed in order to understand the behavior of single unit cells across stations. LaRF analysis also complements ERF results by providing insightful information about the phenomena involved in two-phase slug flow and why average and standard deviations have such behavior. Analyses using both approaches may enrich the results of future researches, as well as to provide new information that would be hard or impossible to measure otherwise. Moreover, correlations were given for the main hydrodynamic parameters average values and standard deviations – which could be useful for use both in field operations and numerical simulations. Table 7 summarizes the proposed correlations for each parameter, as well as the goodness of fit.

Table 7 – Summary of proposed correlations.

Parameter	Statistic	Correlation	R^2
Velocity	Average	$V_{TB} = 1.492J - 0.066\sqrt{gD}$	0.9909
	Standard deviation	$\sigma_V = -0.0048J^3 + 0.1074J^2 - 0.5479J + 1.235$	0.8602
Frequency	Average	$Sr_J = 0.0735\left(\frac{J_G}{J_L}\right)^{-0.3687} - 0.03779$	0.9943
	Standard deviation	$\sigma_{Sr} = 0.003241\left(\frac{J_G}{J_L}\right)^{-1.91} + 0.006405$	0.9542
Bubble length	Average	$\frac{L_B}{D} = 2.175exp\left(5.251\frac{J_G}{J}\right)$	0.9785
	Standard deviation	$\sigma_{L_B} = 131.6\left(\frac{J_G}{J}\right)^{5.322} + 2.732$	0.9958
Intermittence factor	Average	$\beta = -5.126\left(\frac{J_G}{J}\right)^{-0.07274} + 6.079$	0.9313
	Standard deviation	$\sigma_\beta = 1.223 \cdot 10^{-7}\left(\frac{J_G}{J}\right)^{-11.26} + 0.05452$	0.9634
Bubble void fraction	Average	$R_{GB} = 0.4469\left(\frac{J_G}{J}\right) + 0.2716$	0.9378
	Standard deviation	$\sigma_{R_{GB}} \approx 0.035$	–

Source: The author.

5 Conclusion

The present study has proposed a novel methodology for data analysis, which can be used simultaneously to the widely used Eulerian analysis proposed in literature. In order to develop the novel approach, a literature review was made to identify possible gaps and to elucidate open questions left by them. Moreover, the proposed methodology was used in order to suit numerical simulations needs, extracting experimental parameters which would otherwise be impossible to measure – such as the behavior and phenomena behind the slug length oscillation. The data analysis procedure was documented as clearly as possible in order to be used as a reference for future works.

The current work inserts itself in an interesting gap: although the phenomena investigated with the Lagrangian reference frame are widely investigated by numerical simulations, there is no experimental studies capable of provide these details in order to validate the findings. Furthermore, the novel procedure also provides insightful information regarding the behavior of single unit cells, which can be used to deeper understand two-phase slug flow phenomena and help modeling them. Insightful information was retrieved using the proposed methodology, which could not be gathered using a traditional literature approach: LaRF analysis has made possible to track changes in hydrodynamic parameters within a unit-cell along the pipe. Numerical procedures often evaluate unit-cell hydrodynamic parameters and evaluate the histogram afterwards in order to compare to ERF experimental results, which could be hiding discrepancies that may end up compensating themselves – culminating to accurate average values, but failing to test the accuracy of the model itself.

Applying the proposed methodology, it was found that averaging results may mask an alternative behavior – intrinsic to the unsteadiness of slug flow – which could be limiting physical interpretation of phenomena: although average slug length were found to vary by as much as 30% at most, lagrangian analysis found up to 800% change between individual structures. Slug lengths were found to oscillate at all times – even though their average was shown to differ slightly between measuring stations –, indicating that bubble movement would oscillate as well, which, indeed, is reported in literature.

Bubble velocity was shown to increase most of the time – such as in P8, where average bubble velocity increased by 5.59% between stations 1 and 3 and by 3.58% between stations 3 and 5, and P16, for which average bubble velocity increased 4.35% between stations 1 and 3 and 28.8% between stations 3 and 5 –, even though sometimes it may decrease – as seen in P2, where the average velocity increased by 1.9% between stations 1 and 3, but decreased 3.62% between stations 3 and 5. A reasonable explanation found

was that the slug length in front of the bubble was getting larger, lowering the wake effect, which, therefore, slows down the bubble. When the slug in front of the bubble had considerable aeration, though, the average velocity was shown to increase, and similar reasoning is applied: as bubbles would disturb the velocity profile in front of the bubble, which ultimately culminates to bubble acceleration.

Bubble length is also shown to be dependent of the quantity of gas inside the pipe. It was found that the more gas inside the pipe, the more gas expansion is noticeable. The effects of gas expansion for low aeration points were found to be negligible when compared to concurrent effects, but were also found to be a driver phenomenon in highly aerated conditions.

5.1 Suggestion for future work

The present work aimed to develop a novel methodology to analyze slug flow. Its applications, though, are not limited to the ones given in this paper; in fact, the current research provides sample results and applications. Future work can be further developed using the proposed methodology in order to:

- pair void fraction a pressure time series and evaluate their behavior and interaction along the pipe with time;
- use Lagrangian reference frame analysis with images in order to track unit cells along the pipeline and deeply investigate the changes in hydrodynamic parameters with a precision only obtainable through image processing techniques;
- investigate the coalescence and break processes and the behavior of hydrodynamic variables through the process;
- analyze mass and momentum balances for each structure individually and model their transfer across the interface;
- improve the current algorithm and methodology.

References

Abdelsalam, A.; Cem, S.; Eduardo, P. New dimensionless number for gas-liquid flow in pipes. *International Journal of Multiphase Flow*, Elsevier Ltd, v. 81, p. 15–19, 5 2016. ISSN 03019322.

Abed, E. Gas-liquid slug frequency and slug unit length in horizontal pipes. *The Iraqi Journal for Mechanical and Material Engineering*, v. 15, n. 3, p. 166–180, 2015.

Al-Safran, E. Investigation and prediction of slug frequency in gas/liquid horizontal pipe flow. *Journal of Petroleum Science and Engineering*, v. 69, n. 1-2, p. 143–155, 11 2009. ISSN 09204105.

Al-Safran, E. M. Probabilistic modeling of slug frequency in gas/liquid pipe flow using the Poisson probability theory. *Journal of Petroleum Science and Engineering*, Elsevier, v. 138, p. 88–96, 2016. ISSN 09204105. Available in: <http://dx.doi.org/10.1016/j.petrol.2015.12.008>.

Al-Safran, E. M.; Taitel, Y.; Brill, J. P. Prediction of slug length distribution along a hilly terrain pipeline using slug tracking model. *Journal of Energy Resources Technology, Transactions of the ASME*, v. 126, n. 1, 2004. ISSN 01950738.

Alves, I. N.; Shoham, O.; Taitel, Y. Drift velocity of elongated bubbles in inclined pipes. *Chemical Engineering Science*, v. 48, n. 17, 1993. ISSN 00092509.

Araújo, J. D.; Miranda, J. M.; Campos, J. B. Flow of two consecutive Taylor bubbles through a vertical column of stagnant liquid-A CFD study about the influence of the leading bubble on the hydrodynamics of the trailing one. *Chemical Engineering Science*, Elsevier Ltd, v. 97, p. 16–33, 6 2013. ISSN 00092509.

Araújo, J. D.; Miranda, J. M.; Campos, J. B. Simulation of slug flow systems under laminar regime: Hydrodynamics with individual and a pair of consecutive Taylor bubbles. *Journal of Petroleum Science and Engineering*, v. 111, p. 1–14, 11 2013. ISSN 09204105.

Araújo, J. D.; Miranda, J. M.; Pinto, A. M.; Campos, J. B. Wide-ranging survey on the laminar flow of individual Taylor bubbles rising through stagnant Newtonian liquids. *International Journal of Multiphase Flow*, v. 43, p. 131–148, 7 2012. ISSN 03019322.

Barnea, D.; Taitel, Y. A model for slug length distribution in gas-liquid slug flow. *International Journal of Multiphase Flow*, v. 19, n. 5, 1993. ISSN 03019322.

Barr, G. The air-bubble viscosimeter. *The London, Edinburgh, and Dublin Philosophical Magazine and Journal of Science*, v. 1, n. 2, p. 395–405, 1926.

Barros, H. et al. Experimental analysis of two-phase slug flow evolution with a slight upward direction change. In: *Cong. B. Eng. Mec.* [S.l.: s.n.], 2019.

Bendiksen, K. H. An experimental investigation of the motion of long bubbles in inclined tubes. *International Journal of Multiphase Flow*, v. 10, n. 4, p. 467–483, 1984. ISSN 03019322.

Benjamin, T. B. Gravity currents and related phenomena. *Journal of Fluid Mechanics*, v. 31, n. 2, 1968. ISSN 14697645.

Brill, J. P.; Schmidt, Z.; Coberly, W. A.; Herring, J. D.; Moore, D. W. Analysis of two-phase tests in large-diameter flow lines in Prudhoe Bay field. *Society of Petroleum Engineers journal*, v. 21, n. 3, 1981. ISSN 01977520.

Brown, R. A. The mechanics of large gas bubbles in tubes: I. Bubble velocities in stagnant liquids. *The Canadian Journal of Chemical Engineering*, v. 43, n. 5, 1965. ISSN 1939019X.

Campos, J. B.; Carvalho, J. R. G. D. An experimental study of the wake of gas slugs rising in liquids. *Journal of Fluid Mechanics*, v. 196, 1988. ISSN 14697645.

Collins, R.; Moraes, F. F. D.; Davidson, J. F.; Harrison, D. The motion of a large gas bubble rising through liquid flowing in a tube. *Journal of Fluid Mechanics*, v. 89, n. 3, 1978. ISSN 14697645.

Conte, M. G.; Hegde, G. A.; Silva, M. J. da; Sum, A. K.; Morales, R. E. Characterization of slug initiation for horizontal air-water two-phase flow. *Experimental Thermal and Fluid Science*, v. 87, 2017. ISSN 08941777.

Costigan, G.; Whalley, P. B. Slug flow regime identification from dynamic void fraction measurements in vertical air-water flows. *International Journal of Multiphase Flow*, v. 23, n. 2, 1997. ISSN 03019322.

Diaz, M. J. C. Two-Phase Slug Flow Experiments with Viscous Liquids (electronic version). In: . [S.l.: s.n.], 2016. p. 109. ISBN 978-82-326-1557-5. ISSN 1503-8181.

Dinaryanto, O. et al. Experimental investigation on the initiation and flow development of gas-liquid slug two-phase flow in a horizontal pipe. *Experimental Thermal and Fluid Science*, Elsevier Inc., v. 81, p. 93–108, 2 2017. ISSN 08941777.

Direito, F. J.; Campos, J. B.; Miranda, J. M. A Taylor drop rising in a liquid co-current flow. *International Journal of Multiphase Flow*, Elsevier Ltd, v. 96, p. 134–143, 2017. ISSN 03019322.

Dukler, A. E.; Hubbard, M. G. A Model for Gas-Liquid Slug Flow in Horizontal and Near Horizontal Tubes. *Industrial and Engineering Chemistry Fundamentals*, v. 14, n. 4, 1975. ISSN 01964313.

Dumitrescu, D. T. Strömung an einer Luftblase im senkrechten Rohr. *ZAMM - Journal of Applied Mathematics and Mechanics / Zeitschrift für Angewandte Mathematik und Mechanik*, v. 23, n. 3, 1943. ISSN 15214001.

Fabre, J. Gas-Liquid Slug Flow. In: . [S.l.: s.n.], 2003. p. 117–156.

Fabre, J.; Grenier, P.; Gadoin, E. Evolution of slug flow in long pipe. In: . [S.l.: s.n.], 1993. p. 165–177.

Fanchi, J. R.; Christiansen, R. L. *Introduction to petroleum engineering*. [S.l.: s.n.], 2016. 1–335 p. ISBN 9781119193463.

Ferre, D. *Ecoulments gaz-liquide a poches et a bouchons dans les conduites de section circulaire*. Tese (Doutorado) — Inst. National Polytech Toulouse, 1981.

Fossa, M.; Guglielmini, G.; Marchitto, A. Intermittent flow parameters from void fraction analysis. *Flow Measurement and Instrumentation*, v. 14, n. 4-5, 2003. ISSN 09555986.

Gokcal, B.; Al-Sarkhi, A. S.; Sarica, C.; Al-Safran, E. M. Prediction of slug frequency for high-viscosity oils in horizontal pipes. *SPE Projects, Facilities and Construction*, v. 5, n. 3, 2010. ISSN 19422431.

Goldsmith, H. L.; Mason, S. G. The movement of single large bubbles in closed vertical tubes. *Journal of Fluid Mechanics*, v. 14, n. 1, 1962. ISSN 14697645.

Gomez, L. E.; Shoham, O.; Schmidt, Z.; Chokshi, R. N.; Northug, T. Unified mechanistic model for steady-state two-phase flow: Horizontal to vertical upward flow. *SPE Journal*, v. 5, n. 3, 2000. ISSN 1086055X.

Gregory, G. A.; Nicholson, M. K.; Aziz, K. Correlation of the liquid volume fraction in the slug for horizontal gas-liquid slug flow. *International Journal of Multiphase Flow*, v. 4, n. 1, 1978. ISSN 03019322.

Gregory, G. A.; Scott, D. S. *Correlation of liquid slug velocity and frequency in horizontal cocurrent gas-liquid slug flow*. 1969.

Greskovich, E. J.; Shrier, A. L. Slug Frequency in Horizontal Gas-Liquid Slug Flow. *Industrial and Engineering Chemistry Process Design and Development*, v. 11, n. 2, 1972. ISSN 01964305.

Hassanlouei, R. N.; Firouzfar, H.; Kasiri, N.; Khanof, M. H. A simple mathematical model for slug liquid holdup in horizontal pipes. *Scientia Iranica*, v. 19, n. 6, p. 1653–1660, 12 2012. ISSN 10263098.

Hernandez-Perez, V.; Abdulkadir, M.; Azzopardi, B. J. Slugging frequency correlation for inclined gas-liquid flow. *World Academy of Science, Engineering and Technology*, v. 61, 2010. ISSN 2010376X.

Heywood, N. I.; Richardson, J. F. Slug flow of air-water mixtures in a horizontal pipe: Determination of liquid holdup by γ-ray absorption. *Chemical Engineering Science*, v. 34, n. 1, 1979. ISSN 00092509.

Hibiki, T.; Ishii, M. One-dimensional drift-flux model and constitutive equations for relative motion between phases in various two-phase flow regimes. *International Journal of Heat and Mass Transfer*, v. 46, n. 25, 2003. ISSN 00179310.

Hill, T. J.; Wood, D. G. New approach to the prediction of slug frequency. In: *Proceedings - SPE Annual Technical Conference and Exhibition*. [S.l.: s.n.], 1990. Pi.

Hout, R. V.; Barnea, D.; Shemer, L. Evolution of statistical parameters of gas-liquid slug flow along vertical pipes. *International Journal of Multiphase Flow*, v. 27, n. 9, 2001. ISSN 03019322.

Jepson, W. P.; Taylor, R. E. Slug flow and its transitions in large-diameter horizontal pipes. *International Journal of Multiphase Flow*, v. 19, n. 3, 1993. ISSN 03019322.

Joseph, D. D. Rise velocity of a spherical cap bubble. *Journal of Fluid Mechanics*, n. 488, 2003. ISSN 00221120.

Kadri, U.; Mudde, R. F.; Oliemans, R. V. Influence of the operation pressure on slug length in near horizontal gas-liquid pipe flow. *International Journal of Multiphase Flow*, v. 36, n. 5, p. 423–431, 5 2010. ISSN 03019322.

Kaichiro, M.; Ishii, M. Flow regime transition criteria for upward two-phase flow in vertical tubes. *International Journal of Heat and Mass Transfer*, v. 27, n. 5, 1984. ISSN 00179310.

Kang, C.; Wilkens, R.; Jepson, W. P. The effect of slug frequency on corrosion in high pressure, inclined pipelines. In: *NACE - International Corrosion Conference Series*. [S.l.]: National Assoc. of Corrosion Engineers International, 1996. v. 1996-March. ISSN 03614409.

Laird, A. D.; Chisholm, D. Pressure and Forces along Cylindrical Bubbles in a Vertical Tube. *Industrial and Engineering Chemistry*, v. 48, n. 8, 1956. ISSN 00197866.

Malnes, D. *Slug flow in vertical, horizontal and inclined pipes*. [S.l.]: Institute for Energy Technology, 1983. 47 p.

Mao, Z.-S.; Dukler, A. E. *Experiments in Fluids An experimental study of gas-liquid slug flow*. [S.l.], 1989. v. 8, 169–182 p.

Marcano, R.; Chen, X. T.; Sarica, C.; Brill, J. P. Study of slug characteristics for two-phase horizontal flow. In: *Proceedings of the SPE International Petroleum Conference & Exhibition of Mexico*. [S.l.: s.n.], 1998. ISSN 09205489.

Massoud, E. Z.; Xiao, Q.; El-Gamal, H. A.; Teamah, M. A. Numerical study of an individual Taylor bubble rising through stagnant liquids under laminar flow regime. *Ocean Engineering*, Elsevier Ltd, v. 162, p. 117–137, 8 2018. ISSN 00298018.

Mayor, T. S.; Ferreira, V.; Pinto, A. M.; Campos, J. B. Hydrodynamics of gas-liquid slug flow along vertical pipes in turbulent regime-An experimental study. *International Journal of Heat and Fluid Flow*, v. 29, n. 4, p. 1039–1053, 8 2008. ISSN 0142727X.

Mi, Y.; Ishii, M.; Tsoukalas, L. H. *Vertical two-phase flow identification using advanced instrumentation and neural networks*. [S.l.], 1998. v. 184, 409–420 p.

Mohmmed, A. O.; Nasif, M. S.; Al-Kayiem, H. H. Experimental data for the slug two-phase flow characteristics in horizontal pipeline. *Data in Brief*, Elsevier Inc., v. 16, p. 527–530, 2 2018. ISSN 23523409.

Moissis, R.; Griffith, P. Entrance effects in a two-phase slug flow. *Journal of Heat Transfer*, v. 84, n. 1, 1962. ISSN 15288943.

Morgado, A. O.; Miranda, J. M.; Araújo, J. D.; Campos, J. B. *Review on vertical gas–liquid slug flow*. 2016.

Nicholson, M. K.; Aziz, K.; Gregory, G. A. Intermittent two phase flow in horizontal pipes: Predictive models. *The Canadian Journal of Chemical Engineering*, v. 56, n. 6, 1978. ISSN 1939019X.

Nicklin, D.; Wilkes, J.; Davidson, J. Two-phase slug flow in vertical tubes. *Trans. Inst. of Chemical Engrs*, v. 40, p. 61, 1961.

Nydal, O. J.; Pintus, . S.; Andreussi, P. *STATISTICAL CHARACTERIZATION OF SLUG FLOW IN HORIZONTAL PIPES*. [S.l.], 1992. v. 18, n. 3, 439–453 p.

Nydal, O. J.; Pintus, S.; Andreussi, P. Statistical characterization of slug flow in horizontal pipes. *International Journal of Multiphase Flow*, v. 18, n. 3, 1992. ISSN 03019322.

OGE. *Visualisation examples*. 2020. Available in: <http://www.ogegraphics.com/visualisation-examples.html>.

Orell, A.; Rembrand+, R. *A Model for Gas-Liquid Slug Flow in a Vertical Tube*. [S.l.]. v. 2, n. 5, 196–206 p.

Polonsky, S.; Barnea, D.; Shemer, L. *Averaged and time-dependent characteristics of the motion of an elongated bubble in a vertical pipe*. [S.l.]. Available in: <www.elsevier.com/locate/ijmulflow>.

Pringle, C. C.; Ambrose, S.; Azzopardi, B. J.; Rust, A. C. The existence and behaviour of large diameter Taylor bubbles. *International Journal of Multiphase Flow*, Elsevier Ltd, v. 72, p. 318–323, 6 2015. ISSN 03019322.

Quan, S. Co-current flow effects on a rising Taylor bubble. *International Journal of Multiphase Flow*, v. 37, n. 8, p. 888–897, 10 2011. ISSN 03019322.

Radovcich, N. A.; Moissis, R. *THE TRANSITION FROM TWO PHASE BUBBLE FLOW TO SLUG FLOW*. [S.l.], 1962.

Reis, E. dos; Leonardo, J. G. Characterization of slug flows in horizontal piping by signal analysis from a capacitive probe. *Flow Measurement and Instrumentation*, v. 21, n. 3, 2010. ISSN 09555986.

Rodrigues, H.; Morales, R.; Rosa, E.; Mazza, R. Modeling and simulation of two-phase horizontal and vertical slug flow patterns with a slug tracking numerical model. *Boletim Tecnico da Producao de Petroleo*, Petroleo Brasileiro S.A., v. 4, n. 1, p. 105–124, 2009. ISSN 18096751.

Rodrigues, R. L. P. et al. Statistical features of the flow evolution in horizontal liquid-gas slug flow. *Experimental Thermal and Fluid Science*, v. 119, p. 110203, 2020. ISSN 0894-1777. Available in: <http://www.sciencedirect.com/science/article/pii/S089417772030707X>.

Rosa, E. S. *Escoamento Multifásico Isotérmico*. [S.l.: s.n.], 2012. ISBN 9788540700727.

Sæther, G.; Bendiksen, K.; Müller, J.; Frøland, E. The fractal statistics of liquid slug lengths. *International Journal of Multiphase Flow*, v. 16, n. 6, 1990. ISSN 03019322.

Santim, C. G.; Gaspari, E. F.; Paternost, G. M. A transient analysis of gas-liquid slug flow inside a horizontal pipe using different models. *Journal of Petroleum Science and Engineering*, Elsevier B.V., v. 151, p. 62–76, 2017. ISSN 09204105.

Scott, S. L.; Shoham, O.; Brill, J. P. Prediction of slug length in horizontal, large-diameter pipes. *SPE Production Engineering*, v. 4, n. 3, 1989. ISSN 08859221.

Shoham, O. Mechanistic Modeling of Gas-Liquid Two-Phase Flow in Pipes. *Society of Petroleum Engineers*, p. 2006, 2006.

Sylvester, N. D. *A Mechanistic Model for Two-Phase Vertical Slug Flow in Pipes*. [S.l.], 1987. Available in: <http://asme.org/terms>.

Taitel, Y.; Barnea, D. Two-Phase Slug Flow. *Advances in Heat Transfer*, v. 20, n. C, 1990. ISSN 00652717.

Taitel, Y.; Barnea, D. Slug-tracking model for hilly terrain pipelines. *SPE Journal*, v. 5, n. 1, 2000. ISSN 1086055X.

Taitel, Y.; Dukler, A. E. A model for predicting flow regime transitions in horizontal and near horizontal gas-liquid flow. *AIChE Journal*, v. 22, n. 1, 1976. ISSN 15475905.

Thomas, J. E. *Fundamentos de engenharia de petróleo*. [S.l.: s.n.], 2001. Único. ISSN 00394521.

Trononi, E. Prediction of slug frequency in horizontal two-phase slug flow. *AIChE Journal*, v. 36, n. 5, 1990. ISSN 15475905.

Viana, F.; Pardo, R.; Yánez, R.; Trallero, J. L.; Joseph, D. D. Universal correlation for the rise velocity of long gas bubbles in round pipes. *Journal of Fluid Mechanics*, n. 494, p. 379–398, 11 2003. ISSN 00221120.

Vicencio, F. E. C. *Caracterização experimental do escoamento intermitente líquido-gás em tubulações horizontais*. 129 p. Tese (Doutorado) — Federal University of Technology of Paraná, 2013.

Wang, X.; Guo, L.; Zhang, X. An experimental study of the statistical parameters of gas-liquid two-phase slug flow in horizontal pipeline. *International Journal of Heat and Mass Transfer*, v. 50, n. 11-12, 2007. ISSN 00179310.

Weber, M. E. *Drift in intermittent two-phase flow in horizontal pipes*. 1981.

White, E. T.; Beardmore, R. H. *The velocity of rise of single cylindrical air bubbles through liquids contained in vertical tubes*. [S.l.], 1962. v. 17, 351–361 p.

Widyatama, A.; Dinaryanto, O.; Indarto; Deendarlianto. The development of image processing technique to study the interfacial behavior of air-water slug two-phase flow in horizontal pipes. *Flow Measurement and Instrumentation*, Elsevier Ltd, v. 59, p. 168–180, 3 2018. ISSN 09555986.

Yadigaroglu, G.; Hewitt, G. *Introduction to Multiphase Flow*. [S.l.: s.n.], 2018. 214 p. ISBN 978-3-319-58718-9.

Yin, P.; Cao, X.; Li, Y.; Yang, W.; Bian, J. Experimental and numerical investigation on slug initiation and initial development behavior in hilly-terrain pipeline at a low superficial liquid velocity. *International Journal of Multiphase Flow*, Elsevier Ltd, v. 101, p. 85–96, 4 2018. ISSN 03019322.

Zabaras, G. J. Prediction of slug frequency for gas/liquid flows. *SPE Journal*, v. 5, n. 3, 2000. ISSN 1086055X.

Zheng, D.; Che, D. Experimental study on hydrodynamic characteristics of upward gas-liquid slug flow. *International Journal of Multiphase Flow*, v. 32, n. 10-11, p. 1191–1218, 10 2006. ISSN 03019322.

APPENDIX A – Statistical distribution fitting

The result of the present study consists in a data bank. Part of the data analysis consists in fitting statistical distribution to the data, which can be done by using the chi-square test method.

The chi-square test measures the goodness of fit (or adherence) of observed occurrences during an experiment against the expected occurrences for a given distribution. Furthermore, the test can also be used to determine the association degree between two variables. One of its limitations, though, is relative to the number of observations made. If the interval has less than five samples, it is recommended to agglutinate it with another adjacent interval.

The statistic of interest of the test is the chi-square, defined in Eq. A.1.

$$\chi^2 = \sum_{i=1}^{k} \frac{(O_i - E_i)^2}{E_i}, \tag{A.1}$$

where O_i is the i-th observed value, E_i is the i-th expected value and k is the total number of values.

The chi-square test null hypothesis presuppose that values observed and expected are equal, given the significance level. The computed chi-square value for the current data set should be compared to its critical value, which depends on the degrees of freedom of the data set, as well as the desired level of significance. If the critical chi-square is less or equal than the computed chi-square, the null hypothesis is confirmed and the data can be represented by the chosen distribution.

APPENDIX B – Eulerian results

Figure 63 – Histograms and log-logistic fits for P1 hydrodynamic parameters.

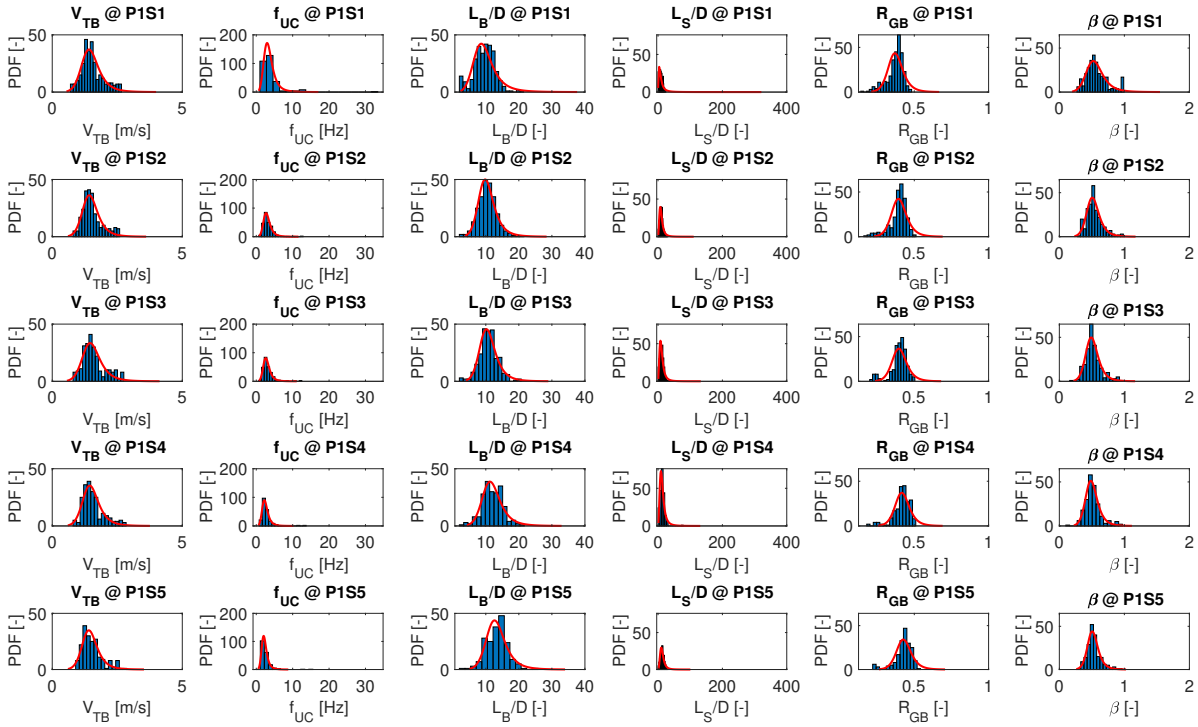

Source: The author.

Figure 64 – Histograms and log-logistic fits for P2 hydrodynamic parameters.

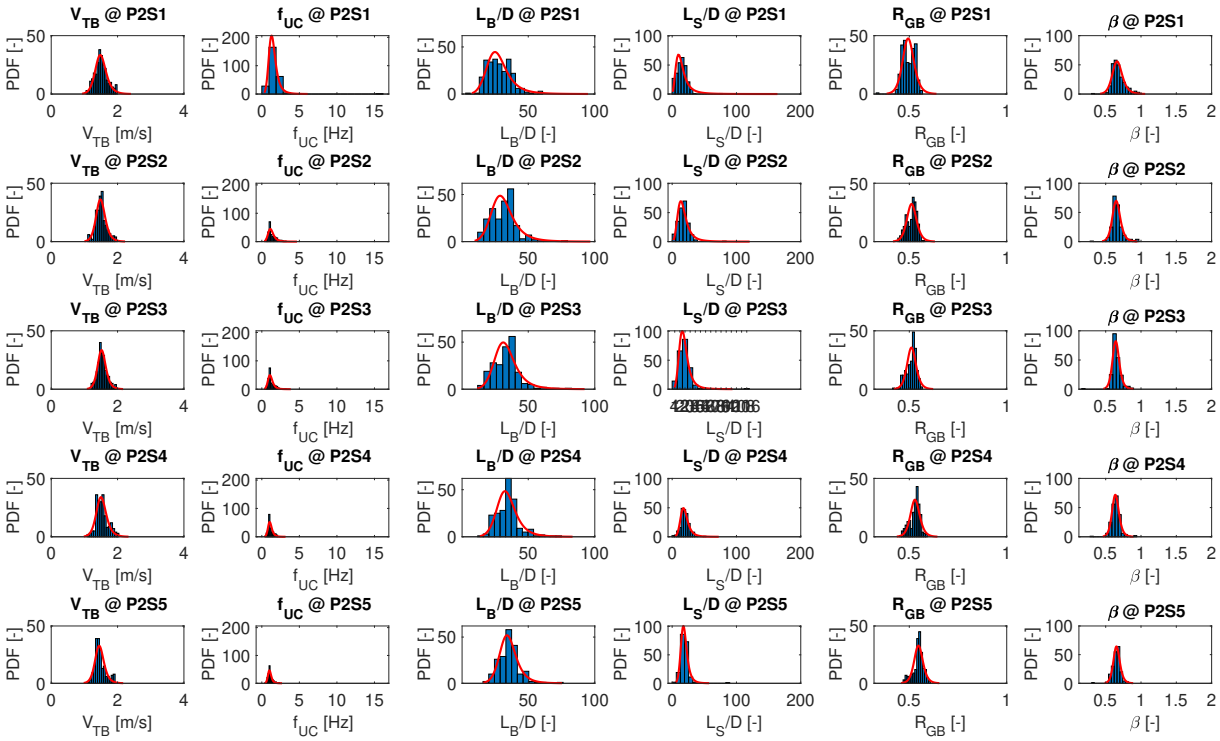

Source: The author.

Figure 65 – Histograms and log-logistic fits for P3 hydrodynamic parameters.

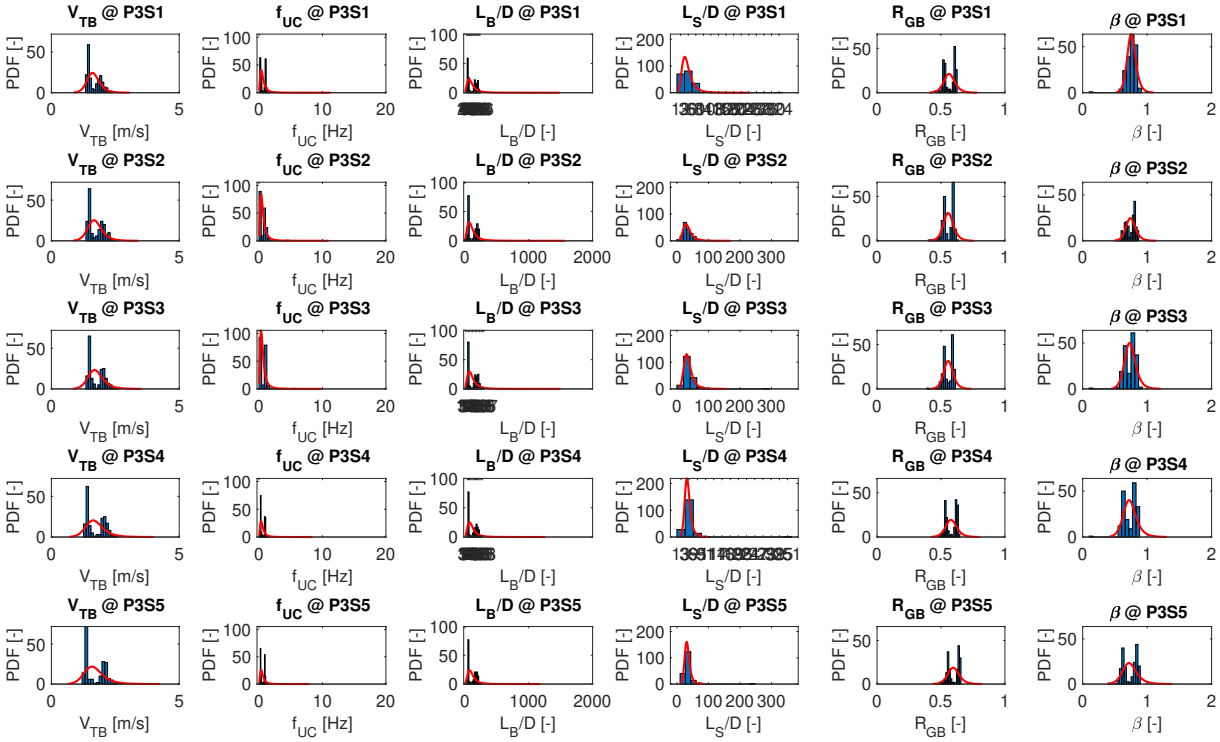

Source: The author.

Figure 66 – Histograms and log-logistic fits for P4 hydrodynamic parameters.

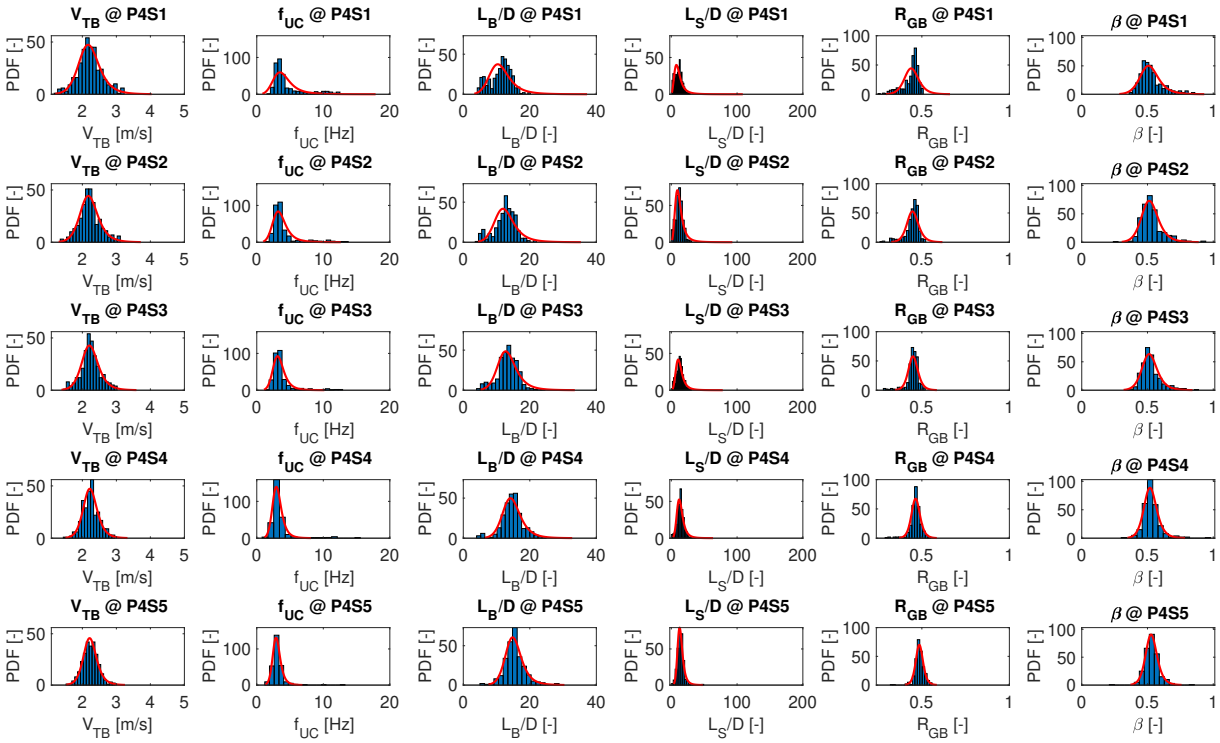

Source: The author.

Figure 67 – Histograms and log-logistic fits for P5 hydrodynamic parameters.

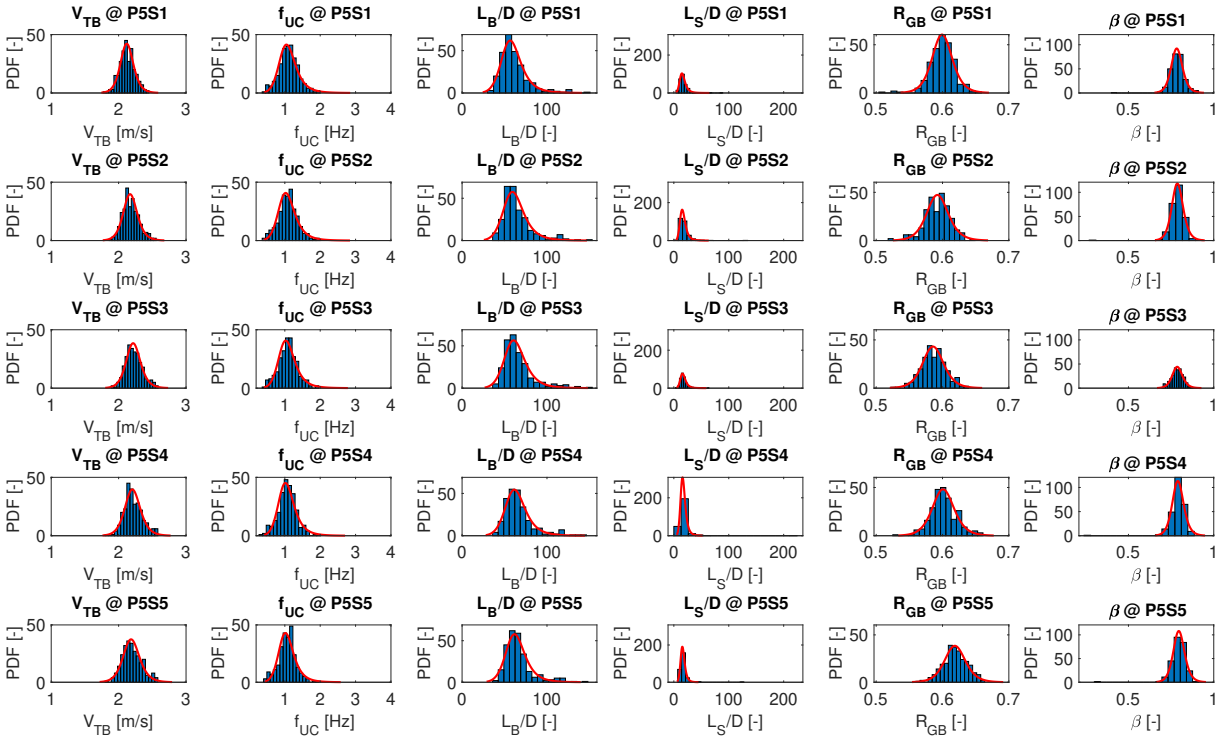

Source: The author.

Figure 68 – Histograms and log-logistic fits for P6 hydrodynamic parameters.

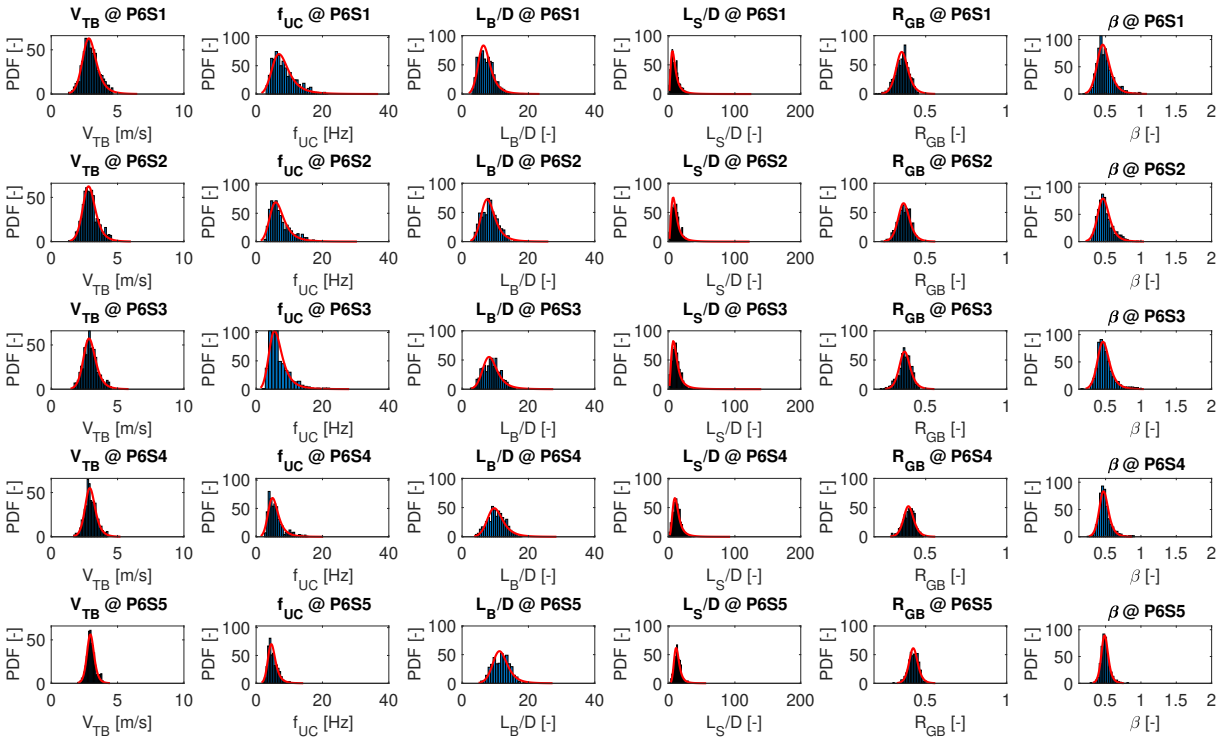

Source: The author.

Figure 69 – Histograms and log-logistic fits for P7 hydrodynamic parameters.

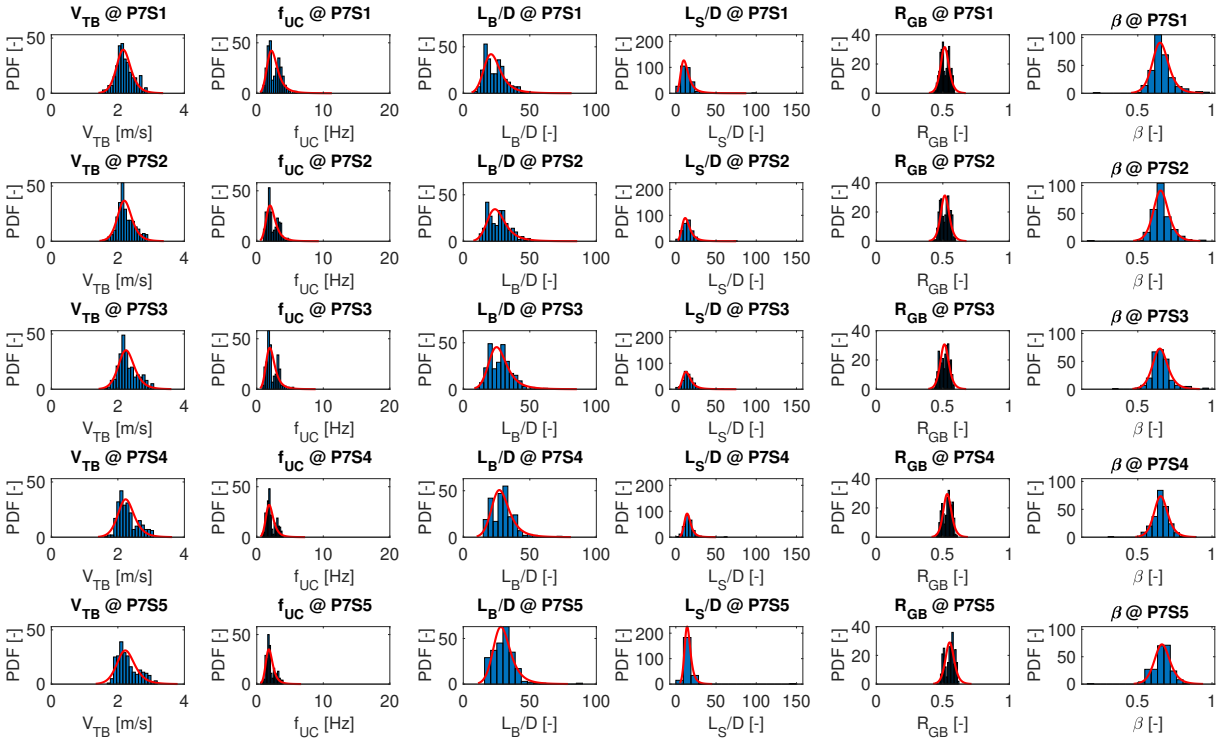

Source: The author.

Figure 70 – Histograms and log-logistic fits for P8 hydrodynamic parameters.

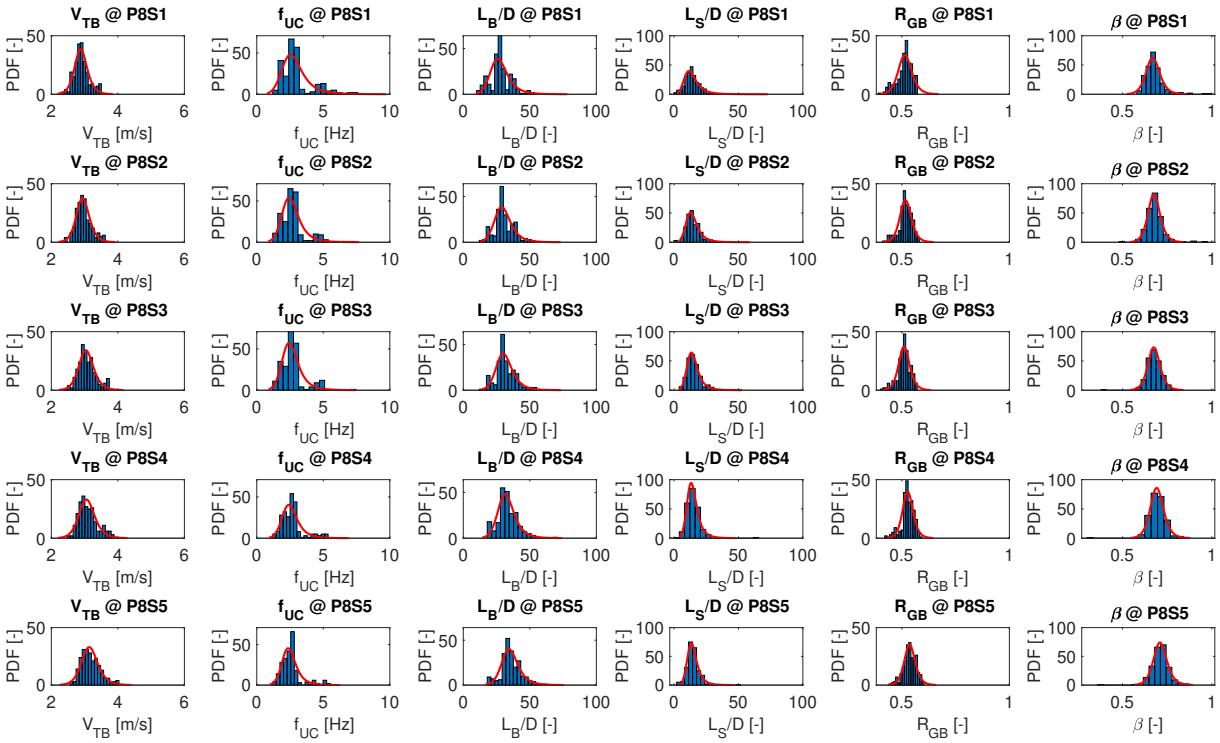

Source: The author.

Figure 71 – Histograms and log-logistic fits for P9 hydrodynamic parameters.

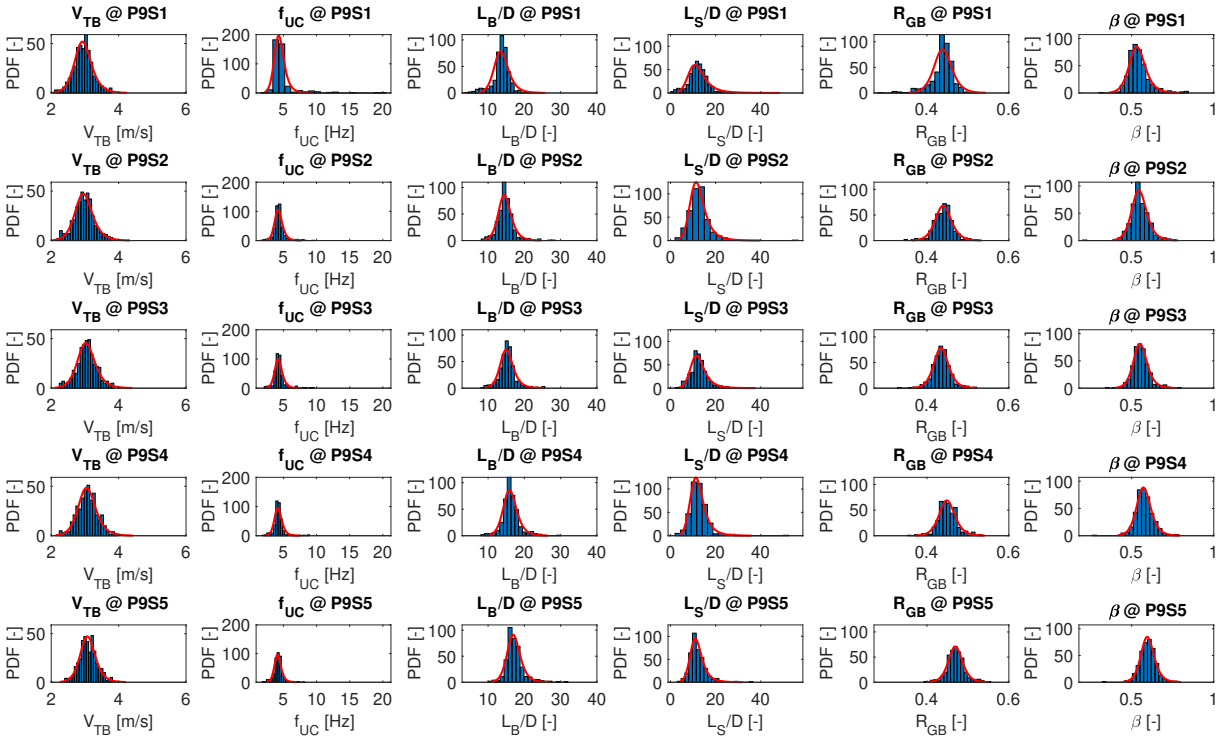

Source: The author.

Figure 72 – Histograms and log-logistic fits for P10 hydrodynamic parameters.

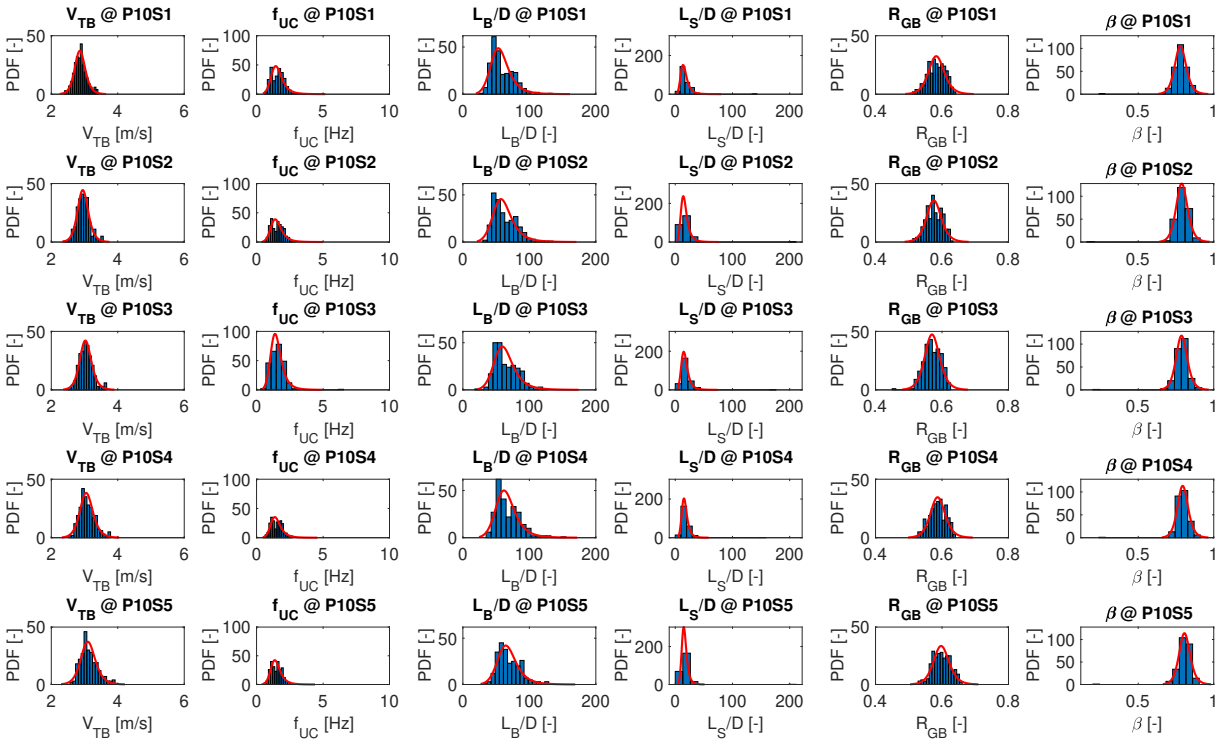

Source: The author.

Figure 73 – Histograms and log-logistic fits for P11 hydrodynamic parameters.

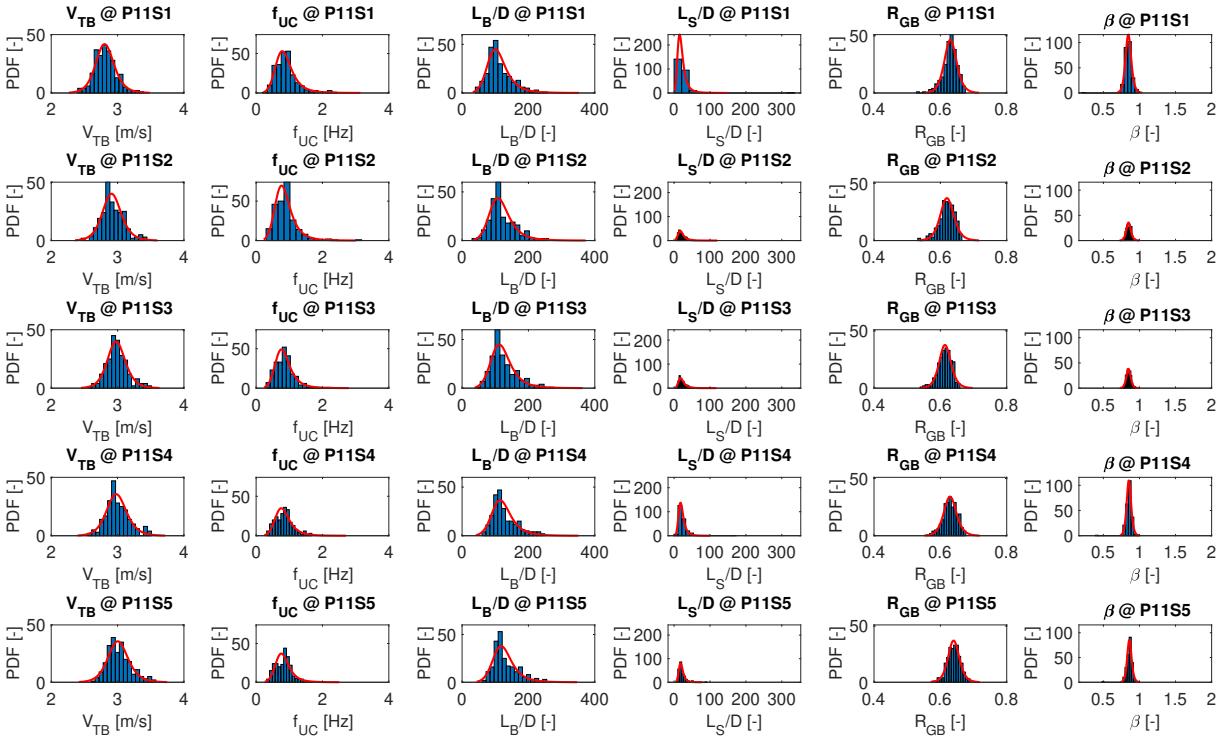

Source: The author.

Figure 74 – Histograms and log-logistic fits for P12 hydrodynamic parameters.

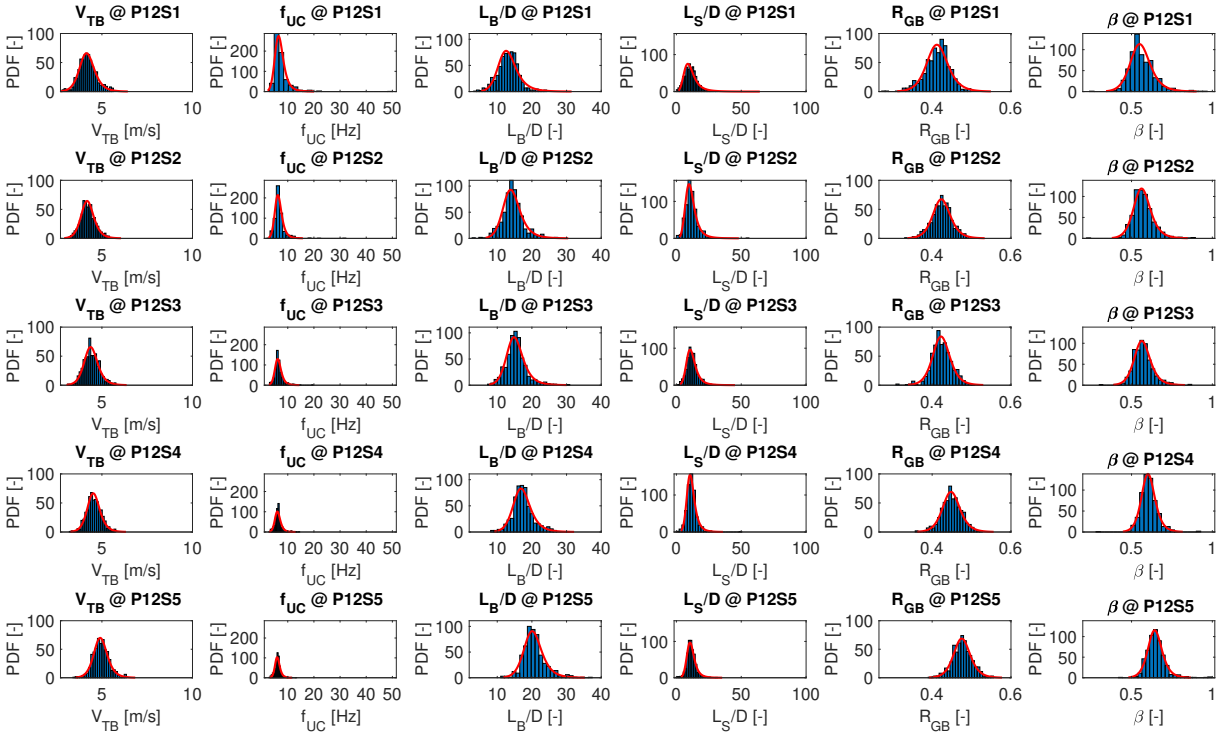

Source: The author.

Figure 75 – Histograms and log-logistic fits for P13 hydrodynamic parameters.

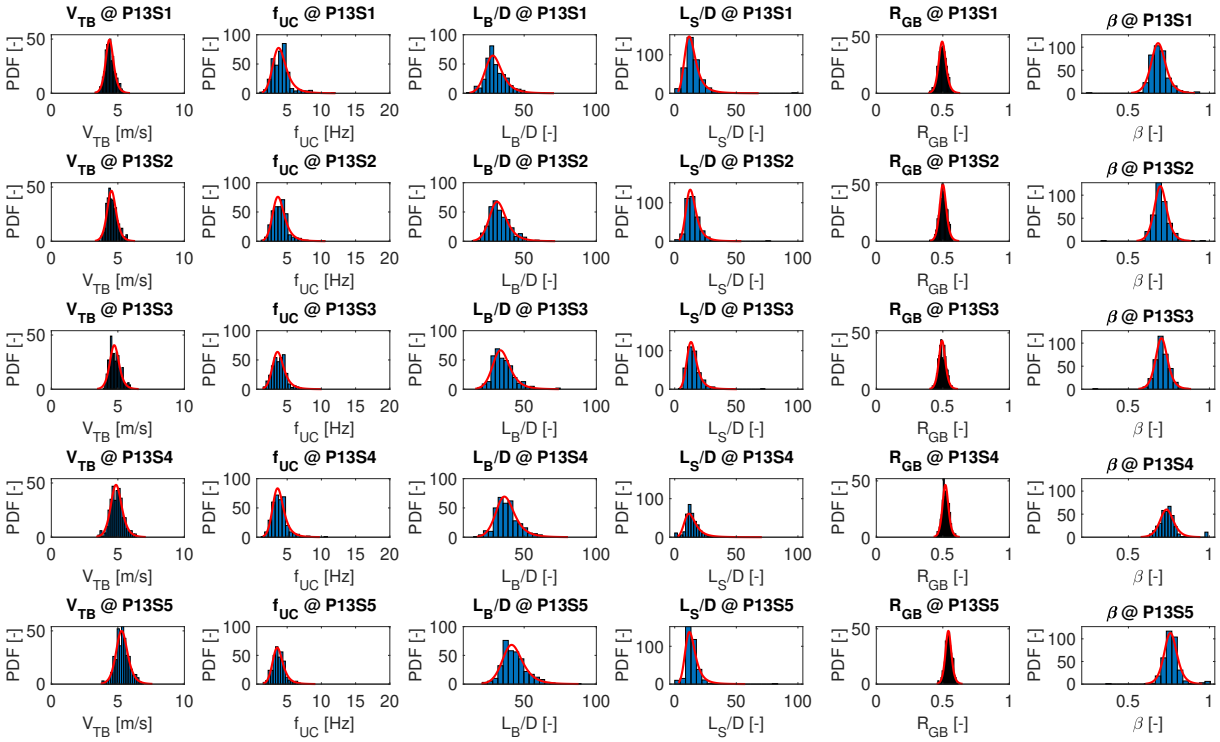

Source: The author.

Figure 76 – Histograms and log-logistic fits for P14 hydrodynamic parameters.

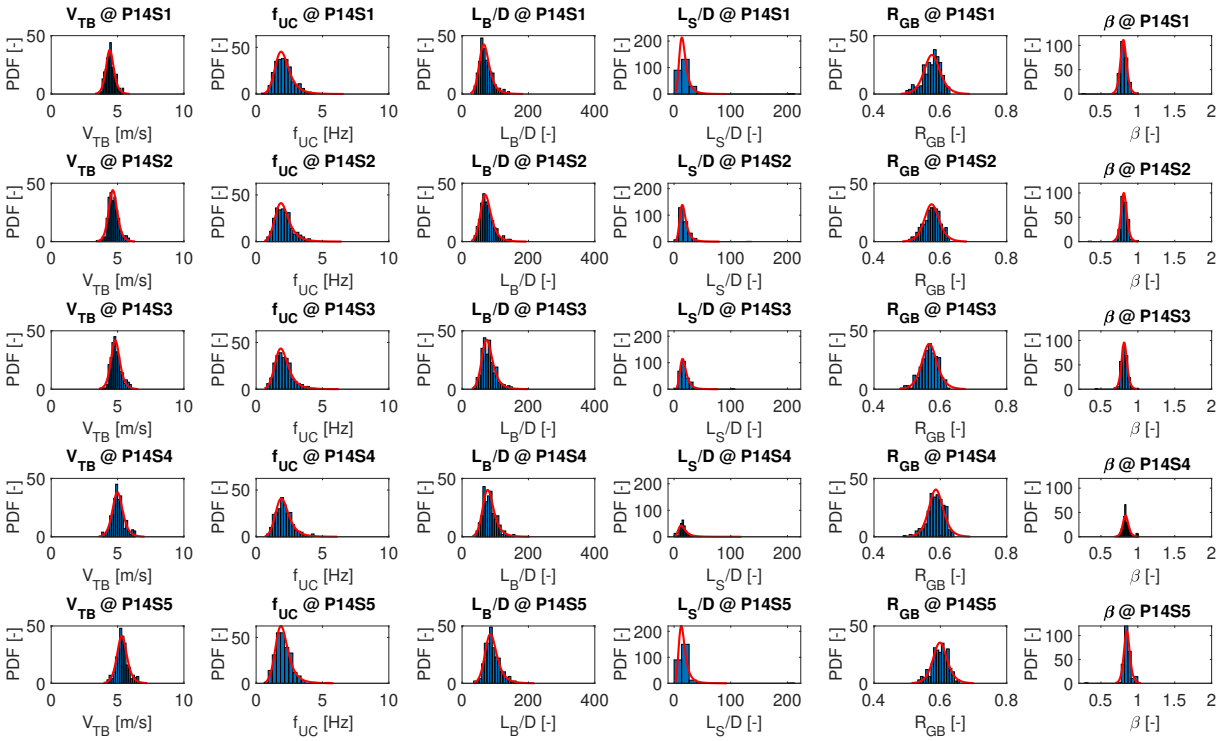

Source: The author.

Figure 77 – Histograms and log-logistic fits for P15 hydrodynamic parameters.

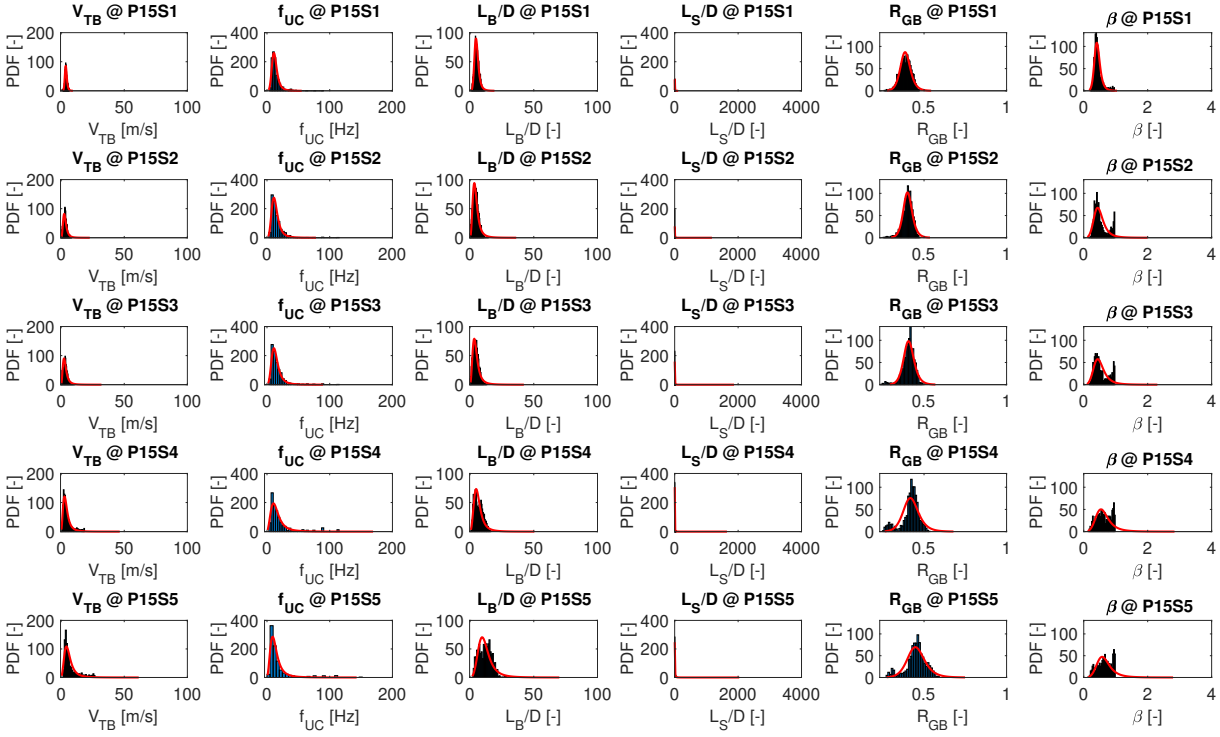

Source: The author.

Figure 78 – Histograms and log-logistic fits for P16 hydrodynamic parameters.

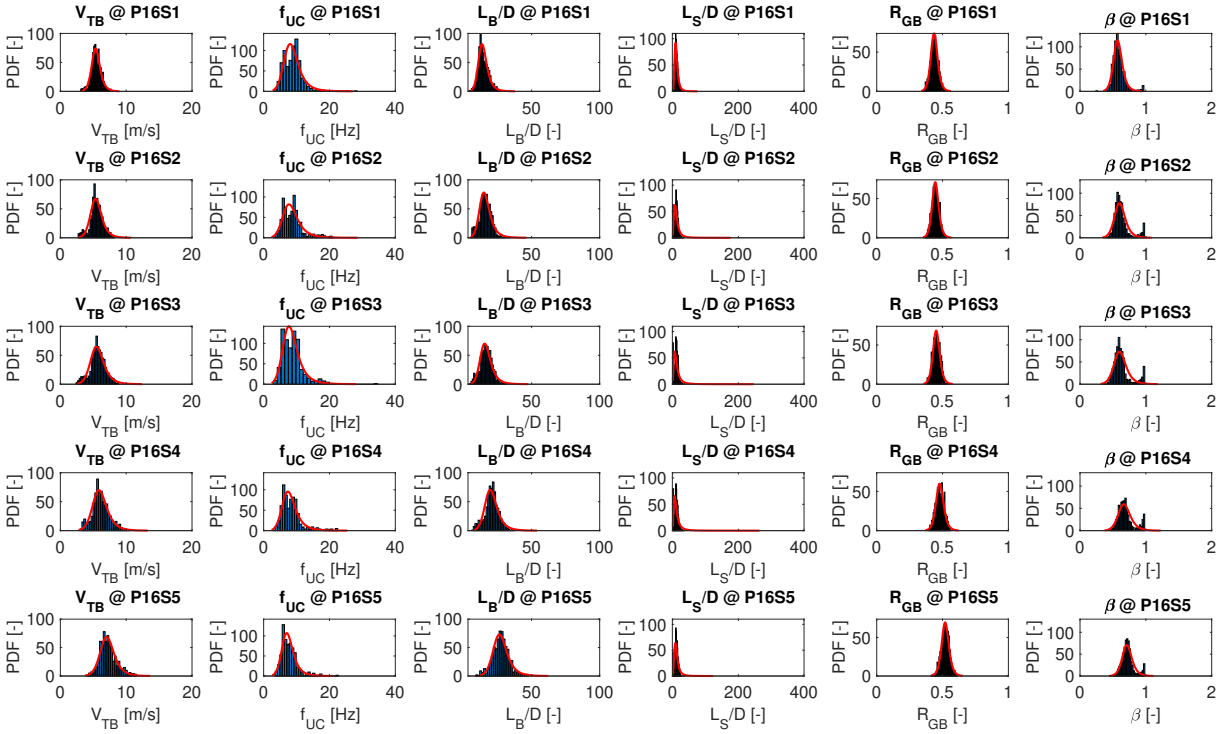

Source: The author.

Figure 79 – Histograms and log-logistic fits for P17 hydrodynamic parameters.

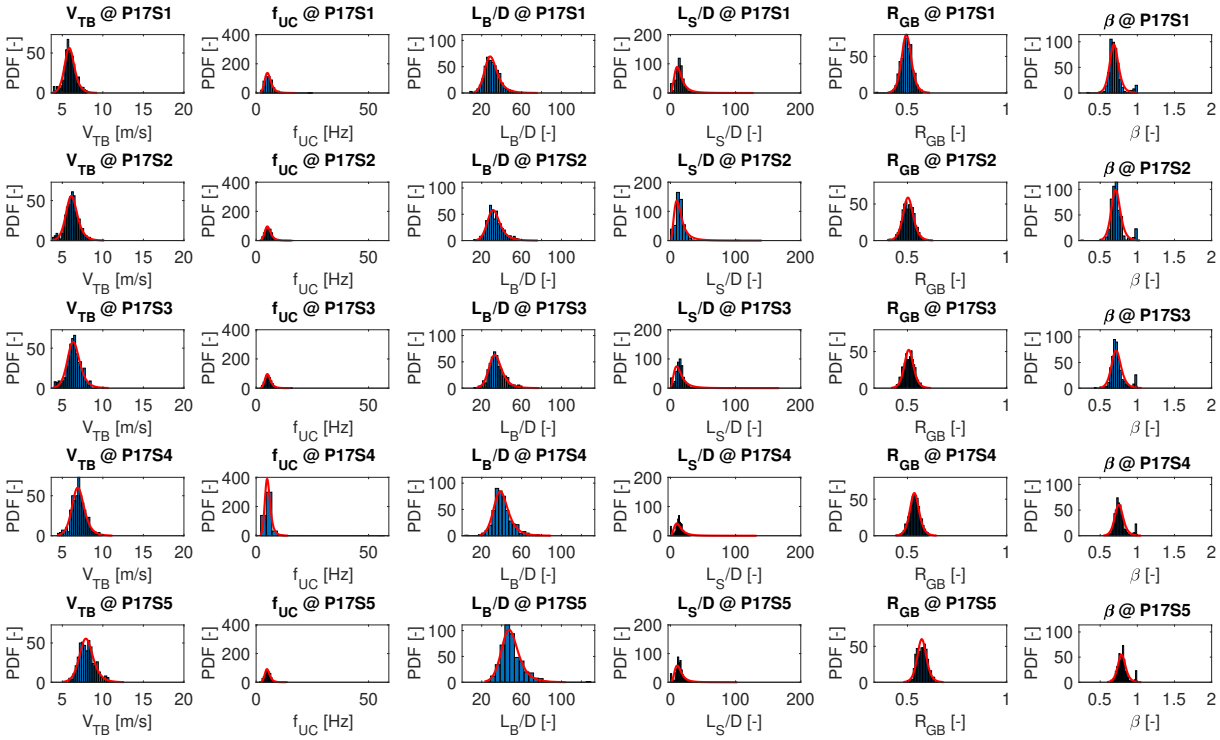

Source: The author.

Figure 80 – Histograms and log-logistic fits for P18 hydrodynamic parameters.

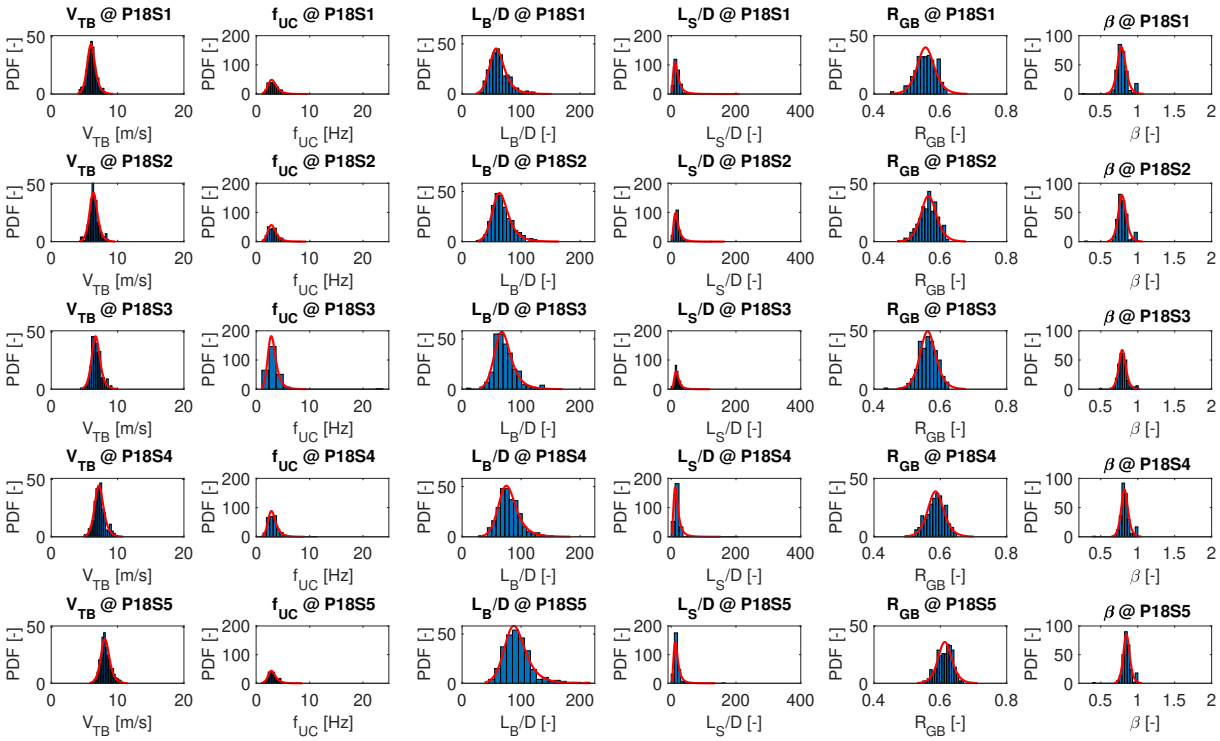

Source: The author.

APPENDIX C – Lagrangian results

Figure 81 – P1 hydrodynamic parameters percent change between stations 1 and 5.

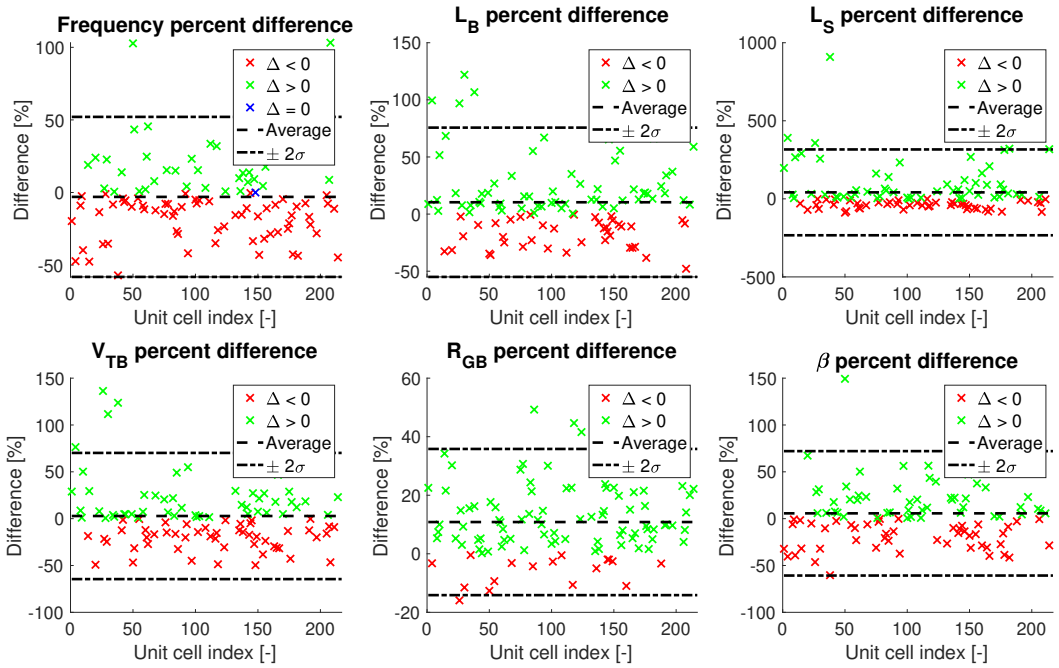

Source: The author.

Figure 82 – P2 hydrodynamic parameters percent change between stations 1 and 5.

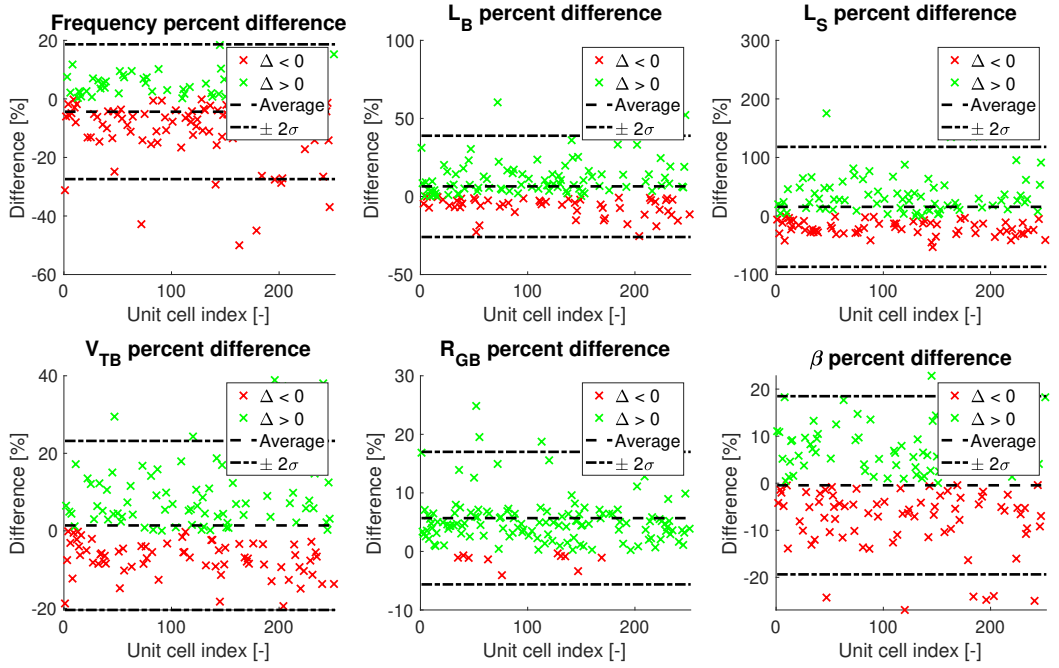

Source: The author.

Figure 83 – P3 hydrodynamic parameters percent change between stations 1 and 5.

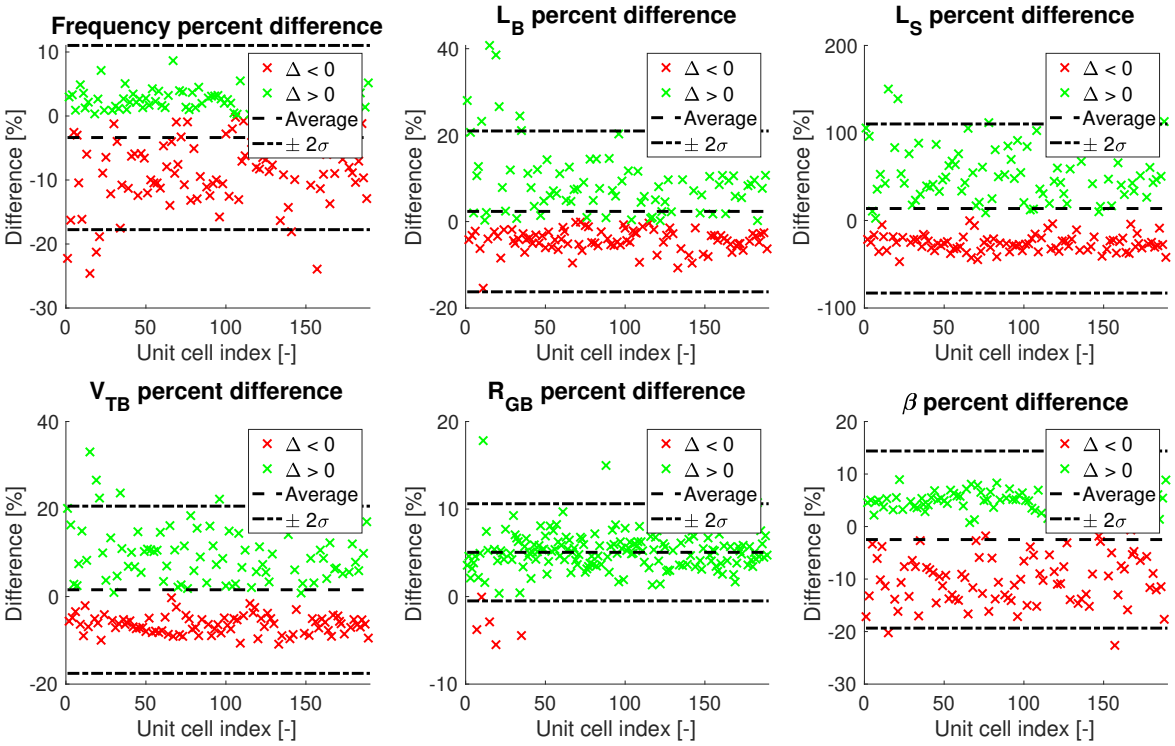

Source: The author.

Figure 84 – P4 hydrodynamic parameters percent change between stations 1 and 5.

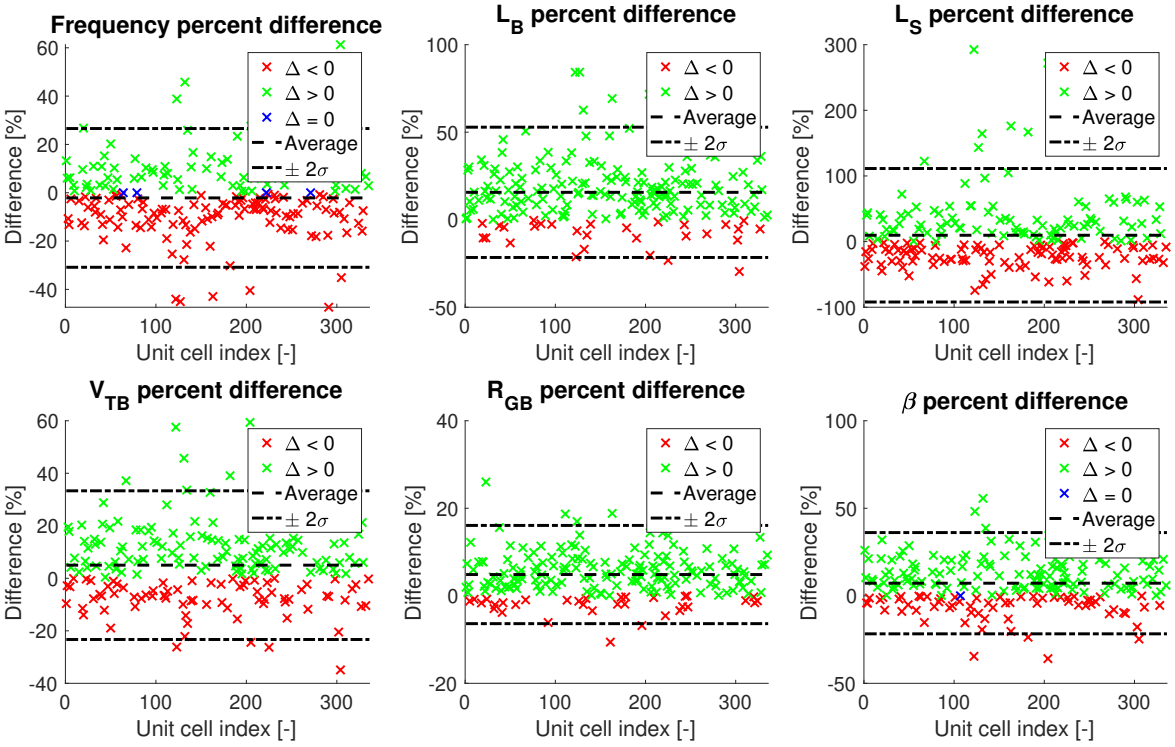

Source: The author.

Figure 85 – P5 hydrodynamic parameters percent change between stations 1 and 5.

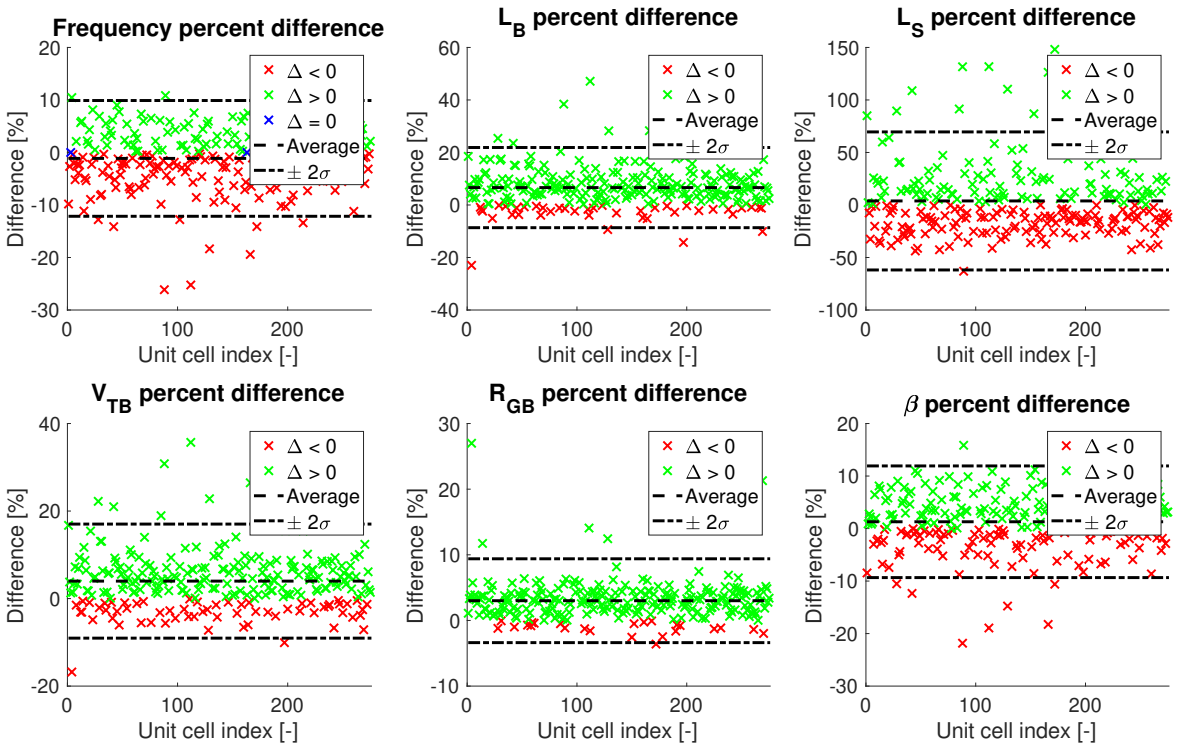

Source: The author.

Figure 86 – P6 hydrodynamic parameters percent change between stations 1 and 5.

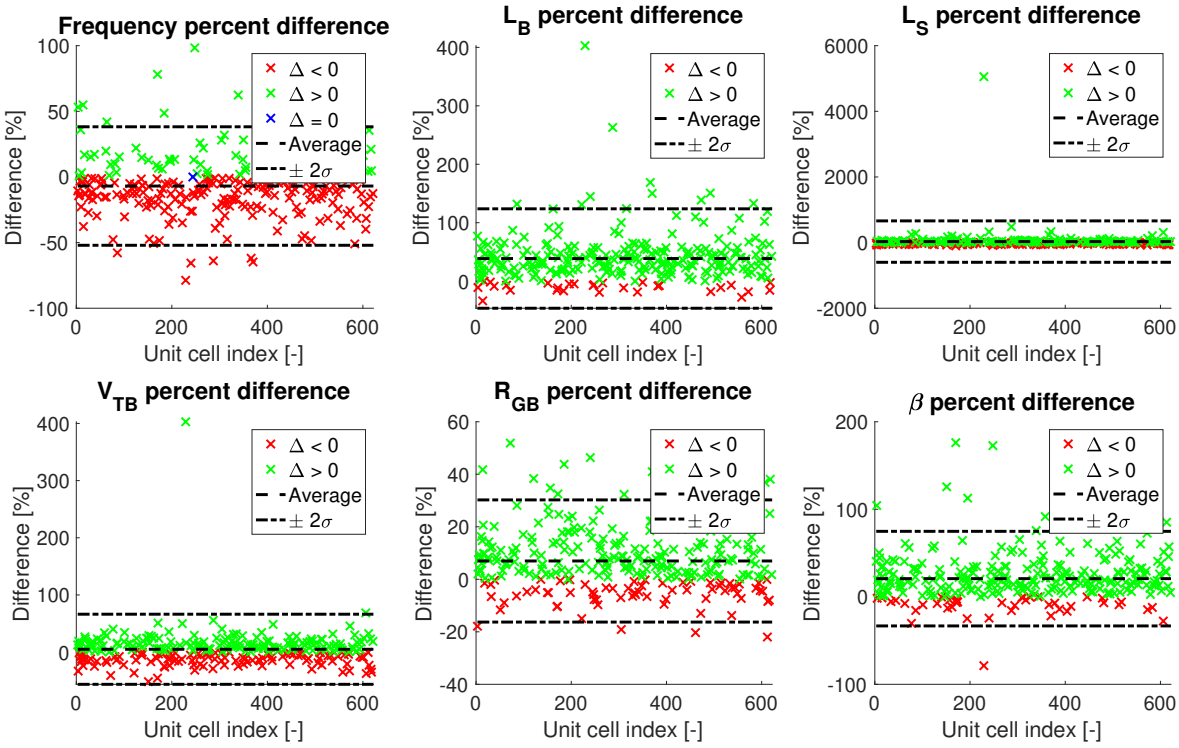

Source: The author.

Figure 87 – P7 hydrodynamic parameters percent change between stations 1 and 5.

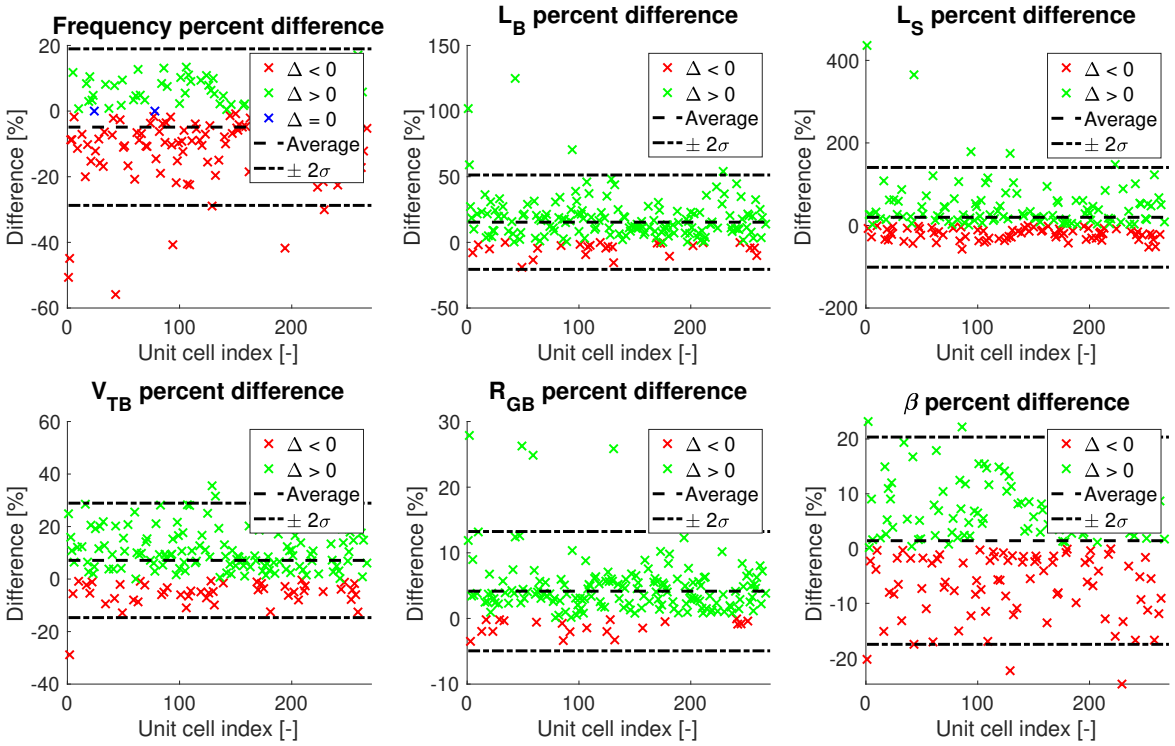

Source: The author.

Figure 88 – P8 hydrodynamic parameters percent change between stations 1 and 5.

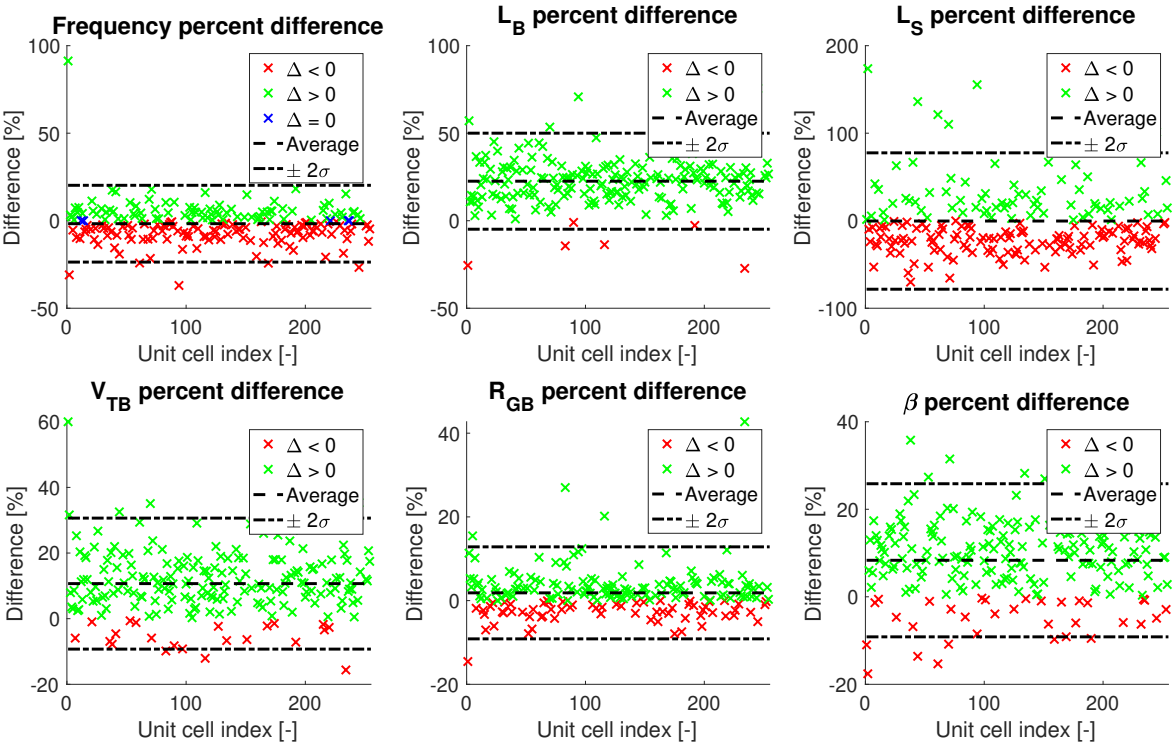

Source: The author.

Figure 89 – P9 hydrodynamic parameters percent change between stations 1 and 5.

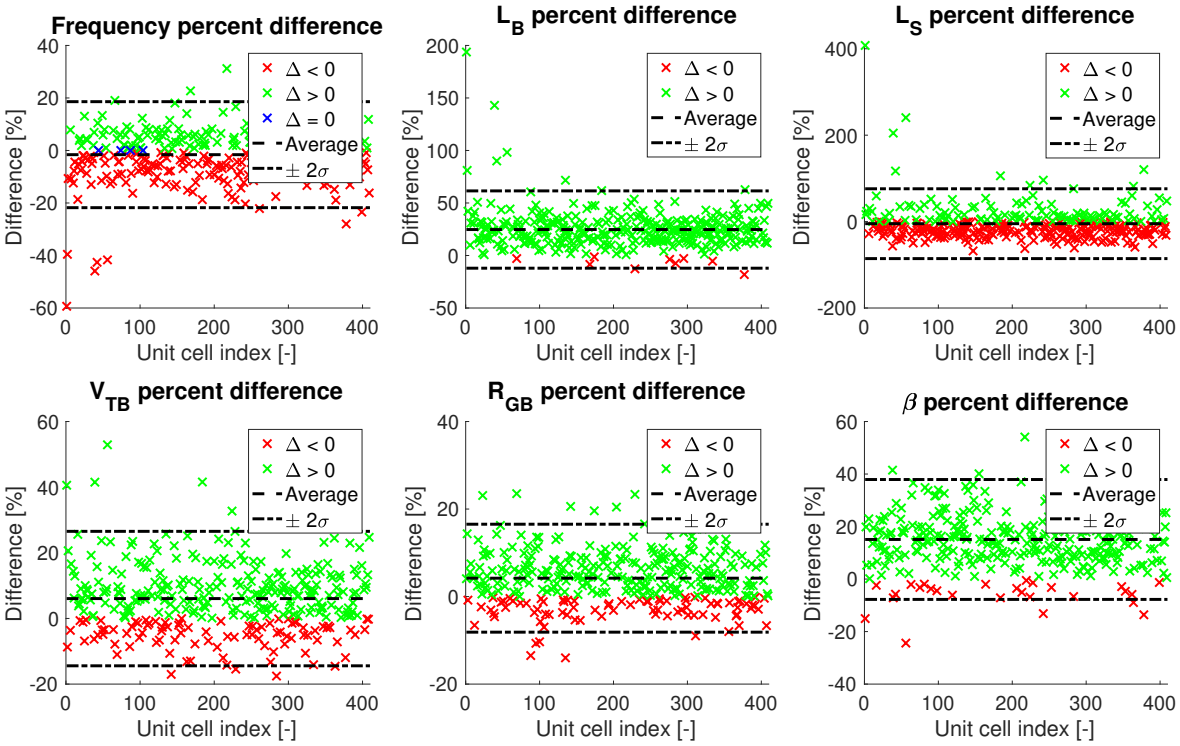

Source: The author.

Figure 90 – P10 hydrodynamic parameters percent change between stations 1 and 5.

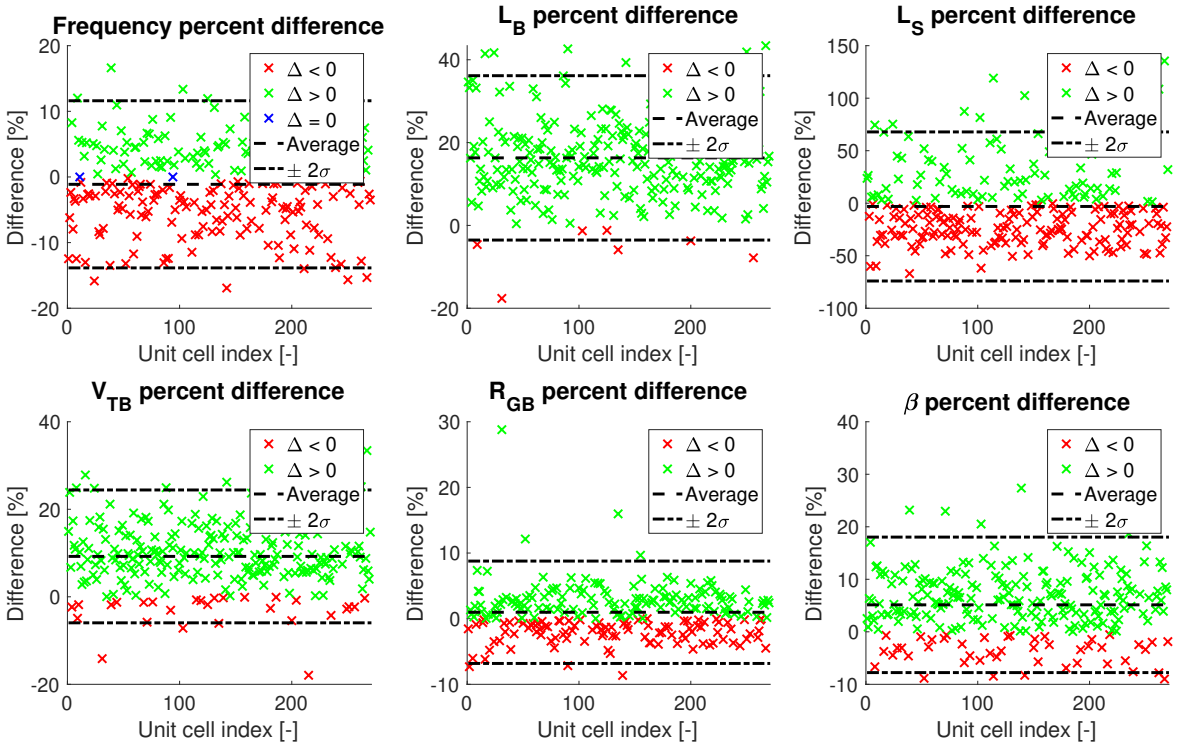

Source: The author.

Figure 91 – P11 hydrodynamic parameters percent change between stations 1 and 5.

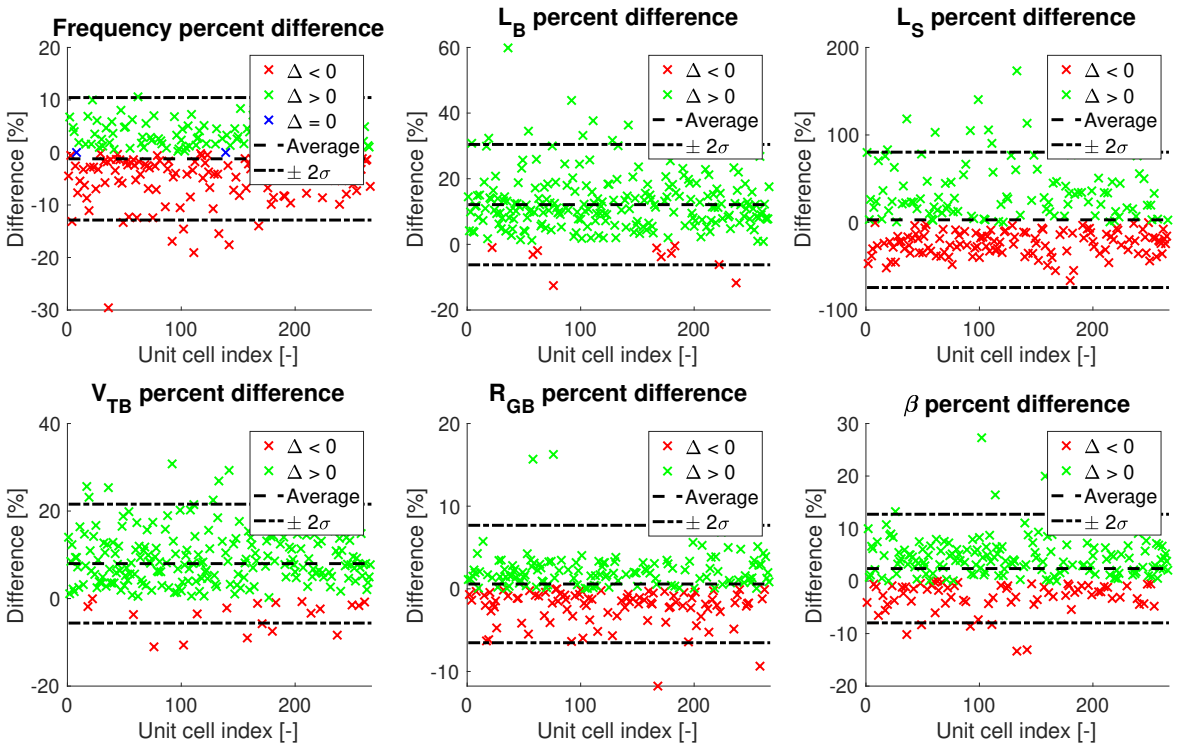

Source: The author.

Figure 92 – P12 hydrodynamic parameters percent change between stations 1 and 5.

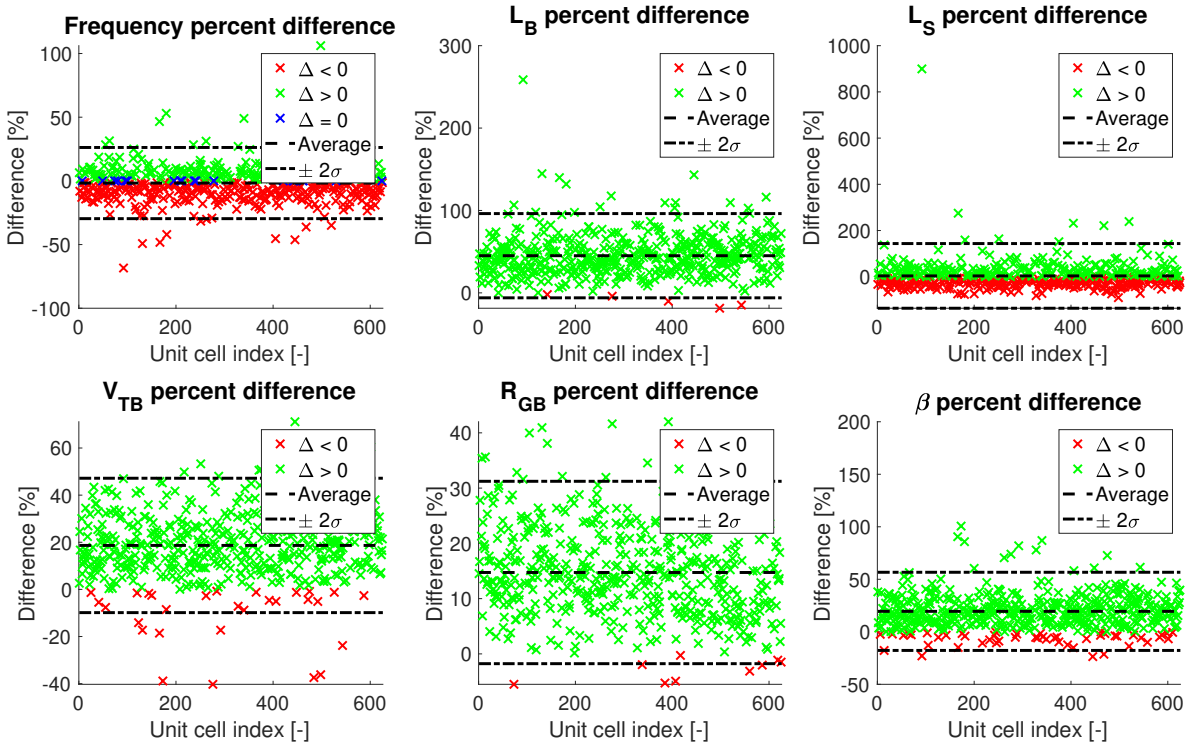

Source: The author.

Figure 93 – P13 hydrodynamic parameters percent change between stations 1 and 5.

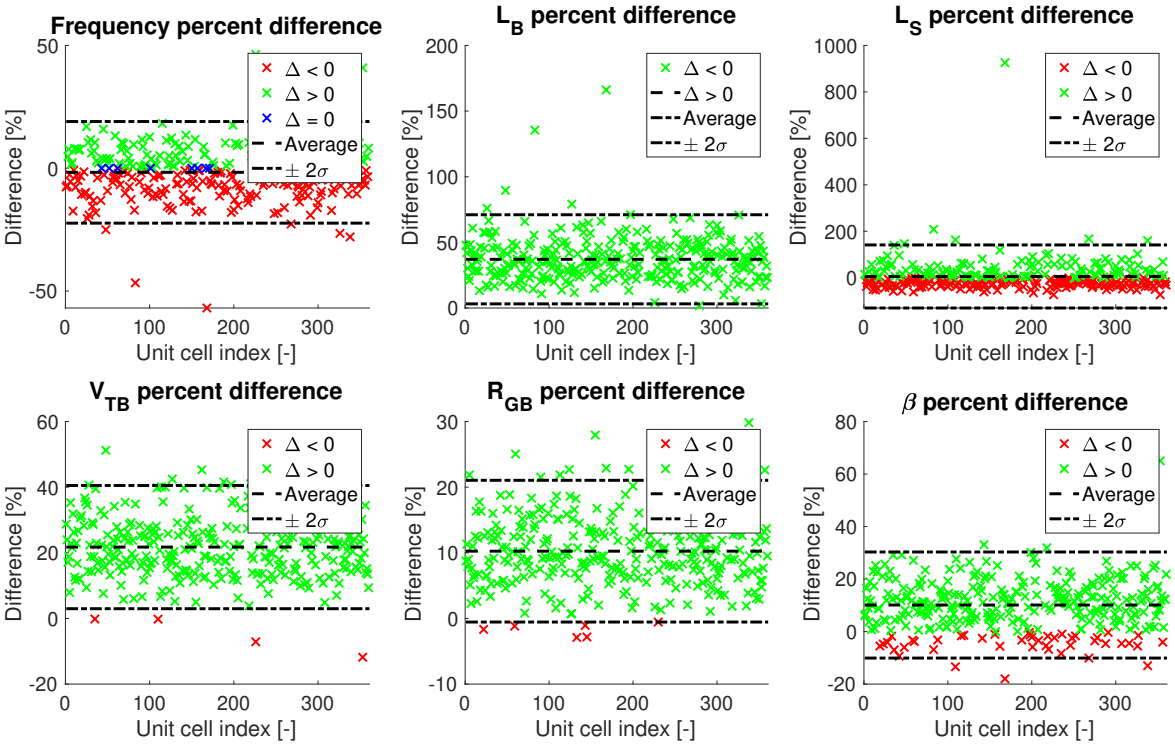

Source: The author.

Figure 94 – P14 hydrodynamic parameters percent change between stations 1 and 5.

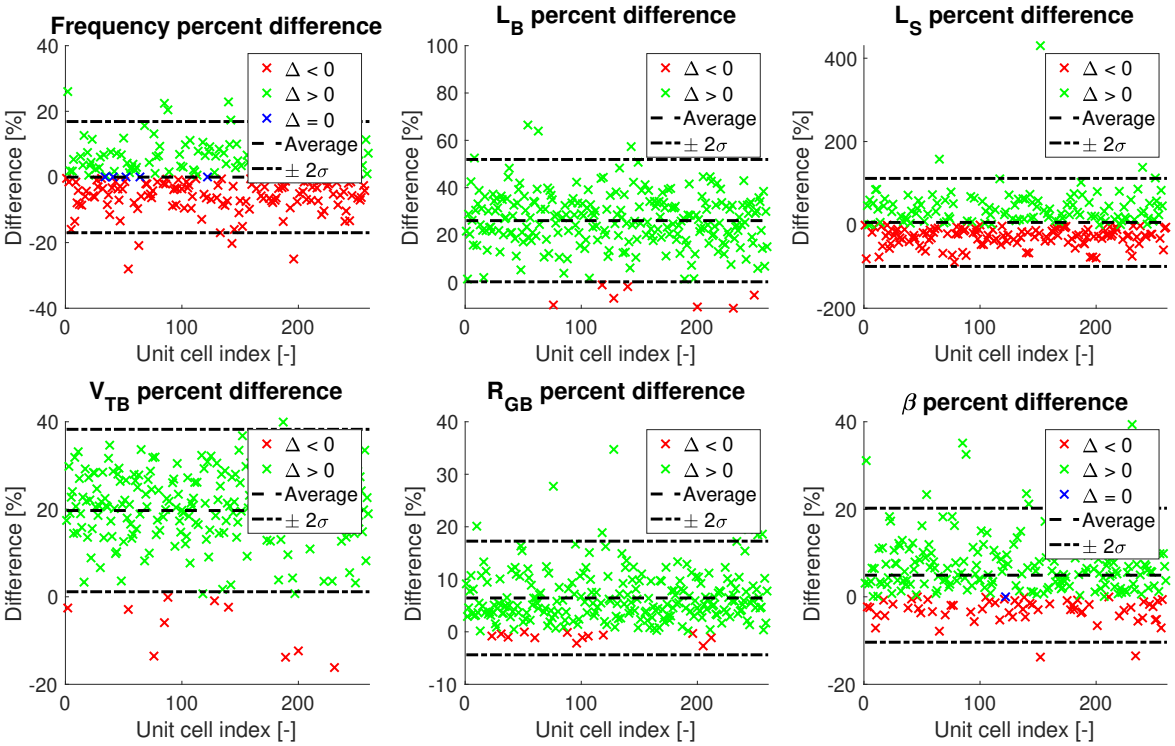

Source: The author.

Figure 95 – P15 hydrodynamic parameters percent change between stations 1 and 5.

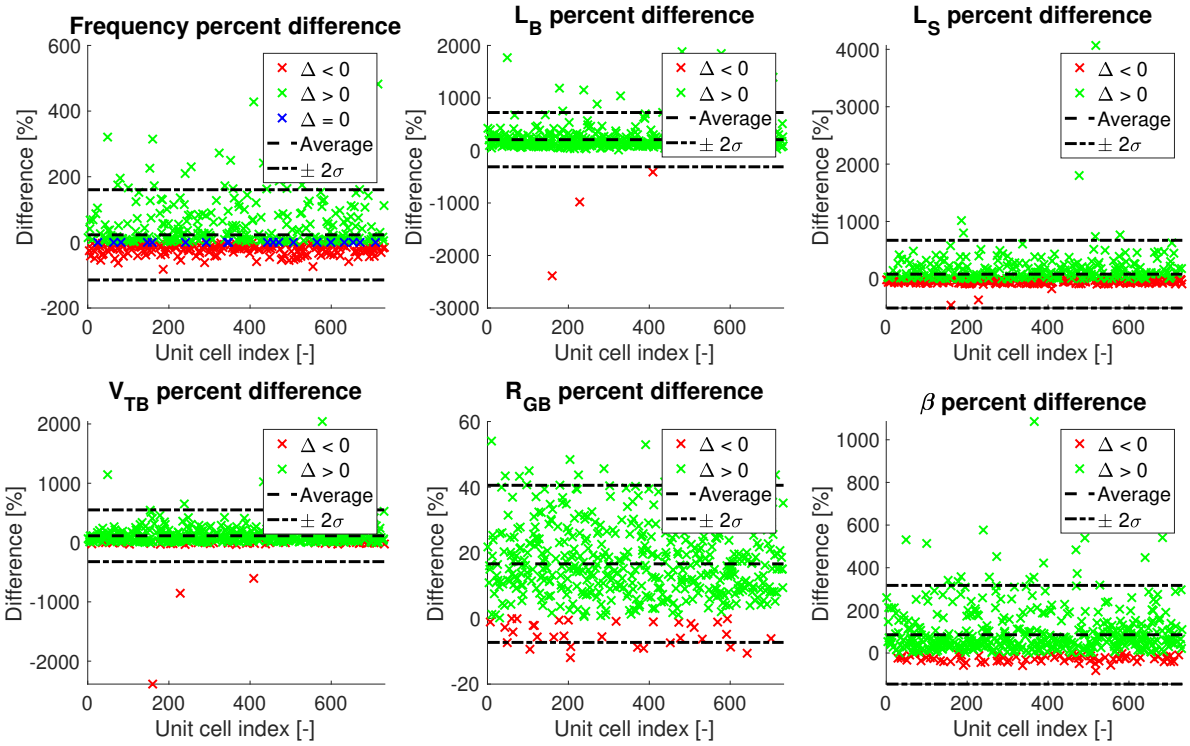

Source: The author.

Figure 96 – P16 hydrodynamic parameters percent change between stations 1 and 5.

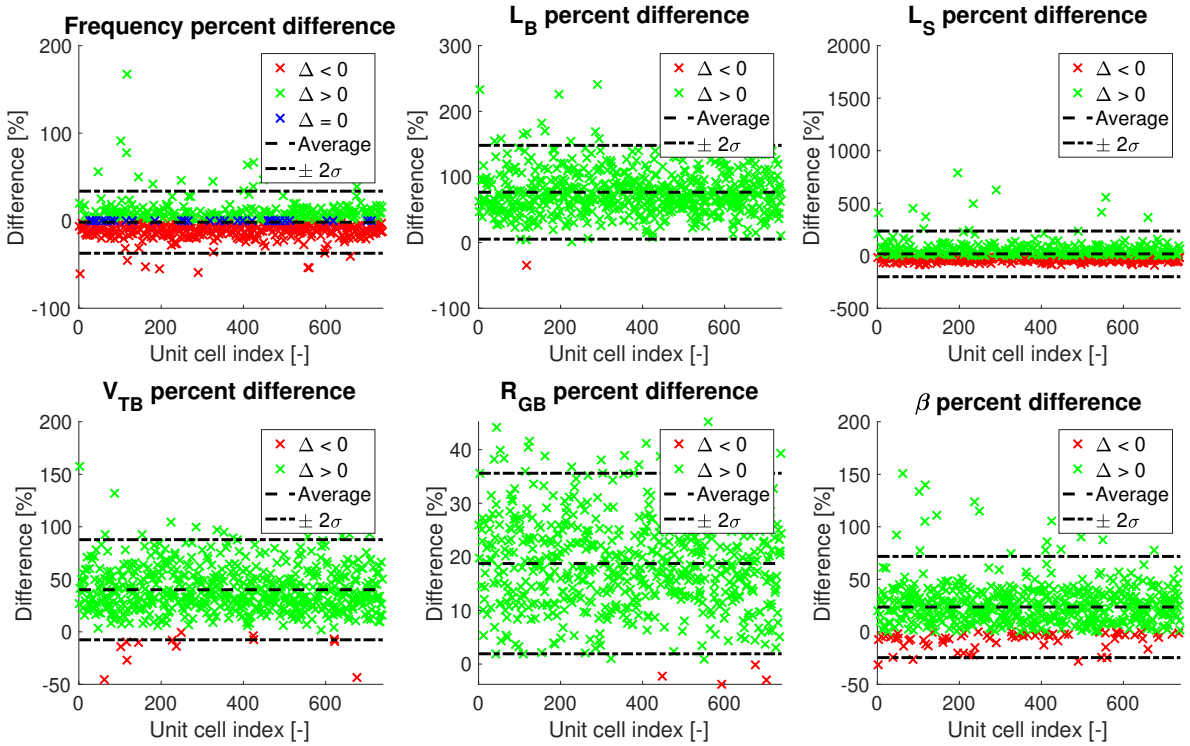

Source: The author.

Figure 97 – P17 hydrodynamic parameters percent change between stations 1 and 5.

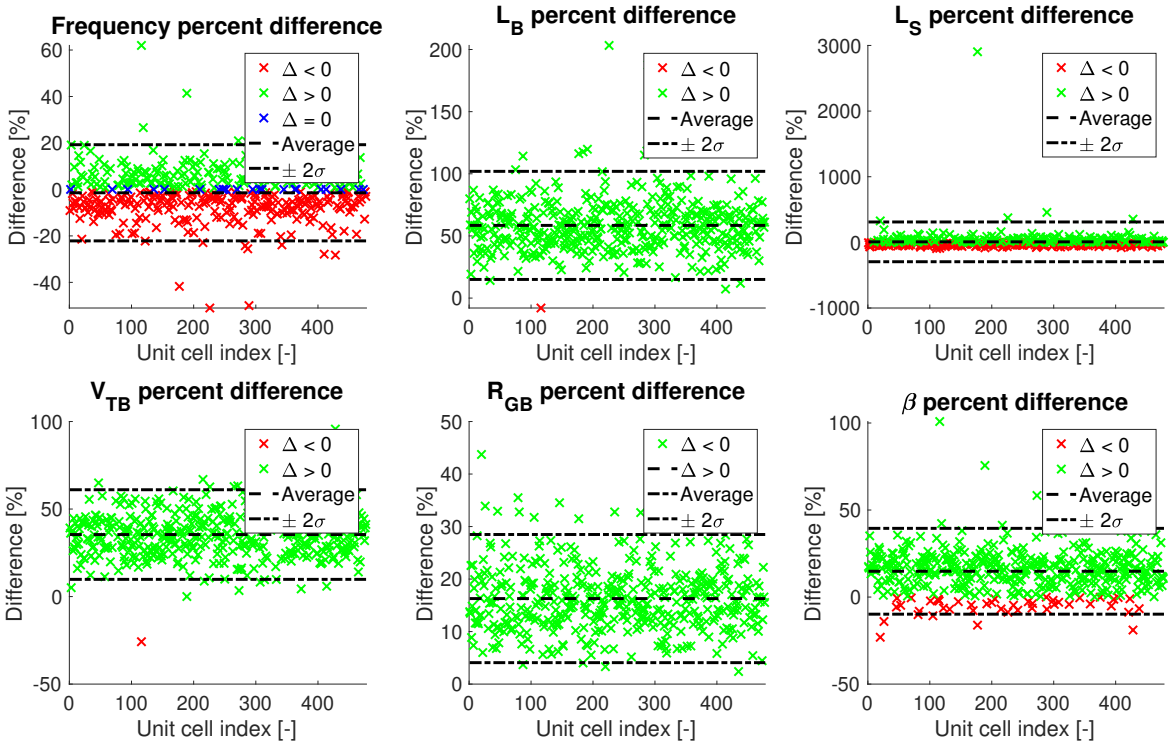

Source: The author.

Figure 98 – P18 hydrodynamic parameters percent change between stations 1 and 5.

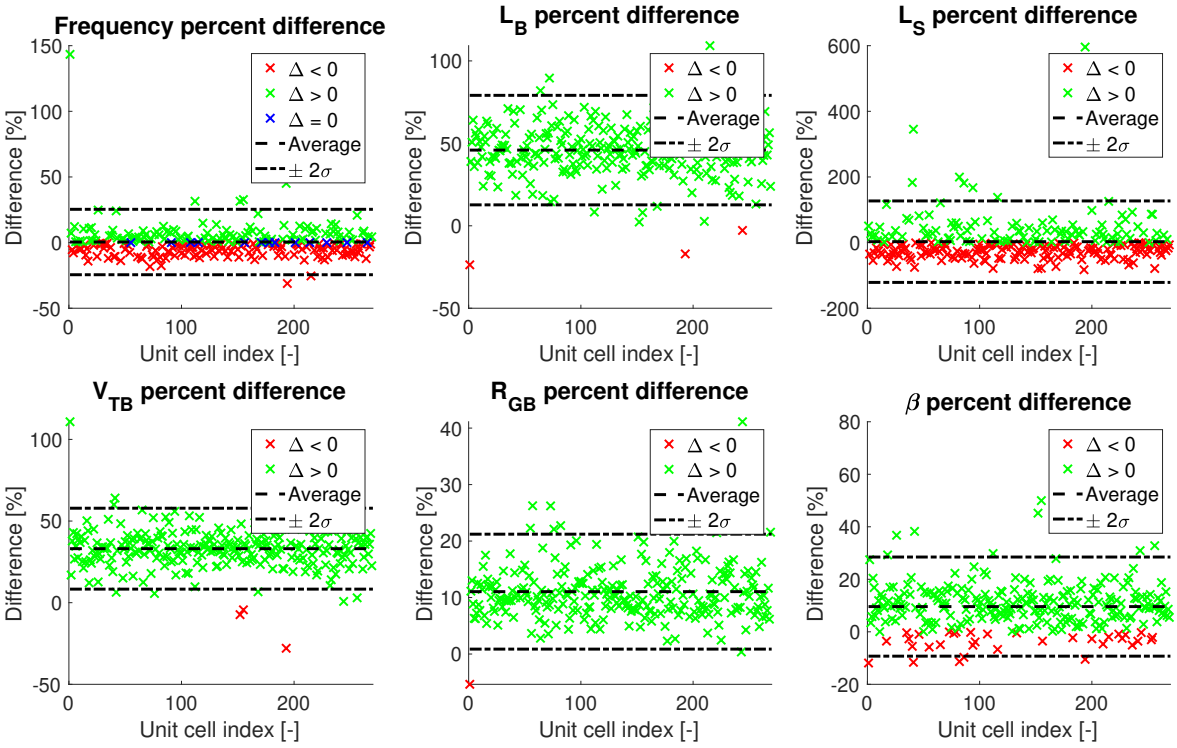

Source: The author.